International
Progress Report

IPR-02-33

Äspö Hard Rock Laboratory

TRUE Block Scale project

Evaluation of block scale tracer retention understanding experiments at Äspö HRL

Vladimir Cvetkovic
Hua Cheng

Water Resources Engineering
KTH Stockholm

December 2002

Svensk Kärnbränslehantering AB
Swedish Nuclear Fuel
and Waste Management Co
Box 5864
SE-102 40 Stockholm Sweden
Tel +46 8 459 84 00
Fax +46 8 661 57 19

Äspö Hard Rock
Laboratory

Report no.	No.
IPR-02-33	F56K
Author	Date
Vladimir Cvetkovic Hua Cheng	Dec. 2002
Checked by	Date
Anders Winberg	June 2003
Approved	Date
Christer Svemar	Sept. 2003

Äspö Hard Rock Laboratory

TRUE Block Scale project

Evaluation of block scale tracer retention understanding experiments at Äspö HRL

Vladimir Cvetkovic
Hua Cheng

Water Resources Engineering
KTH Stockholm

December 2002

Keywords: Tracer retention, crystalline rock, fracture network, tracer tests, transport modelling, rim zone, diffusion/sorption in rocks, TRUE, Äspö

Contents

Foreword

We gratefully acknowledge valuable comments provided by Anders Winberg (Conterra AB) and Jan-Olof Selroos (SKB) which improved the original version of the report. Also, we would like to thank the participants of the TRUE Block Scale programme: Peter Andersson, Johan Byegård, Jan Hermanson, Henrik Widestrand and Eva-Lena Tullborg (SKB team), Bill Dershowitz and Masahiro Uchida (JNC/Golder, Japan), David Holton (Nirex, UK), Jaime Gomez-Hernandez and Agustin Medina (Enresa, Spain), Daniel Billaux (Itasca Consultants SA, France), Antti Poteri and Aimo Hautojärvi (Posiva, Finland), for valuable discussions and exchanges. Finally, we thank the TRUE Block Scale reviewers Wolfgan Kinzelbach (ETH, Switzerland), Jane Long (University of Nevada Systems, US) and Ivars Neretnieks (KTH, Sweden) for critical and constructive comments on the entire TRUE Block Scale programme, which was helpful for the preparation of the final version of this report.

All modelling calculations of the report have been carried out using codes written in *Fortran 77*; these codes are available from the authors upon request. The text of the report was prepared by LaTeX typesetting on a *Red Hat Linux* platform (v 5.2). All the original figures of the report have been generated using *Tecplot* plotting software (v 7.5).

Abstract

The breakthrough curves [MT^{-1}] of the TRUE Block Scale non-reactive and reactive tracer tests at Äspö (Phase C) have been evaluated and interpreted adopting the LaSAR modelling framework (Cvetkovic et al., 1999). The fact that different tracers with strongly varying sorption properties were injected simultaneously, constitutes a key constraint in our analysis. Another important constraint is the assumption that the immobile water ("matrix") porosity and diffusivity can be deterministically related by an empirical relationship referred to as "Archie's law". Evaluation results indicate that the basic dual porosity transport model with diffusion-controlled sorption in the matrix, seems to account for the most dominant effects on the experimental time scales of the TRUE Block Scale tests. Retention parameters are grouped as material properties pertinent to the immobile zones (porosity θ, formation factor F, sorption coefficients K_d and K_a) and flow-related (hydrodynamic control) parameter $\beta = k\tau$ pertinent to the mobile zone. We have estimated ranges for all *in-situ* retention parameters, including the flow-dependent parameter k, assuming uniform (effective) values of the material properties; the full parameter range is presented for all flow paths in Tables 6.4-6.6. The estimate of the sorption coefficient K_d is most robust, whereas the estimate of k (and consequently of K_a) is least robust. We showed the potential complexity and impact of three-dimensional retention heterogeneity. The interplay between extent of penetration for a given tracer and depth-wise variability is investigated, as well as the effect of longitudinal variability in porosity and the formation factor for diffusion. The penetration depth over the TRUE Block Scale time scales for the strongly sorbing tracers seems to be limited to a few millimeters , and hence the depth-wise porosity over the first few millimeters is important for estimates of K_d. Estimates of k are less sensitive to the depth-dependence (since non-sorbing tracers penetrate relatively long into the "matrix"), but are sensitive to the longitudinal variability, as quantified by the log-standard deviation, $\sigma_{\ln\theta}$. We have derived an expression for effective porosity Eq.(7.16), relevant for non-sorbing tracers and estimation k, and showed that increasing variability implies enhanced retention. Effective porosity substitutes the uniform (constant) porosity in the transport model, and is related to the underlying heterogeneous field. For non-sorbing tracers effective porosity is shown to be always greater than the arithmetic mean porosity, if Archie's law is applicable; if Archie's law is not applicable, and the formation factor is a constant independent of porosity, then effective porosity is the arithmetic mean. For relatively strongly sorbing tracers, we derived the effective porosity as Eq.(7.19). Comparison of retention parameter estimates from TRUE-1 Feature A scale of 5 m with TRUE Block Scale estimates indicate that material effective properties are comparable; thus it appears that no particular spatial upscaling considerations are required for effective material properties from 5 m to say 15-30 m.

Sammanfattning

Vi har utvärderat genombrottskurvor av icke-reaktiva och reaktiva spårämnen från TRUE Block Scale-experimenten i Äspölaboratoriet med hjälp av modelleringskonceptet LaSAR (Cvetkovic et al., 2000). Den viktigaste förutsättningen för vår utvärdering är att olika spårämnen har distinkt olika sorptionsegenskaper. Ett viktigt antagande i utvärderingen är att vi kan tillämpa Archies lag, som relaterar matrisporositet och diffusivitet på empirisk basis. Resultaten antyder att ”dual porosity”-konceptet är tillämpbart för de förhållanden som gäller vid spårämnesförsöken inom TRUE Block Scale-experimenten Retentionsparametrarna är grupperade som dels materialegenskaper (porositet θ, ”formation factor” F, sorptionskoefficienter K_a och K_d) dels den strömningsrelaterade (hydrodynamisk kontrollerade) parametern $\beta = k\tau$, som är relaterad till den mobila zonen. Vi uppskattar alla *insitu* -retentionsparametrarna, inklusive k, som beror på strömningsfältet, med antagandet att de alla representerar konstanta, effektiva retentionsegenskaper; resultatet av denna uppskattning visas i Tabellen 6.4- 6.6. Uppskattningen av K_d är minst känslig, medan den av k (och därmed av K_a) är mest känslig. Vi visar den potentiella komplexiteten och påverkan av tredimensionell heterogenitet i retentionsegenskaperna, särskilt samspelet mellan spårämnespenetrationsdjupet och den longitudinella variabiliteten i porositet och diffusivitet. Penetrationsdjupet för starkt sorberande spårämnen för TRUE Block Scale-tidsskalorna verkar vara ett par millimeter; därför är porositeten över de första få millimetrarna den viktigaste faktorn för uppskattningen av K_d. Uppskattningen av k är mindre känslig för porositetsvariationen med djupet (eftersom icke-sorberande spårämnen penetrerar relativt djupt i matrisen);uppskattningen av k är däremot känslig för den longitudinella variabilitet i porositet och diffusivitet som kvantifieras av standardavvikelsen σ_θ. Vi härleder uttryck för effektiv porositet Ekv. (7.16), som är relevant för icke-sorberande spårämnen och särskilt för uppskattningen av k. Effektiv porositet ersätter den konstanta porositeten i transportmodellen och är relaterad till statistiken av det heterogena fältet. För icke-sorberande spårämnen visas den effektiva porositeten alltid vara större än det aritmetiska medelvärdet av porositeten, om Archies lag är tillämpbar. Om Archies lag ej är tillämpbar och ”formation factor” är konstant och oberoende av porositeten, så är den effektiva porositet lika med det aritmetis medelvärdet. För starkt sorberande spårämnen härleder vi Ekv.(7.19) som effektiv porositet. Jämförelse av retentionsparametrarna uppskattade inom TRUE-1 Feature A på 5-meterskalan med samma parametrar uppskattade inom TRUE Block Scale visar att de materiella retentionsegenskaperna är jämförbara. Det tyder på att inga speciella uppskalningar behövs för effektiva materiella egenskaper från 5 m till säg 15-30m-skalan.

Executive summary

The measured TRUE Block Scale tracer breakthrough curves (BTCs) indicate relatively strong retention compared to what would be predicted using unaltered matrix retention data. Retention observed in TRUE Block Scale tests is comparable to the retention observed in the TRUE-1 tests. Judging from K_d and K_a estimates, as well as by the dimensionless measure RC ("retention capacity"), Feature A has somewhat stronger retention properties than the TRUE Block Scale flow paths. The flow paths II and III (C-2 and C-3 tests) appear to have stronger retention properties than flow path I (C-1), however, the number of sorbing tracers recovered in C-2 and C-3 tests is limited and hence estimation of retention properties for C-2 and C-3 flow paths is less reliable.

The measured TRUE Block Scale BTCs (20-100 m scale) exhibit characteristics which are consistent with those found in the interpreted single fracture, Feature A (5 m scale) investigated as part of the TRUE-1 tests. There is a consistency in the TRUE Block Scale BTCs, in the successive arrival of sorbing tracers, and corresponding peak magnitudes, both following the strength of sorption properties. In other words, tracers which sorb most strongly, are retained most strongly, with a lowest peak.

Our TRUE Block Scale predictions proposed two limiting cases, one using the MIDS laboratory retention data for the unaltered matrix, and one with estimated TRUE-1 *in-situ* retention data (Cvetkovic et al., 2000). Using the t_5, t_{50} and t_{95} measures (Table 5.3), the predictions of tracer breakthrough were reasonably good, where data is essentially found between the two limits; the estimated *in-situ* TRUE-1 retention parameters generally yielded somewhat better predictions. The BTCs for the more strongly sorbing tracers (e.g., K, Rb and Cs in C-1 tests), where in between the two limits, somewhat more closely represented by the TRUE-1 data (Figure 6.1) For the C-2 and C-3 tests (which covers only weakly sorbing tracers), *in-situ* retention was generally underestimated by the predictions, with both MIDS and TRUE-1 retention data. In particular, the tracers Na, Sr and Ca, exhibited surprisingly strong retention, which has yet to be fully explained (Figure 6.2-6.3).

Assuming uniform (effective) retention material properties, we estimated ranges for all *in-situ* retention parameters, including the flow-dependent parameter k; the full parameter range is presented for all flow paths in Table 6.4-6.6. In view of the relatively limited statistical base for retention heterogeneity, as well as the aperture variability, the estimated *in-situ* ranges we provide here are non-unique and uncertain. New data, for instance from pore space characterization, could provide further independent information (constraints) for assessing the validity of the estimated ranges.

There is sufficient information available both from Feature A (TRUE-1) (Byegård et al., 2001) and TRUE Block Scale structure intercepts (Kelokaski et al., 2001) to conclusively establish that porosity of the rock matrix varies statistically in three-dimensions, with a depth-wise trend normal to the fracture surface. The variability found, for instance, on Feature A intercepts is relatively large (log-standard deviation in the range 1.1-1.5, Figure 7.3) on a small sample (5 cm scale). Unless the integral scale of the longitudinal variability is comparable to the sample size, we anticipate this variability to be larger on larger scales, with log-standard deviations greater than 1.5. However, the structural complexity of different retention (immobile) zones along a flow path (including coating, fault breccia, fault gouge, stagnant water) makes statistical characterization from intercepts less relevant, even with a large number of samples from various locations. Thus we regard the available data on retention heterogeneity primarily as qualitative, and have used, for instance, the log-standard deviation of the porosity as a sensitivity parameter in the range 1.1-1.5.

The potential complexity and impact of three-dimensional retention heterogeneity was demonstrated, in particular the interplay between penetration and depth-wise variability, and the longitudinal variability, in porosity. The penetration depth of the strongly sorbing tracers over TRUE Block Scale time scales seems to be limited to a few millimeters, and hence the depth-wise porosity over the first few millimeters is important for estimates of K_d. Estimates of k are less sensitive to the depth-dependence (since non-sorbing tracers penetrate relatively long into the "matrix"), but are sensitive to the longitudinal variability, as quantified by the log-standard deviation, $\sigma_{\ln\theta}$. Our methodology to account for retention heterogeneity is approximate for the three-dimensional reality. Further analysis, with more comprehensive simulations, would reveal a greater level of detail in particular regarding tracer penetration and its impact of retention.

An expression for effective porosity Eq.(7.16) was derived, relevant for non-sorbing tracers and in particular for estimating k. Effective porosity substitutes the uniform (constant) porosity in the transport model, and is related to the underlying heterogeneous field. In Table 9.4 of Cvetkovic et al. (2000) for TRUE-1, and in Tables 6.4- 6.6 in Chapter 6, all estimated *in-situ* parameters are *effective* values. The interesting issue is whether effective properties can be related to statistical parameters which in principle can be measured. Our expression (7.16) links effective porosity with the log-normal porosity parameters and the exponent m in Archie's law. We showed that for non-sorbing tracers effective porosity is always greater than the arithmetic mean porosity. If Archie's law is applicable; if Archie's law is not applicable, and the formation factor F is a constant independent of porosity, then effective porosity is the arithmetic mean. For relatively strongly sorbing tracers, we derived the corresponding Eq.(7.19).

We have showed that porosity variability along a flow path *enhances retention*. Specifically, effective porosity for retention depends on the degree of variability, and *increases* with increasing variability, in our case quantified by the log-standard deviation, $\sigma_{\ln\theta}$. In fact, effective porosity can become quite large with increasing $\sigma_{\ln\theta}$ if Archie's law is applicable. This result is in our view important for at least partly explaining the relatively

strong *in-situ* retention that has been observed both in the TRUE-1 and the TRUE Block Scale tests. Because porosity varies longitudinally, predictions on the TRUE Block Scale scale are inherently uncertain if we do not have sufficient characterization of the retention heterogeneity, such that basic statistical parameters can be inferred. Thus, characterization of retention variability, in particular the porosity, can in principle serve as a basis for improving the prediction accuracy of tracer tests performed in the block scale.

Chapter 1

Background

1.1 General

Concepts for deep geological disposal of spent nuclear fuel include multi-barrier systems for isolation of nuclear waste from the biosphere. Waste forms, and concepts for encapsulation of the waste and engineered barriers may vary between countries, but most concepts rely on a natural geological barrier which should provide a stable mechanical and chemical environment for the engineered barriers, and should also reduce and retard transport of radionuclides released from the engineered barriers. In case of an early canister damage, the retention capacity of the host rock for short-lived radionuclides such as Cs and Sr becomes important.

In planning the experiments to be performed during the Operating Phase of the Äspö Hard Rock Laboratory, the Swedish Nuclear Fuel and Waste management Company (SKB) identified the need for a better understanding of radionuclide transport and retention processes. The needs of performance assessment included improved confidence in models to be used for quantifying transport of sorbing radionuclides. It was also considered important from the performance assessment perspective to be able to show that adequate transport data and parameters (distribution coefficients, diffusivity, "flow-wetted surface", etc.) could be obtained from site characterisation, or field experiments, and that laboratory results could be related to retention parameters obtained *in-situ*.

To answer these needs, SKB in 1994 initiated a tracer test programme referred to as the Tracer Retention Understanding Experiments (TRUE). The overall objectives of the Tracer Retention Understanding Experiments (TRUE) are to (Winberg et al., 2000):

- develop an understanding of radionuclide migration and retention in fractured rock;
- evaluate to what extent concepts used in models are based on realistic descriptions of a rock volume and if adequate data can be collected in site characterisation;
- evaluate the usefulness and feasibility of different approaches to model radionuclide migration and retention;
- provide *in-situ* data on radionuclide migration and retention.

The First Stage of TRUE (Winberg et al, 2000) was performed on the detailed scale (0-10 m) and was focused on characterisation, experimentation and modelling of an interpreted single feature. Work performed included drilling of five boreholes, site characterisation, and installation of multi-packer systems to isolate interpreted hydraulic structures. Subsequent cross-hole hydraulic tests and a comprehensive series of tracer tests were used to plan a series of three tracer tests with radioactive sorbing tracers, in three separate flow paths. The *in-situ* tests were supported by a comprehensive laboratory programme performed on generic (Byegård et al., 1998; Byegård et al., 2001), as well as on site-specific material from the studied interpreted features (Andersson et al., 2002b; Kelokaski et al., 2001; Dershowitz et al., 2001).

1.2 TRUE Block Scale project

When the TRUE Programme was set up it was identified that the understanding of radionuclide transport and retention in the block scale (10-100 m) also required attention in terms of a separate experiment; the TRUE Block Scale Project was designed for this purpose.

The specific objectives of the TRUE Block Sale Project given in the developed test plan (Winberg, 1997) were to:

- increase understanding of tracer transport in a fracture network and improve predictive capabilities;
- assess the importance of tracer retention mechanisms (diffusion and sorption) in a fracture network;
- assess the link between flow and transport data as a means for predicting transport phenomena.

The TRUE Block Scale project is an international partnership funded by ANDRA (France), ENRESA (Spain), Nirex (UK), Posiva (Finland), PNC (Japan) and SKB (Sweden). The Block Scale project is one part of the Tracer Retention Understanding Experiments (TRUE) conducted at the Äspö Hard Rock Laboratory. The TRUE Block Scale project, initiated mid 1996, is divided into a series of consecutive stages (Winberg, 1997): Scoping Stage - Preliminary Characterisation Stage - Detailed Characterisation Stage (Winberg et al., 2000) - Tracer Test Stage - Evaluation and Reporting Stage. The staged approach has also an embedded iterative approach to characterisation and evaluation.

1.3 Summary of characterization and experiments

Results of the characterisation of each drilled borehole have been used to plan the subsequent borehole. During the initial four stages of TRUE Block Scale, a total of 5 boreholes have been drilled and characterised as part of the project. Additional four boreholes have been completed as part of other adjacent projects and have been utilised as verification and

monitoring boreholes. The principal characterisation tools used to establish the conductive geometry have been BIPS borehole imaging supported by logging of the boreholes with the Posiva difference flow meter and hydraulic connectivity established from responses to drilling and performed cross-hole interference tests. During the course of the project 6 versions of a descriptive structural model have been developed. At the conclusion of the Detailed Characterisation Stage in mid 1999, the feasibility of performing tracer tests in the identified network of structures in the block scale (10- 100 m) had been firmly demonstrated (Winberg, 2000). As a consequence a series of tests with radioactive sorbing tracers were performed as part of the Tracer Test Stage which has run from mid 1999 through 2000 (Andersson et al., 2002a). The respective updates of the structural model have been used to simulate, and in some cases perform blind predictions, of performed hydraulic and tracer tests (Poteri et al., 2002).

In support of the *in-situ* experimentation a series of laboratory investigations have been performed on geological material from the interpreted structures which make up the studied fracture network. The analyses include mineralogical and geochemical analyses, porosity determinations using water absorption and PMMA techniques (Andersson et al., 2002b; Kelokaski et al., 2001). In addition water samples collected during drilling and from packed off sections have been analysed for chemical composition and isotope content and used in support of the structural models. Cation exchange capacity for fault breccia material from different intercepts, deduced from mineralogical composition, have been used in combination with ambient groundwater chemistry from the different test sections to estimate volumetric distribution coefficients (Andersson et al., 2002b).

1.4 Scope of report

In Chapter 2 we present the model which is used for the SKB/WRE evaluation of the TRUE Block Scale tracer breakthrough curves (BTCs). Chapter 3 summarizes the C-1, C-2 and C-3 tracer tests which are the subject of the evaluation and interpretation. Flow dependent parameters, as obtained from JNC/Golder discrete fracture network (DFN) (FracMan) simulations is the subject of Chapter 4. Results of predictions of TRUE Block Scale BTCs, obtained by the SKB/WRE team, are briefly presented in Chapter 5. In Chapter 6, we summarize evaluation results assuming uniform retention parameters, and compare the evaluated *in-situ* values with retention data/parameters based on laboratory experiments on unaltered Äspö diorite. The potential impact of retention heterogeneity and methods to account for it, are discussed in Chapter 7. In Chapter 8 we interpret the observed BTCs accounting for *retention heterogeneity*[1], and provide estimates of block scale *in-situ* retention parameters. Finally, in Chapter 9 we discuss the results and in Chapter 10 summarize our main findings and conclusions.

[1]By "retention heterogeneity" we mean in the present context three-dimensional variations of rock material properties which control retention; the material properties are both physical (e.g., porosity, diffusivity) and chemical/mineralogical (e.g., sorption coeffi cient).

Chapter 2

Evaluation model

2.1 LaSAR approach

The Lagrangian Stochastic Advection-Reaction (LaSAR) modelling approach, as applied to the TRUE Block Scale tracer tests, derives from the parallel plate diffusion/sorption model originally proposed for retention in crystalline fractures by Neretnieks (1980). The model of Neretnieks (1980) was extended as part of the TRUE program to account for aperture variability as well as for longitudinal heterogeneity in retention parameters (Cvetkovic et al, 1999, 2000).

We have further extended the LaSAR methodology to a network of fractures, and implemented it for evaluating and interpreting the TRUE Block Scale tracer tests.

2.2 Conceptualization and assumptions

Interpreted deterministic structures (fractures) of the TRUE Block Scale site are heterogeneous with a relatively complex microscopic structure. Based on available data, we identify four principle immobile zones of retention: (i) rim zone of the fracture wall rock, (ii) fault breccia, (iii) fault gouge material, and (iv) stagnant water (Figure 2.2). Our conceptualization of the retention zones is given in Figure 2.3. Matrix porosity, diffusivity and presumably K_d, are assumed heterogeneous in three dimensions, with a trend in the z-direction (orthogonal to the fracture plane), decreasing from the rim zone toward the intact rock. Fault breccia is viewed as part of the microscopic heterogeneity with sorption limited by diffusion, and the effect of fault gouge is viewed as part of (equilibrium) surface sorption.[1] The effect of stagnant water on retention (due to diffusion) is not explicitly accounted for.[2]

[1] The rationale for this is based on the assumption that fault breccia consists of suffi ciently large particle such that diffusion/sorption can be approximated as unlimited on the time scale of experiments, and fault gouge is assumed to consist of suffi ciently small particles such that diffusion capacity is satuurated and sorption is essentially at equilibrium.

[2] Following a similar reasoning as presented in (Cvetkovic et al., 2000), we consider diffusion into lateral stagnant water zones as a second order retention process compared to diffusion/sorption in the immobile matrix, and therefore neglect it.

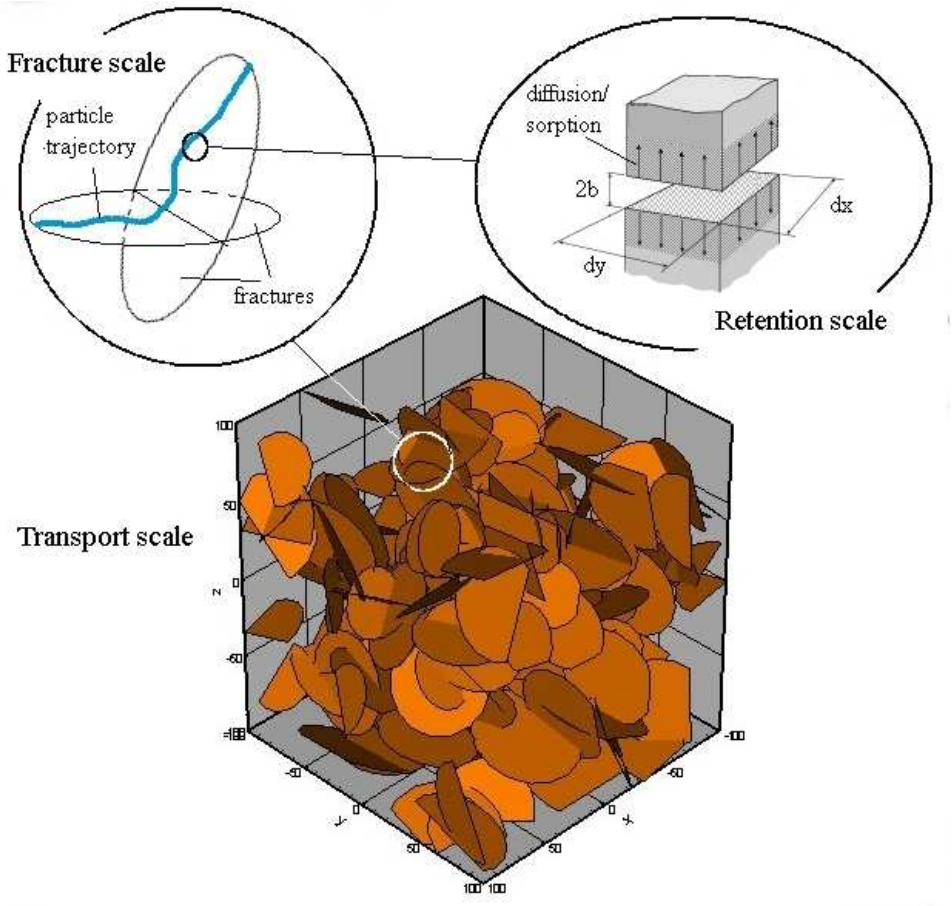

Figure 2.1: *Relevant scales for TRUE Block Scale (from Cvetkovic et al., 2002).*

The LaSAR modelling approach, as applied to the TRUE Block Scale tests, is based on the following assumptions:

- Flow is assumed to be steady state.
- Dominant hydrodynamic mode of transport in fractures is variable advection.
- Tracers are fully mixed in the fracture in the z-direction (orthogonal to the fracture plane).
- Advective transport in the rock matrix is negligible.
- Tracer diffuses into the rock matrix in the direction orthogonal to the fracture plane, i.e., diffusion into the rock matrix is one dimensional.
- All mass transfer processes are assumed linear.
- Diffusion in the rock matrix is assumed unlimited.
- Sorption in the rock matrix is assumed to be at equilibrium.
- Sorption on the fracture surfaces is assumed to be at equilibrium.

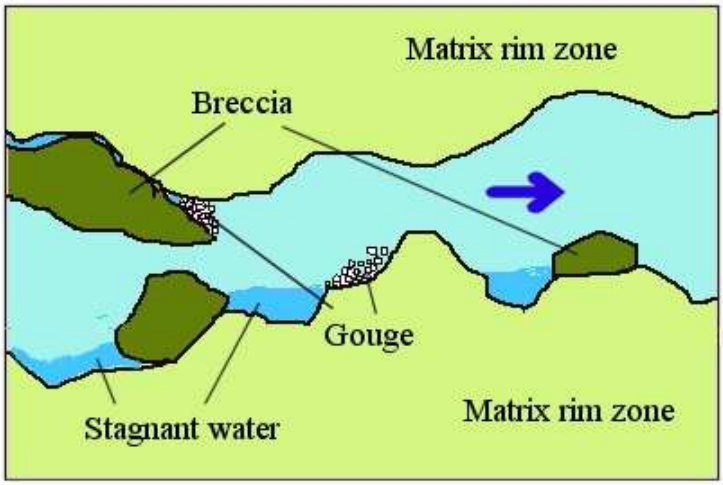

Figure 2.2: *Schematic illustration of four principle immobile zones of retention for conductive structures/fractures of the TRUE Block Scale site.*

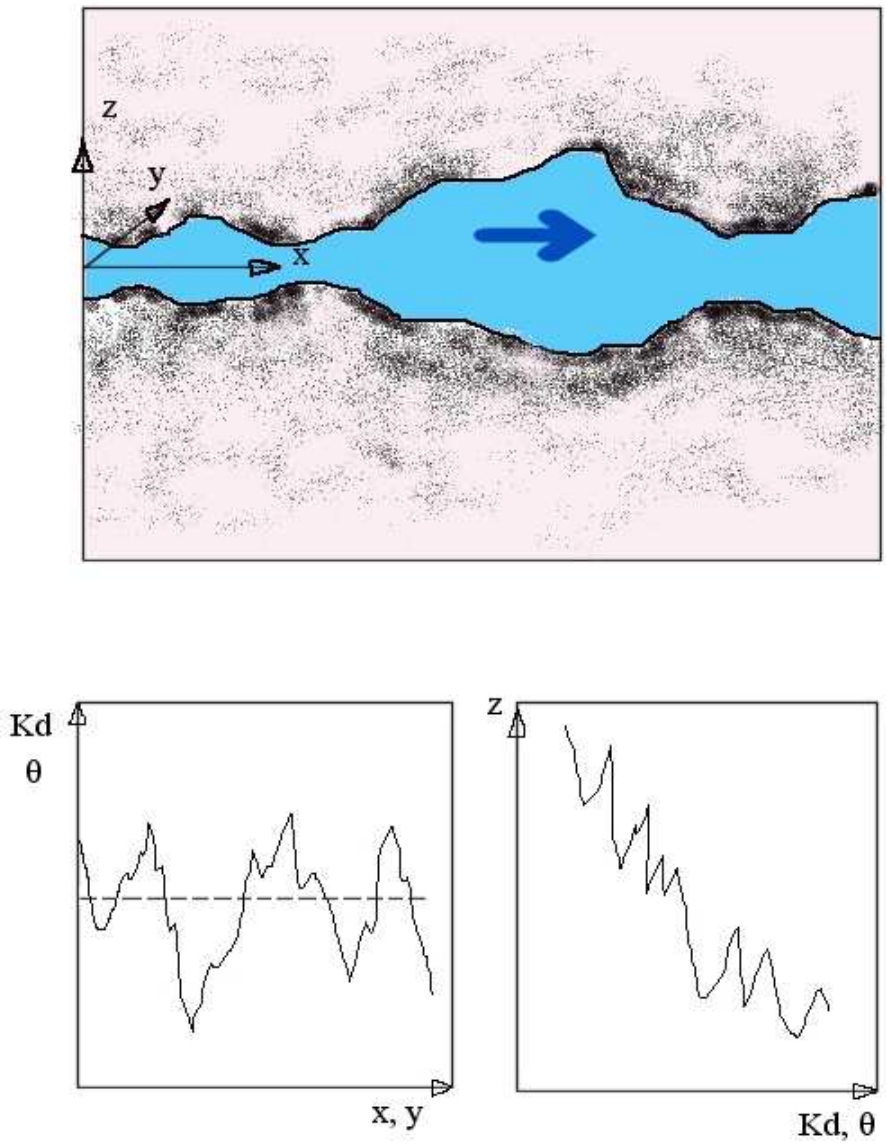

Figure 2.3: *Conceptualization of retention zones for modelling. Darker shading implies greater porosity, and possibly even greater K_d; retention in the four principle zones of Figure 2.2 are "lumped" into two mass transfer (retention) processes: Unlimited diffusion/sorption in the rim zone and fault breccia pieces/fragments, and equilibrium sorption on fracture surface, including fault gouge. Variability in three dimensions is also schematically illustrated as a trend in the z-direction, whereas no trend is assumed in the longitudinal direction.*

2.3 Transport model

The basic expression of our transport model is the probability density function (pdf) for a single tracer particle residence time from the injection to the detection (pumping) borehole which couples the processes of advection, diffusion and sorption (neglecting decay):

$$\gamma(t,\tau) = \frac{H(t-\tau)\,B}{2\sqrt{\pi}(t-\tau-A)^{3/2}}\,\exp\left[\frac{-B^2}{4(t-\tau-A)}\right] \tag{2.1}$$

where

$$B = \sum_{i=1}^{N} \beta_i \kappa_i \quad ; \quad \beta_i = \frac{l_i}{V_i b_i} \quad ; \quad \tau = \sum_{i=1}^{N} \frac{l_i}{V_i} \tag{2.2}$$

$$A = \sum_{i=1}^{N} K_a^i \beta_i \quad ; \quad \kappa_i \equiv \theta_i \left[D_i(1+\frac{\rho_b K_d^i}{\theta_i})\right]^{1/2} \tag{2.3}$$

and H is the Heaviside step function. The density γ [1/T] Eq.(2.1) is conditioned on the water residence time τ, and on parameters A [T] and B [$T^{1/2}$]. If there is no retention, then $\gamma(t,\tau) = \delta(t-\tau)$, i.e., particle residence time is equivalent to the water residence time through the fracture network.

The index "i" designates either a fracture (if the particle is transported through a series of fractures), and/or discretization segments if we consider a single heterogeneous fracture; N is the total number of segments, which could also cover transport through a few heterogeneous fractures. K_d [L^3/M] is the distribution coefficient in the matrix, K_a [L] is the sorption coefficient on the fracture surface, b [L] is the fracture half-aperture, D [L^2/T] is pore diffusivity and ρ_b [M^3/L] the bulk density of the rock matrix. All of the above parameters are in general segment-dependent, hence index "i".

If the retention parameters θ , D, K_d are constant (effective) values for all segments, we have

$$B = \beta\kappa \quad ; \quad \kappa = \theta\left[D\ (1+K_d\rho/\theta)\right]^{1/2} \quad ; \quad \beta = \sum_{i=1}^{N} \frac{l_i}{V_i b_i} \tag{2.4}$$

The parameter β [T/L] integrates incremental advective water residence time for segments along a trajectory, normalized by the half-aperture of the segments. It is dependent only on the advective (water) movement, i.e., on fracture hydrodynamics, which in turn is determined by the aperture variations as well as the network features, and on the prevailing boundary conditions. Our basic evaluation model is based on Eq.(2.4); however, we will also use Eqs.(2.2)-(2.3) in order to account for spatial variability in porosity.

2.4 Modelling tracer test results

Let m_0 [M] denote the total mass (or activity) of a tracer released in the injection borehole with a rate $\phi(t)$ [1/T]. Let $g(\tau)$ [1/T] denote the pdf of the water residence time τ from the injection to the detection borehole. If dispersion due to advection variability is neglected, then $g(t) = \delta(\tau - \tau_0)$ where τ_0 is the plug-flow water residence time for a given flow path.

Numerical simulations under various conditions have indicated that β is strongly correlated to τ (Cvetkovic et al., 1999; Cvetkovic et al., 2000). In general, the correlation between β and τ is non-linear and follows a power-law. However, for the variability range encountered in TRUE Block Scale, a linear relationship seems to provide a reasonable approximation. We therefore postulate

$$\beta = k\tau \tag{2.5}$$

where k [1/L] is an *in-situ* parameter associated with a given flow path. Note that Eq.(2.5) simplifies the estimation problem significantly, since the entire distribution of β is replaced by the distribution of τ and a single parameter k; this parameter has been referred to as "flow-wetted surface per unit volume of water" (Andersson et al., 1998).

Substituting Eq.(2.5) into Eq.(2.2)-(2.3) with Eqs.(2.4), we get $A = \tau\zeta$ and $B = \tau\psi$ where the two key parameter groups ζ [-] and ψ [$T^{-1/2}$] are defined as:

$$\zeta \equiv kK_a \quad ; \quad \psi \equiv k\kappa \tag{2.6}$$

The tracer discharge (or breakthrough), Q, in the detection borehole is evaluated as

$$Q(t) = m_0 \int_0^\infty [\phi(t) * \gamma(t,\tau)] g(\tau) d\tau \tag{2.7}$$

where γ is given in Eq.(2.1) and "*" denotes the convolution operator. Thus to predict Q, we require the knowledge of all *in-situ* retention parameters (assuming effective, uniform values), we require k, the water residence time density $g(\tau)$, the injection rate $\phi(t)$ and the total tracer mass m_0.

2.5 Calibration steps

The calibration procedure consists of two steps:

1. Determining $g(\tau)$ by "deconvoluting" BTCs for non-sorbing tracers; the actual form of $g(\tau)$ is assumed to be inverse-gaussian, and the first two water residence time moments are calibrated for each flow path.

2. Calibrating the two parameter groups ψ and ζ on the TRUE Block Scale BTC data, using the "deconvoluted" $g(\tau)$ from step 1.

2.6 Accounting for heterogeneity

Equations (2.1)-(2.3) directly account for lateral heterogeneity (i.e., in the x, y-directions of the fracture plane) for all parameters involved. As indicated by Eqs.(2.2)-(2.3), the heterogeneity affects the transport in an integrated sense with quantities A and B. The key problem is in relating the effective retention parameters in Eq. (2.4) to point measurements of say the porosity θ and K_d.

Retention parameters in Eqs.(2.2)-(2.3) strictly assume that the parameters are constant in the direction orthogonal to the fracture plane (z-direction, Figure 2.3). Clearly there is spatial variability in all retention parameters from the fracture plane, through the rim zone, to the unaltered rock; there is evidence that porosity systematically decreases (as a trend) with increasing z and presumably so does K_d (Figure 2.3), although such data for K_d is currently unavailable. The key issue related to heterogeneity in the z-direction is the penetration depth for individual tracers. In particular, the values of say θ and K_d at any given point of the x, y -plane (which appear in expressions Eqs.(2.2)-(2.3)), will depend on the extent to which a given tracer penetrates the rim zone.

Currently available data are insufficient for constructing statistical models of retention parameter variability under TRUE Block Scale conditions. Thus our attempt to investigate potential effects of heterogeneity must be considered as qualitative. In particular, we shall use a log-normal distribution model for porosity in the x, y-plane (consistent with data available), and show that this lateral heterogeneity in porosity is relevant for interpreting effective porosity. We will also account for heterogeneity in the z-direction indirectly, by estimating the penetration depth for different tracers, and using this estimate to define a depth-averaged, tracer-dependent porosity, again using the limited data available.

2.7 Estimation of *in-situ* retention parameters

If all effective *in-situ* retention parameters were available, we could insert them into Eq.(2.4) for each tracer. Based on Eq.(2.5), we could then use the calibrated ζ and ψ to infer the parameter k. In this case, the estimation problem would be over-determined, since we would have several equations and only one unknown (k). In reality, we do not have the *in-situ* retention parameters, and in fact, wish to estimate these. Since we calibrate ζ and ψ, the estimation problem is undetermined since we have more unknowns than equations (see Cvetkovic et al. (2000) for a discussion related to the evaluation of TRUE-1 experiments). In fact, we have precisely two more unknowns than equations, and hence require two additional constraints (assumptions, or independent estimates) in order to close the system of equations and estimate all *in-situ* retention parameters (including k).

We summarize below three possible, alternative constraints:

1. Parameter k. The parameter k can be independently estimated in several ways; we list three possibilities:

- Numerical Monte Carlo simulations of particle transport in a discrete fracture network. Relevant DFN simulations were run, for instance, by JNC/Golder. These data include all tracer trajectories and necessary properties (velocities and apertures) along trajectories between the injection and detection borehole. The parameter k is obtained through linear regression between τ and β. Based on the results from the C-1 test, and also combining the results from C-2 and C-3 tests, we estimated $k = 6000$ 1/m. This possibility will be discussed in Chapter 4.
- Assuming a streamtube model, we have $\beta = 2WL/q$ where W is prescibed (say the borehole diameter, 0.056 m), L is the estimated distance between the injection and detection borehole (e.g., 14 m for C-1 tests) and q is the estimated injection flow rate (e.g., 45 ml/min for C-1 tests). The parameter k is then approximately $k = \beta/\tau$ where τ is the estimated mean water residence time.
- Following the definition of β Eq. (2.5), k can be interpreted as an inverse effective half-aperture. If we consider any particular value (obtained from hydraulic tests, or borehole imaging) as representative (say 1 mm as a representative aperture for TRUE Block Scale conditions), we would then estimate $k = 1/0.5$ mm$= 2000$ 1/m.

2. Relationship between porosity and diffusivity. We can relate D and θ using "Archies law" in the form $F = \theta^m$ (Clennell, 1997) where F [-] is the formation factor and m is an exponent in the range say $1.3 < m < 1.8$. The value $m \approx 1.6$ was obtained from a wide range of core data in petroleum engineering, and 1.8 is consistent with TRUE-1 "modelling input data set" (MIDS) (e.g., Cvetkovic et al., 2000).[3] The limit $m = 1$ is for an ideal case of perfectly parallel microfissures, or micro-pores, from the fracture surface into the rim zone. Since we do not have m for TRUE Block Scale conditions, it is appropriate to consider sensitivity to the entire range $1.3-1.8$. In our following analysis, we shall take advantage of Archie's law and use it as a constraint.

3. Matrix sorption coefficient. We could assume that *in-situ* K_d for any tracer is a particular value obtained in the laboratory, say from batch tests on 1-2 mm fraction. If emphasis is on sorption, then it is appropriate here to consider a more strongly sorbing tracer, such as Cs. For instance, the value for Cs is $K_d = 0.053$ m^3/kg for 1-2 mm fraction from a batch tests of 36 days duration using unaltered Äspö diorite (Byegård et al., 1998). This possibility is taken advantage of in Section 6.4.

[3]The MIDS formation factor is $F = 0.00005$ and the porosity $\theta = 0.004$; from $F = \theta^\theta$, we get $m \approx 1.8$.

Chapter 3

Experimental setting and summary of tracer test results

This chapter first describes the experimental setting for the TRUE Block Scale tracer tests, i.e., the basic features of the experimental rock volume and the structural model. Experimental tracer test results for the relevant non-sorbing and sorbing tracers are then summarized. Non-sorbing tracer tests, including B-2g, B-2d and B-2b, are presented in Andersson et al. (2000a,b, 2001); sorbing tracer tests C-1, C-2 and C-3 are presented in Andersson et al. (2001, 2002b).

3.1 Setting and structural model

The geophysical and geological investigations in the Äspö region verified three orders of trending zones. The 1^{st} order zones of lineaments are one almost orthogonal system of trending N-S and E-W and extending about 20-50 kilometers. The 2^{nd} order zones of lineaments are also one almost orthogonal system while trending NW and NE. The 3^{rd} order zones of lineaments trend NNW and NNE.

The dominant rocks on the Äspö island belong to the Transscandinavian Igneous Belt (TIB) granitoids in which mineralogical composition ranges from true granites (Ävrö granite) to granodioritic to quartz monzodioritic rock mass (Äspö diorites) (Kornfält and Wikman, 1988).

The TRUE Block Scale site is located at the southwestern part of the experimental level at the Äspö HRL (Figure 3.1). The block is denoted as ”TRUE Block Scale rock volume”. The rock volume is about $200\times250\times100$ m^3. The block containing the fracture network used in the tracer tests is about $100\times100\times50$ m^3 and is denoted as ”TRUE Block Tracer Test volume”.

The lithology of the TRUE Block Scale rock volume is dominated by Äspö diorite intermixed by small sections of fine-grained granite. Greenstone exists in minor fragments in the diorite.

The conductive structures in the TRUE Block Scale rock volume were investigated using different methods (e.g., borehole television, pressure responses, flow logging). The conductive fractures of the rock volume were found to consist of steeply dipping NW struc-

tures and NNW structures. The connectivity of the conductive structures was investigated through pressure responses. Two main groups of the structures were identified in the TRUE Block Scale rock volume through the responses : the structures (#13, #20,#21,#22,#23) and the structures (#5,#6,#7). High inflows and pressure responses in the boreholes were mainly associated with geologically and geometrically identified conductive structures. The structures associated with more than one anomaly were designated as deterministic structures in the structural model. The other conductive structures were assigned to the background fractures. The first three boreholes (KA2563A, KI0025F and KI0023B) were used to develop the basic structural model. Two additional boreholes (KI0025F02 and KI0025F03) were then used to confirm and refine the basic model developed on the first three boreholes. The hydraulic interference tests and dilution tests were performed to identify suitable sink and source sections for subsequent tracer tests. The main interpreted features, along with existing boreholes, are illustrated in Figure 3.2

Sorbing tracer tests in TRUE Block Scale were performed along three different flow paths: injection in KI0025F03:P5 (C-1 test), KI0025F03:P7 (C-2 test) and KI0025F02:P7 (C-3 test), while pumping in KI0023B:P6 for all three flow paths. Flow path I (C-1 test) KI0025F03:P5-KI0023B:P6 is a more or less single structure flow path (Structure #20). Flow path II (C-2 test) KI0025F03:P7-KI0023B:P6 is characterized as a network flow path involved at least three structures (#23,22,20). Flow path III (C-3) KI0025F02:P7-KI0023B:P6 is characterized as a long single flow path in structure #21 to some extent with fracture network characteristics.

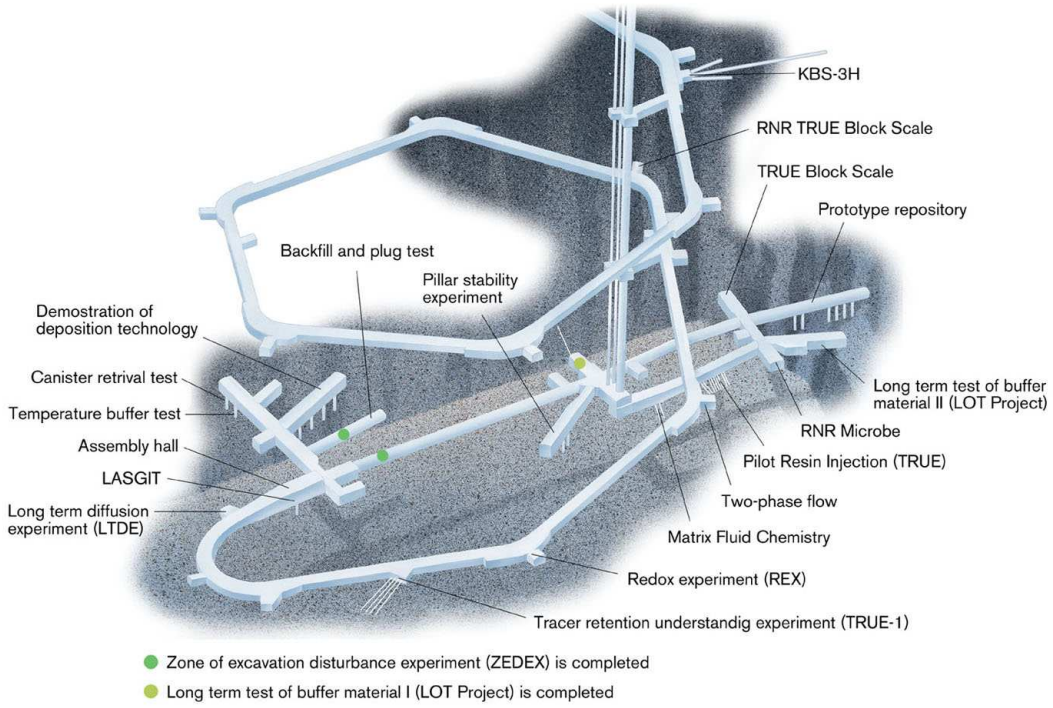

Figure 3.1: *Disposition of the Äspö Hard Rock Laboratory; the locations of TRUE Block Scale experiments are indicated.*

Table 3.1: Summary of tracer tests B-2g, B-2d and B-2b. "*" denotes values calculated by weighing.

Test	Inj. rate [ml/min]	Pump rate [ml/min]	Inj. borehole	Pump borehole	Recovery [%]*
B-2g	45	2060	KI0025F03:P5	KI0023B:P6	100
B-2d	10	2060	KI0025F03:P7	KI0023B:P6	88
B-2b	1.0	2060	KI0025F02:P7	KI0023B:P6	98

3.2 Non-sorbing tracer tests B-2g, B-2d and B-2b

Tracer tests B-2g, B-2d and B-2b (Andersson et al., 2000b) were performed as preparatory tests for sorbing tracer tests C-1, C-2 and C-3, respectively. B-2g is a weak dipole test. The tracers were injected in KI0025F03:P5 with $Q = 45$ ml/min with pumping in KI0023B:P6 at $Q = 2060$ ml/min. B-2d is also a weak dipole test. The tracers were injected in KI0025F03:P7 with $Q = 10$ ml/min with pumping in KI0023B:P6 at $Q = 2060$ ml/min. B-2b is a radially converging test. The tracers were released in KI0025F02:P7 with pumping in KI0023B:P6 at $Q = 2060$ ml/min. These three conservative tracer tests aimed at finding the best suitable flow and transport path with sufficient recovery, for the Phase C sorbing tracer tests. Figure 3.3 shows the tracer injection and resulting breakthrough curves (BTCs) for B-2g, B-2d and B-2b tests.

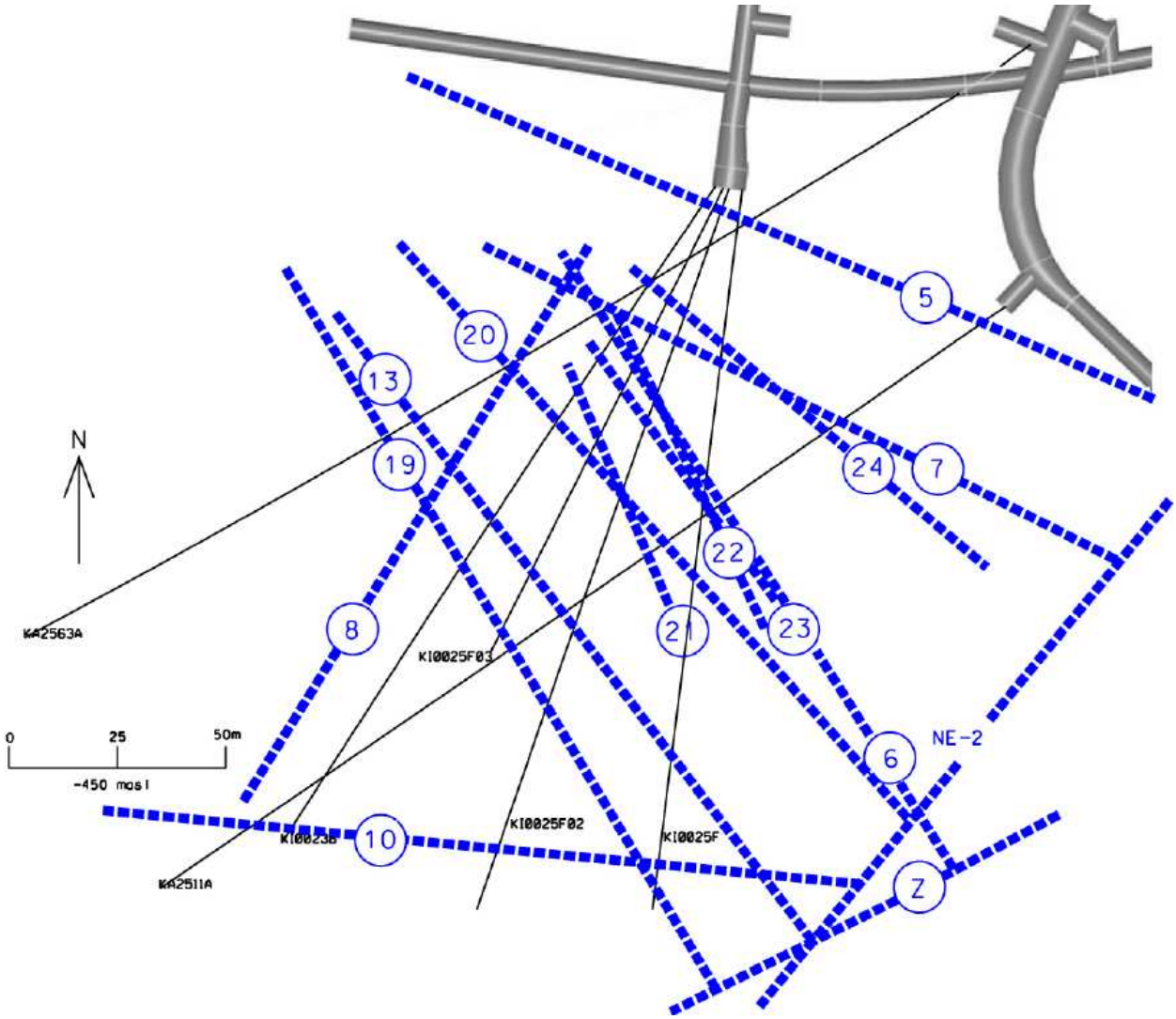

Figure 3.2: *The TRUE Block Scale experimental volume with boreholes and major features (from Poteri et al. (2002)).*

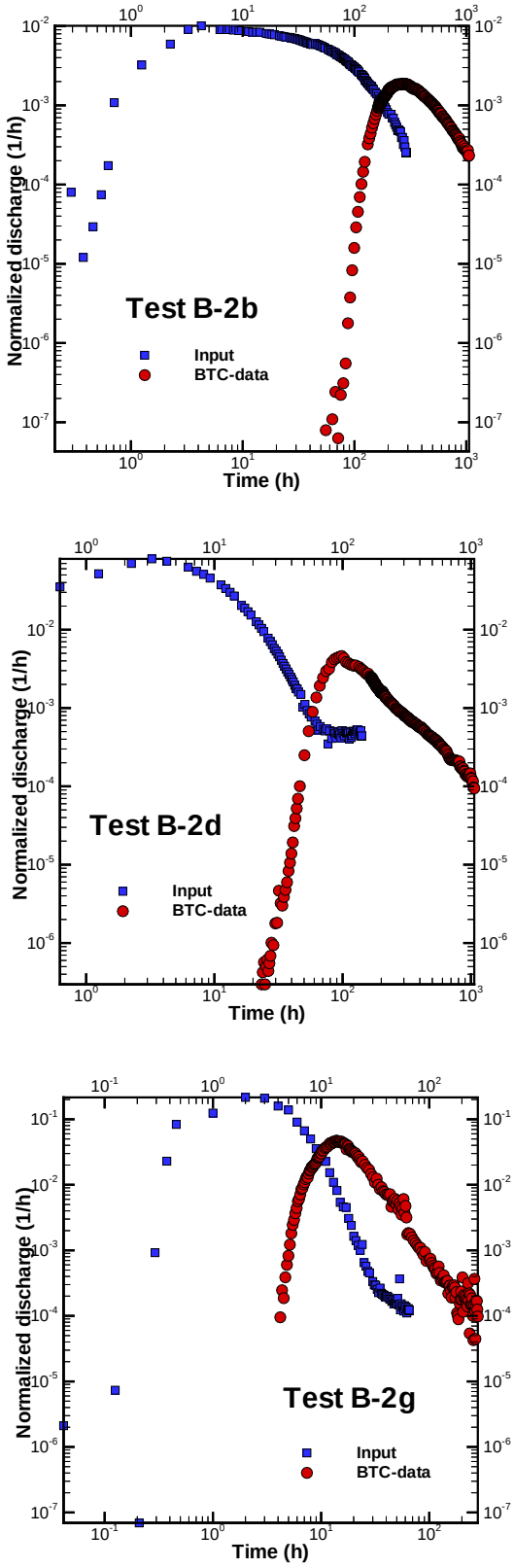

Figure 3.3: *Selected results of the TRUE Block Scale Phase B tracer pre-tests.*

Table 3.2: Phase C sorbing tracer tests configuration.

Test	Inj. rate [ml/min]	Pump rate [ml/min]	Inj. borehole	Pump borehole
C-1	45	2060	KI0025F03:P5	KI0023B:P6
C-2	10	2060	KI0025F03:P7	KI0023B:P6
C-3	1.0	2060	KI0025F02:P7	KI0023B:P6

3.2.1 Sorbing tracer tests C-1, C-2 and C-3

C-1 is a weak dipole test. Six tracers Br-82, Na-24, Ca-47, K-42, Rb-86 and Cs-134 were injected in KI0025F03:P5 with $Q = 45$ ml/min with pumping in KI0023B:P6 at $Q = 2060$ ml/min. C-2 is also a weak dipole test. The four tracers Re-186, Ca-47, Ba-131 and Cs-137 were injected in KI0025F03:P7 with $Q = 10$ ml/min with pumping in KI0023B:P6 at $Q = 2060$ ml/min. C-3 is a radially converging test. The five tracers HTO, Na-22, Sr-85, Rb-83 and Ba-133 were released in KI0025F02:P7 with pumping in KI0023B:P6 at $Q = 2060$ ml/min. The normalized injected and the resulting BTCs for Phase C tests are shown in Figure 3.4.

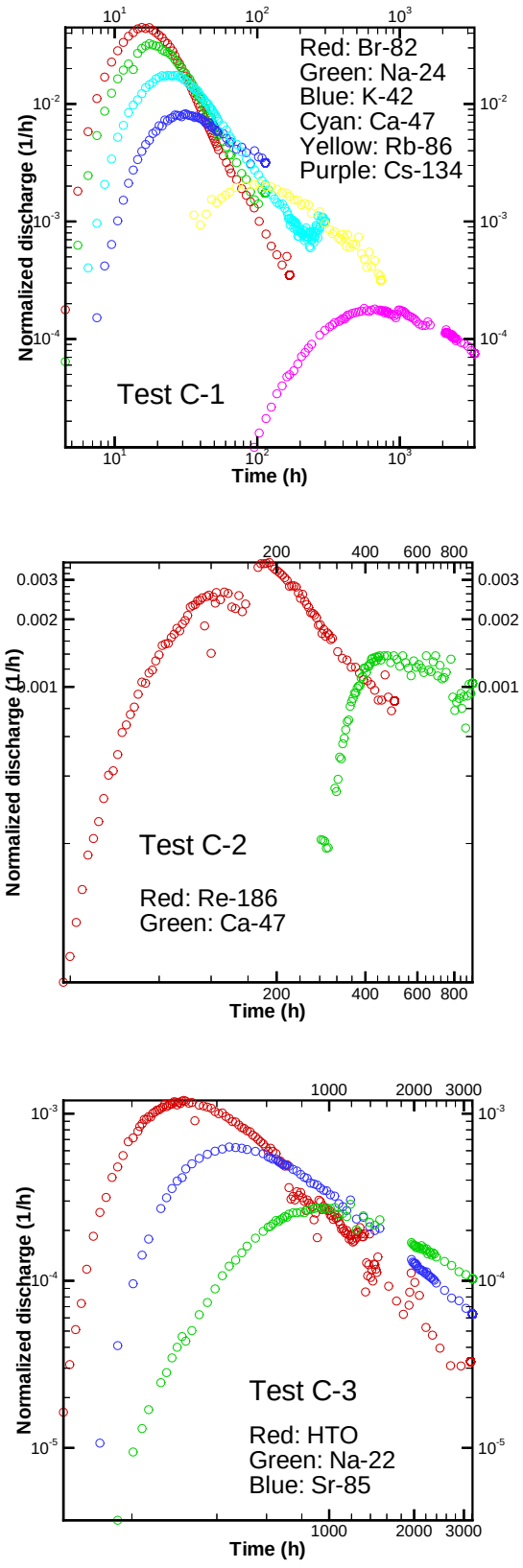

Figure 3.4: *Summary of all BTCs for Phase C tests (Andersson et al., 2001; Andersson et al., 2002a).*

Table 3.3: Injected mass and mass recovery for Phase C tests. "×" indicates tracers not detected at the time BTC data was delivered (Andersson et al., 2001).

Test C-1	Injected Mass	Recovery
	m_0	[%]
Tracer	[MBq]	
Br-82	138	111
Na-24	15.6	96
Ca-47	10.7	98.4
K-42	229	53
Rb-86	13.3	67
Cs-134	7.8	39.5

Test C-2	Injected Mass	Recovery
	m_0	[%]
Tracer	[MBq]	
Re-186	171	80.4
Ca-47	56.4	68.1
Ba-131	25.7	×
Cs-137	23.5	×

Test C-3	Injected Mass	Recovery
	m_0	[%]
Tracer	[MBq]	
HTO	243	73.1
Na-22	21.6	69.5
Sr-85	22	51.9
Ba-133	46	×
Rb-83	0.56	×

Chapter 4

Flow dependent parameters

Two parameters β and τ control advective transport and mass transfer processes, and relate the hydrodynamics to mass transfer processes (see Chapter 3). The flow field of the TRUE Block Scale site is identified as taking place through a fracture network (Andersson et al., 2002b). The fracture network consists of interpreted deterministic structures with heterogeneous properties (e.g., aperture). As tracers are released from the injection borehole into the fracture system, they move along a given flow path following different trajectories.

As mentioned above, the τ, β relationship is important for modelling retention. Both τ and β depend on the flow field. To obtain the necessary site-specific information for computing τ and β along trajectories, simulation results obtained by the JNC/Golder team were used. The JNC/Golder team provided the data necessary to generate τ and β values along individual trajectories. These data include all tracer trajectories with required properties (velocities and apertures). The linear relation between τ and β is assumed as given in Eq.(2.5), and the parameter k is obtained using linear regression.

4.1 JNC/Golder flow and transport simulations

The flow dependent parameters β and τ can be computed by solving the flow equation and calculating aperture and velocity along modelled trajectories. JNC/Golder has performed steady and transient flow modelling for the TRUE Block Scale project using a single porosity, constant fluid density channel network (CN) approach (Klise and Dershowitz, in prep.). The flow and advective transport calculations were obtained using FracMan/PAWorks software (JNC/Golder report, 2001).

The TRUE Block Scale structural model is implemented in the DFN/CN model as a nested model within the 500 m scale to comply with the boundary condition provided by the project. Numbered structures are modelled to the full 500 m scale. However the background fracturing is only modelled on a scale of 50 to 100 m, i.e., close to the discrete structures of interest. Thus detailed modelling was provided in the vicinity of structures #13, #20, #21 and #22.

The JNC/Golder channel network concept is an extension of the discrete fracture network (DFN) concept. Each fracture is treated as a discrete plane. The intersection between fractures defines ”traces” with a line element referred to as “fracture intersection

zone" (FIZ). Each fracture is subdivided into an equivalent number of conductive pipes. The traces are also modelled as pipes. The pipes are described geometrically by the nodal coordinates of the pipe ends, by the pipe width and by the pipe length. Pipe transport aperture is used for transport solutions, but is not considered for flow solutions.

The "pipe" is the finest flow element used in the PAWorks model. Pipes are discretized to a scale of approximately 5 m (the average distance between fracture intersections). Approximately 15000 pipes are used for the calculation. The flow equation is solved numerically using the Galerkin method.

4.2 Transport trajectories

In this section, the transport trajectories based on JNC/Golder data are presented. As tracer particles are released in the injection borehole, they are advected along different trajectories. Individual tracer particles either arrive at the pumping borehole, or are lost in between the injection and pumping boreholes. We are interested in the particles which arrive to the pumping borehole. The trajectories of these particles are referred to as transport trajectories, for which the τ and β distributions are calculated.

Figure 4.1 shows the transport trajectories for C-1 test based on JNC/Golder data from two different geometrical perspectives. The red, green and blue lines are three typical trajectories starting from the injection borehole and ending in the pumping borehole. Figure 4.1a indicates that the C-1 test field is essentially a planar structure. Figure 4.1b shows the trajectories when looking at the trajectories perpendicular to the planar structure although two identified structures are involved. Figure 4.1b indicates that the transport trajectories have quite different lengths and different directions within the plane structure (#20). What is also important is that for a given test these trajectories partly coincide. The average length of trajectories in the C-1 test is 55 m.

Figures 4.2 show transport trajectories for the C-2 and C-3 tests. Again the red, green and blue lines are three typical trajectories for each test. The average length of the trajectories in C-2 and C-3 tests are 74 m and 80 m, respectively.

4.3 β and τ calculation

Let N_1 denote the number of transport trajectories in test C-1, N_2 the number of transport trajectories in test C-2, and N_3 the number of transport trajectories in test C-3. In this evaluation, for C-1 test, we have total trajectories $N_1 = 97$, for C-2 test, $N_2 = 180$ and for C-3 test, $N_3 = 75$ trajectories. Every trajectory starts from the injection borehole and ends in the pumping borehole. Many trajectories partly coincide, and therefore are not independent. However, for the purpose of our calculation of β and τ, we treat them as independent and equally weighted trajectories for the evaluation of Phase C tests. Each trajectory consists of several rectangular segments (pipes), each segment has uniform properties (aperture, transmissivity, velocity, etc.). Different segments of the same trajectory have different properties.

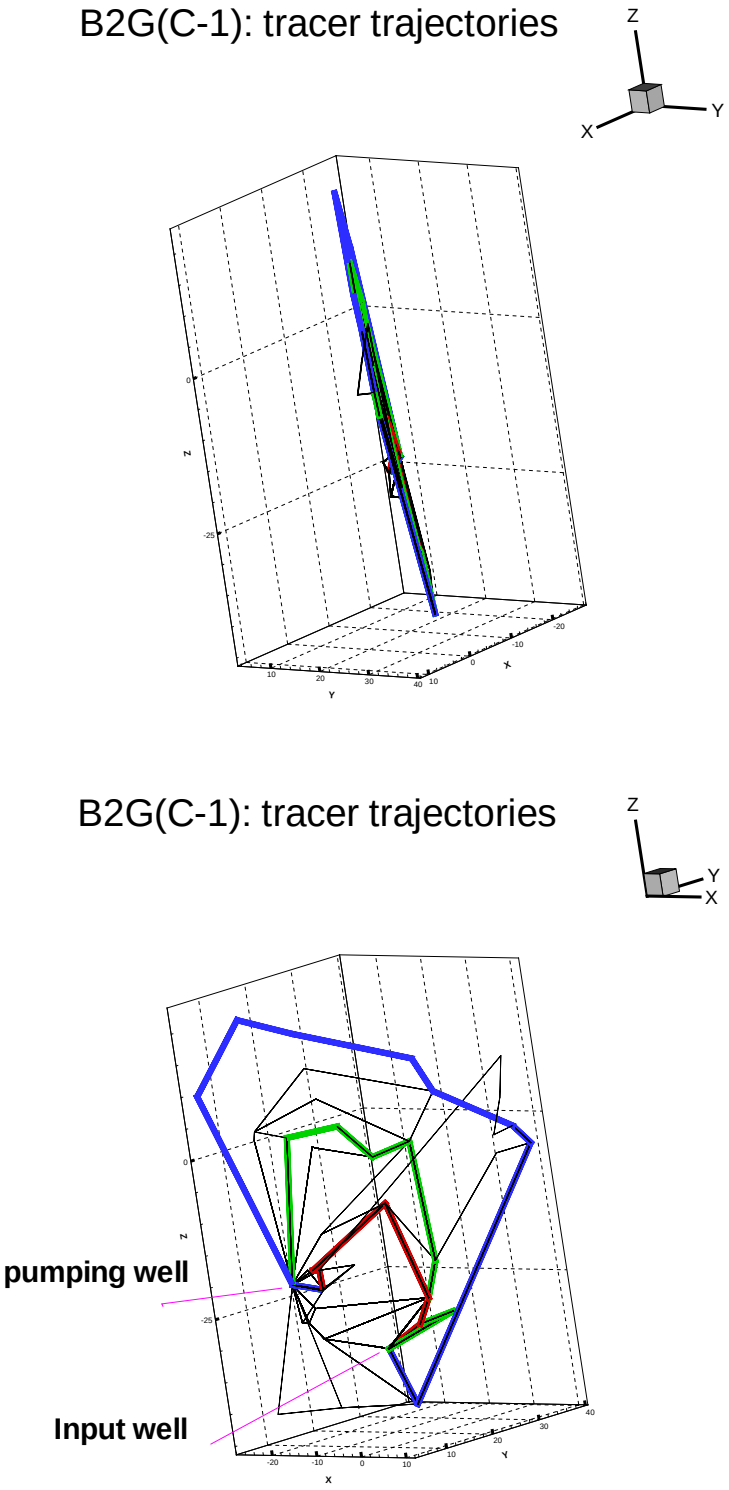

Figure 4.1: *Trajectories for B2G(C-1) test. (a) looking at the trajectories parallel to the planar structure, (b) looking at the trajectories perpendicular to the planar structure*

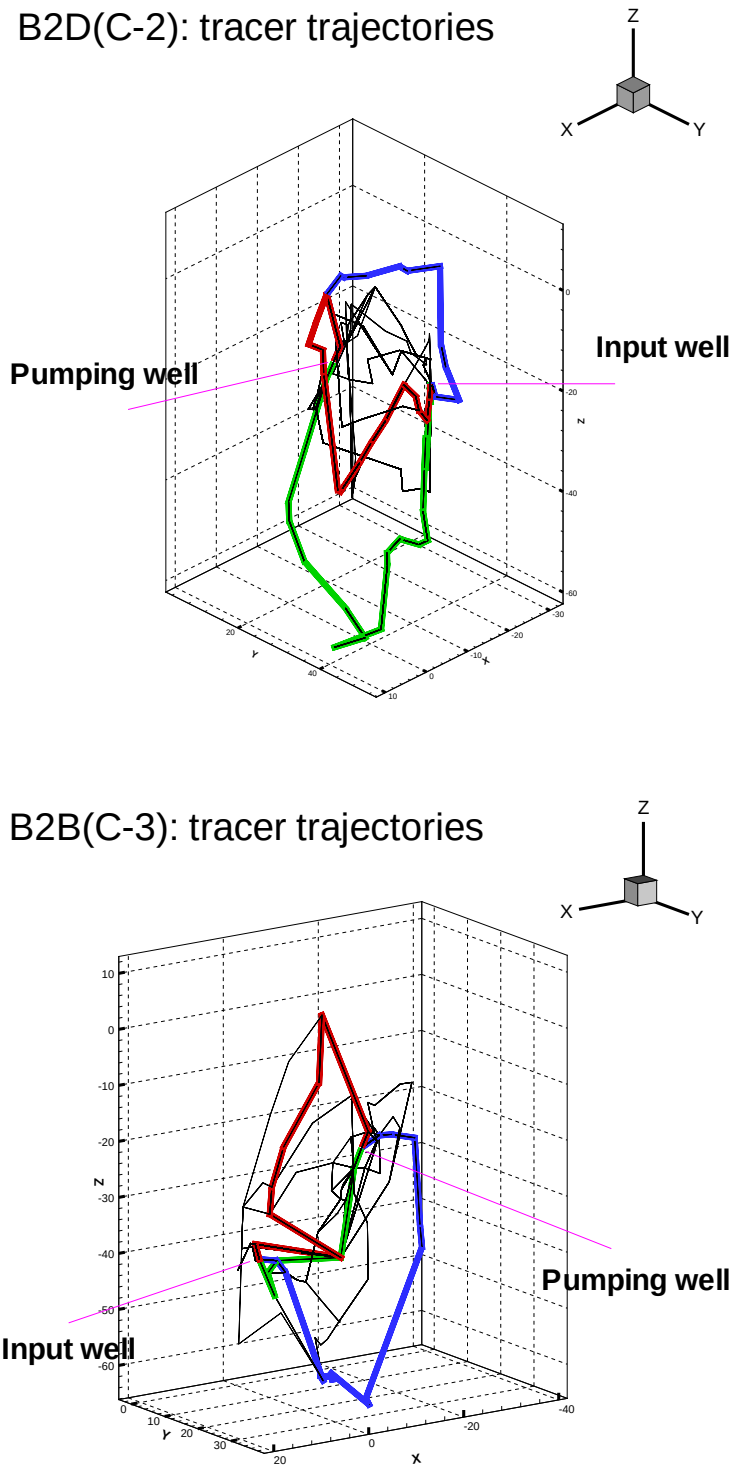

Figure 4.2: *Trajectories for B2D(C-2) and B2B(C-3) tests: (a) B2D(C-2) test, (b) B2B(C-3) test.*

The values of τ and β for the i-th trajectory are computed as:

$$\tau_i = \sum_{j=1}^{n_i} \tau_{ij} \qquad \beta_i = \sum_{j=1}^{n_i} \frac{\tau_{ij}}{b_{ij}} \tag{4.1}$$

where index "i" denotes the trajectories ($i = 1, 2, ..., N_l, l = 1, 2$ and 3), "j" denotes the segments ($j = 1, 2, ...n_i$). There are n_i segments in the i-th trajectory. τ_{ij} is the travel time in j-th segment of i-th trajectory. b_{ij} is the half aperture of j-th segment of i-th trajectory.

4.4 Linearization of β

We plot in Figure 4.3 the scattergram of τ and β for tests C-1, C-2 and C-3 respectively. Computation of β and τ is based on the results from N_1=97 trajectories for the C-1 test (Figure 4.3a), from $N_2 = 180$ trajectories for the C-2 test (Figure 4.3b), and from $N_3 = 75$ trajectories for the C-3 test (Figure 4.3c).

We wish to establish an approximate linear, deterministic relationship Eq. (2.5). In other words, we wish to estimate the value of the slope k based on DFN/CN (JNC/Golder) simulations.

From Figure 4.3a, we see that β and τ for C-1 tests are closely correlated, approximately linear. If we use $\beta = k\tau$, k is about 5000 1/m. For tests C-2 (Figure 4.3b) and C-3 (Figure 4.3c), β and τ are less correlated. Moreover, power law fittings in Figure 4.3b and Figure 4.3c suggest that the slope k should be larger than 5000 1/m.

Combining the results from C-1, C-2 and C-3 tests, we propose a common relationship $\beta = 6000\tau$, i.e., k=6000 1/m, as representative for the three tests (C-1, C-2 and C-3), based on DFN/CN (FracMan) simulations by JNC/Golder. We used the value $k = 6000$ 1/m in the predictions. Note however that we do NOT use $k = 6000$ 1/m (or any other value of k) as a constraint in the subsequent retention parameter estimation; in the evaluation, we consider k as an *unknown in-situ* parameter to be estimated.

4.5 Water residence time distribution

The water residence time distribution can be obtained either by numerical simulations or by direct calibration on the non-sorbing tracer BTCs. In this evaluation, the method of direct calibration on non-sorbing tracer BTCs is used.

The form of $g(\tau)$ is assumed as inverse-gaussian, i.e.,

$$g\left(\tau; x\right) = \left(\frac{\left\langle\tau\right\rangle^3}{2\pi\sigma_\tau^2\tau^3}\right)^{1/2} \exp\left[-\frac{\left\langle\tau\right\rangle}{2\tau}\left(\frac{\tau - \left\langle\tau\right\rangle}{\sigma_\tau}\right)^2\right] \tag{4.2}$$

where $\left\langle\tau\right\rangle$ and σ_τ^2 are the temporal moments (mean and variance of τ, respectively) at a given distance (in our case between the injection and pumping boreholes). Since a non-sorbing tracer is also subject to diffusive mass transfer, these effects have to be accounted

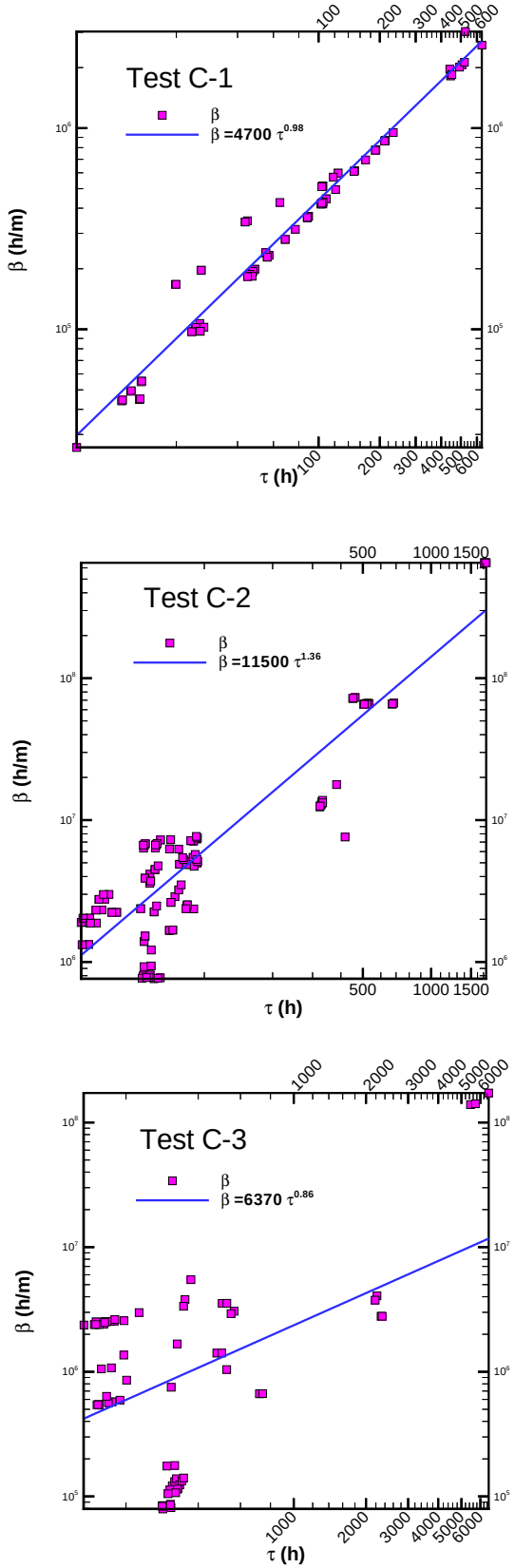

Figure 4.3: *τ-β scattergrams for C1, C2 and C3 tests. Red symbols are the simulated τ, β values, the blues lines are the power-law fits. (a) C-1 test, (b) C-2 test and (c) C-3 test*

for in the calibration of moments $\langle\tau\rangle$ and σ_τ^2. Thus $g(\tau)$ is convoluted with the experimental injection (input) function, as well as with γ Eq.(2.1) (with $K_d = K_a = 0$); the temporal moments and the *in-situ* values of ζ and ψ, Eq.(2.6) are calibrated in order to fit the experimental non-sorbing BTCs, as discussed in Chapter 6.

Chapter 5

Prediction results

The LaSAR approach has been used for performing predictions of Phase C sorbing tracer tests. The following mass transfer processes were accounted for: sorption on fracture surfaces determined by sorption coefficient K_a and diffusion controlled sorption in the rock "matrix" determined by the parameter group κ Eq. (2.4).

Two sets of predictions were made. The first set of predictions was based on modelling input data set for TRUE-1 (abbreviated as MIDS in Winberg et al. (2000)). The second set of predictions was based on estimated *in-situ* retention parameters for the TRUE-1 site (Cvetkovic et al., 2000; Winberg et al., 2000) . These predictions incorporated the parameter k in Eq.(2.5) as obtained from DFN/CN (JNC/Golder) simulations (Klise and Dershowitz, in prep.; see Chapter 4).

5.1 Prediction procedure

The predictions were performed in three steps

- Establishing the $\tau - \beta$ relationship based on DFN/CN simulation results.
- Determining $g(\tau)$ by deconvoluting BTCs from the relevant non-sorbing tracer tests B2g, B2d and B2b; the actual form of $g(\tau)$ was assumed to be inverse-Gaussian Eq. (4.2), and the first two water residence time moments were calibrated for each flow path.
- Predicting BTCs from C-1, C-2 and C-3 tests using $g(\tau)$ by accounting for mass transfer processes with parameters determined from MIDS data and *in-situ* parameters calibrated from TRUE-1 evaluation (Cvetkovic et al., 2000; Winberg et al., 2000).

5.2 Calibration

Based on results from the B2g test, and also combining the results from B2d and B2b tests, we estimated $k = 6000$ 1/m (see discussion in Chapter 4).

Table 5.1: Calibrated water residence time moments for B2g, B2d and B2b tests, based on MIDS data, and on estimated *in-situ* retention parameters for Feature A of the TRUE-1 site.

Test	$\langle\tau\rangle$ [h] MIDS	$\langle\tau\rangle$ [h] TRUE-1	σ_τ^2 [h^2] MIDS	σ_τ^2 [h^2] TRUE-1
B2g	20	12	180	40
B2d	150	65	5000	200
B2b	300	100	20000	300

Table 5.2: Summary of parameters for predicting Phase C test.

Tracer(s)	$K_a \times 10^5$ [m]	$\kappa \times 10^6$ [m/$\sqrt{\text{h}}$] MIDS	$\kappa \times 10^6$ [m/$\sqrt{\text{h}}$] TRUE-1
Br-82,Re-186,HTO	0	1.31	26.2
Na-22,Na-24	0.07	1.34	26.8
Ca-47	0.4	1.61	32.2
Sr-85	0.8	1.55	31
K-47	6	14	280
Ba-131,Ba-133	20	8.83	177
Rb-83,Rb-86	50	20	400
Cs-134,Cs-137	800	76	1520

The temporal moments of $g(\tau)$ were deconvoluted from the B2g, B2d and B2b tests for two sets of diffusion parameters: MIDS and estimated *in-situ* parameters for Feature A of the TRUE-1 site (Cvetkovic et al., 2000; Winberg et al., 2000). The calibrated moments are summarized in Table 5.1.

For both sets of predictions, K_a values from MIDS were used. For the first set of predictions, κ was determined based on MIDS values of θ, D and K_d (Winberg et al., 2000). For the second set of predictions, κ was determined using estimated *in-situ* values of θ, D and K_d from the TRUE-1 site (Cvetkovic et al., 2000; Table 1-2). K_a and κ values used in the predictions are summarized in Table 5.2. The difference in the two estimates stems from the difference in the porosity and diffusivity between MIDS and that estimated *in-situ*. Because MIDS values of porosity and diffusivity are considerably lower than *in-situ* estimates, the water residence time moments are larger for the MIDS case in order to "compensate" for weaker retention.

5.3 Summary of prediction results

The predicted water residence times for a given fraction of tracer recovery (all given in hours) for experimental input are summarized in Table 5.3. The predicted BTCs, along with the data and the best fit curves are given in Chapter 6, c.f.,Figures 6.1- 6.3.

Table 5.3: Summary of prediction results for the transport measures t_5, t_{50} and t_{95} for the C-1, C-2 and C-3 tests, using different input parameters. "Pred.#1" implies MIDS input data, and "Pred.#2" estimated/calibrated TRUE-1 *in-situ* data.

C-1	Tracer	Pred.#1	Pred.#2	Experimental data
t_5	Br-82	9.4	8.5	9.1
	Na-24	9.1	8.1	10.7
	Ca-47	9.2	8.8	14.7
	K-42	12.5	36.3	21.5
	Rb-86	30.6	77	66.4
	Cs-134	365.6	1072	528.1
t_{50}	Br-82	23.2	22.8	20.6
	Na-24	21.2	20.5	27.4
	Ca-47	20.8	23.6	45.9
	K-42	33.3	377	103
	Rb-86	82	779	404.9
	Cs-134	1089	11270	-
t_{95}	Br-82	67.2	157	49.2
	Na-24	45.5	145.6	106.9
	Ca-47	48.1	332.7	263.7
	K-42	182.8	-	-
	Rb-86	375.8	-	-
	Cs-134	5442	-	-

C-2	Tracer	Pred.#1	Pred.#2	Experimental data
t_5	Re-186	74.6	72.8	93.7
	Ca-47	75.9	80.8	375.4
	Ba-131	173	642	-
	Cs-137	4085	40136	-
t_{50}	Re-186	154	191	257.7
	Ca-47	157.4	241	729.6
	Ba-131	416.3	4872	-
	Cs-137	12143	355174	-
t_{95}	Re-186	319	6211	-
	Ca-47	338	9428	-
	Ba-131	4156	-	-
	Cs-137	-	-	-

Table 5.3 (cont.)

C-3	Tracer	Pred.#1	Pred.#2	Exper.data
t_5	HTO	175	154	226.4
	Na-22	172	154	335.6
	Sr-85	180	172	640.1
	Ba-133	398	1538	-
	Rb-83	786	6964	-
t_{50}	HTO	357	441	818.3
	Na-22	355	448	1451.3
	Sr-85	376	538	2958
	Ba-133	1002	11256	-
	Rb-83	2617	58257	-
t_{95}	HTO	765	14729	-
	Na-22	775	15327	-
	Sr-85	839	20066	-
	Ba-133	15460	-	-
	Rb-83	-	-	-

Chapter 6

Evaluation results with uniform retention parameters

We present the evaluation of the TRUE Block Scale tracer tests for each tracer separately. In this Chapter we will obtain the closest possible fit of the measured breakthrough curves (BTCs) to sorbing tracers of the TBS tests, with a minimum number of calibration parameters, using the LaSAR transport model presented in Chapter 2.

In test C-1, six tracers (Br-82, Na-24, K-42, Ca-47, Rb-86 and Cs-134) were injected and all of them were detected in the pumping borehole with variable mass recoveries. In test C-2, four tracers (Re-186, Ca-47, Ba-131 and Cs-137) were injected. The two sorbing tracers Ba-131 and Cs-137 have not been detected at the time the BTC data was provided. Hence, evaluation is performed only for Re-186 and Ca-47 in the C-2 tests. In test C-3, five tracers (HTO, Na-22, Sr-85, Rb-83 and Ba-133) were injected. For the same reason as in the C-2 test, the evaluation is carried out only for the tracers HTO, Na-22 and Sr-85 in the C-3 test.

6.1 Evaluation steps

The retention processes considered in this evaluation are surface sorption quantified by the parameter group ζ, and the diffusion/sorption on the matrix quantified by the parameter group ψ; both ζ and ψ are defined in Eq.(2.6). Our task here is to estimate the "effective" *in-situ* values of κ, K_a and k that most closely reproduce the measured BTCs using the model Eq.(2.7). As ψ is a parameter group, ψ can be calibrated as a single parameter; similarly, ζ is calibrated as a single parameter.

The evaluation procedure consists of two *iterative* steps (Chapter 2):

1. Water residence time distribution of Eq.$g(\tau)$ (4.2) is "deconvoluted" from the non-sorbing tracer BTC, accounting for diffusion into the matrix, whereby the first two moments $\langle\tau\rangle$ and σ_τ^2 are calibrated.

2. Using $g(\tau)$, BTCs of sorbing tracers are modelled accounting for retention processes; *in-situ* values of ψ and ζ are calibrated such that a best fit with the measured

Table 6.1: Calibrated parameters for TRUE Block Scale Phase C tests. "×" indicates that a tracer has not been detected in the pumping borehole at the time when data was delivered.

Tracer	$\psi = k\kappa$ $[1/\sqrt{\mathrm{h}}]$			$\zeta = kK_a$ [-]		
	C-1	C-2	C-3	C-1	C-2	C-3
Br-82	0.03942	-	-	0	-	-
Re-186	-	0.23652	-	-	0	-
HTO	-	-	0.11826	-	-	0
Na-22	-	-	0.18492	-	-	0.42
Na-24	0.1206	-	-	0.0042	-	-
Ca-47	0.2898	0.7728	-	0.24	0.24	-
Sr-85	-	-	0.3534	-	-	0.48
K-42	0.504	-	-	0.432	-	-
Ba-131	-	×	-	-	×	-
Ba.133		–	×	-	-	×
Rb-83	-	-	×	-	-	×
Rb-86	1.44	-	-	3	-	-
Cs-134	5.0292	-	-	9	-	-
Cs-137	-	×	-	-	×	-

BTCs is obtained.

Once ζ and ψ are calibrated, and the water residence distribution, g is calibrated, we shall infer possible ranges of individual retention parameters. Note that the above two steps are iterative in the sense that $g(\tau)$ and the non-sorbing ψ are calibrated *simultaneously* with the sorbing tracers such that the best fit for *all* tracers of a given tests is achieved. Hence the fact that we have a set of tracers with *strongly* varying sorption properties which, for a given flow path, are subject to identical advection-dispersion and diffusive mass transfer, is the most important *constraint* for the evaluation.

6.2 Calibration

In this section, we present the calibrated *in-situ* values of the parameter groups $\psi = k\,\kappa$ and $\zeta = kK_a$, for each tracer and each test. The calibrated ζ and ψ are summarized in Table 6.1. The calibrated temporal moments are summarized in Table 6.2.

In Figure 6.1, calibrated curves for test C-1 are plotted. Several curves are plotted in each figure, the input (injection) function is denoted by "Input", the BTC data denoted by "BTC data", and the best fit curve denoted by "Evaluation". In addition, we plot two prediction curves: "Prediction 1" which was obtained using MIDS data, and "Prediction 2" which was obtained using estimated retention *in-situ* data for Feature A of the TRUE-1

Table 6.2: Calibrated first two moments of the water residence time $g(\tau)$. Note that the values differ from those in Table 5.1 since here the calibration was conditioned on the actual measured BTCs thus indirectly accounting for *in-situ* retention properties, whereas in Table 5.1 either MIDS or TRUE Feature A retention properties were assumed.

Test	$\langle\tau\rangle$ [h]	σ_τ^2 [h^2]
C-1	15	50
C-2	140	4900
C-3	250	10000

tests (see Chapter 5). For all tracers, the initial parts up to the peak of the BTC is closely fitted. For the strongly sorbing tracers, i.e., Cs and Rb, the whole BTC is closely modelled. For the weakly sorbing tracers, some deviation in the tail part is evident.

Figure 6.2 shows the evaluation curves for the test C-2. Only two of the four injected tracers were detected. Our evaluation curve slightly deviates in the initial part, in the peak as well as in the tail part. Figure 6.3 shows the evaluation and prediction curves for the C-3 test. Only three tracers are detected among the five injected. The first part and the peaks are fairly well reproduced. Again, some deviation in the tail part is apparent.

6.3 Range of parameters for a homogeneous matrix

We have calibrated the parameter group ψ as summarized in Table 6.1. We wish to estimate k and κ separately since they are related to entirely different retention processes/effects. Moreover, we would like to estimate the contribution to κ, from physical properties (e.g., variable porosity and/or diffusivity) and chemical processes (variable sorption capacity). However, k and κ cannot be determined separately without additional constraints (or assumptions) (see discussion in Chapter 2).

To facilitate our further discussion, we first write κ as

$$\kappa = \theta \sqrt{D\,R_m} = \theta \left[D \left(1 + \frac{K_d^m\,\rho}{\theta} \right) \right]^{1/2} = \left[D_e \left(\theta + K_d^m\,\rho \right) \right]^{1/2} \tag{6.1}$$

$$= \left[D_w\,F \left(\theta + K_d^m\,\rho \right) \right]^{1/2} \tag{6.2}$$

where $F \equiv D_e/D_w = D\theta/D_w$ is the "formation factor" which accounts for the tortuosity and connectivity of the matrix pore space, D_w is the diffusivity in water, D is "pore diffusivity" and D_e is the "effective diffusivity" with $D_e = D\theta$. For a small porosity, $1-\theta \approx 1$. The values of D_w are given in Table 6.3 for all tracers.

From the expression (2.4) for κ, we write

$$\psi_{(\mathrm{TR})} \equiv k\kappa_{(\mathrm{TR})} = k \left[D_{w(\mathrm{TR})}\,F \left(\theta + \rho\,K_{d(\mathrm{TR})}^m \right) \right]^{1/2} \tag{6.3}$$

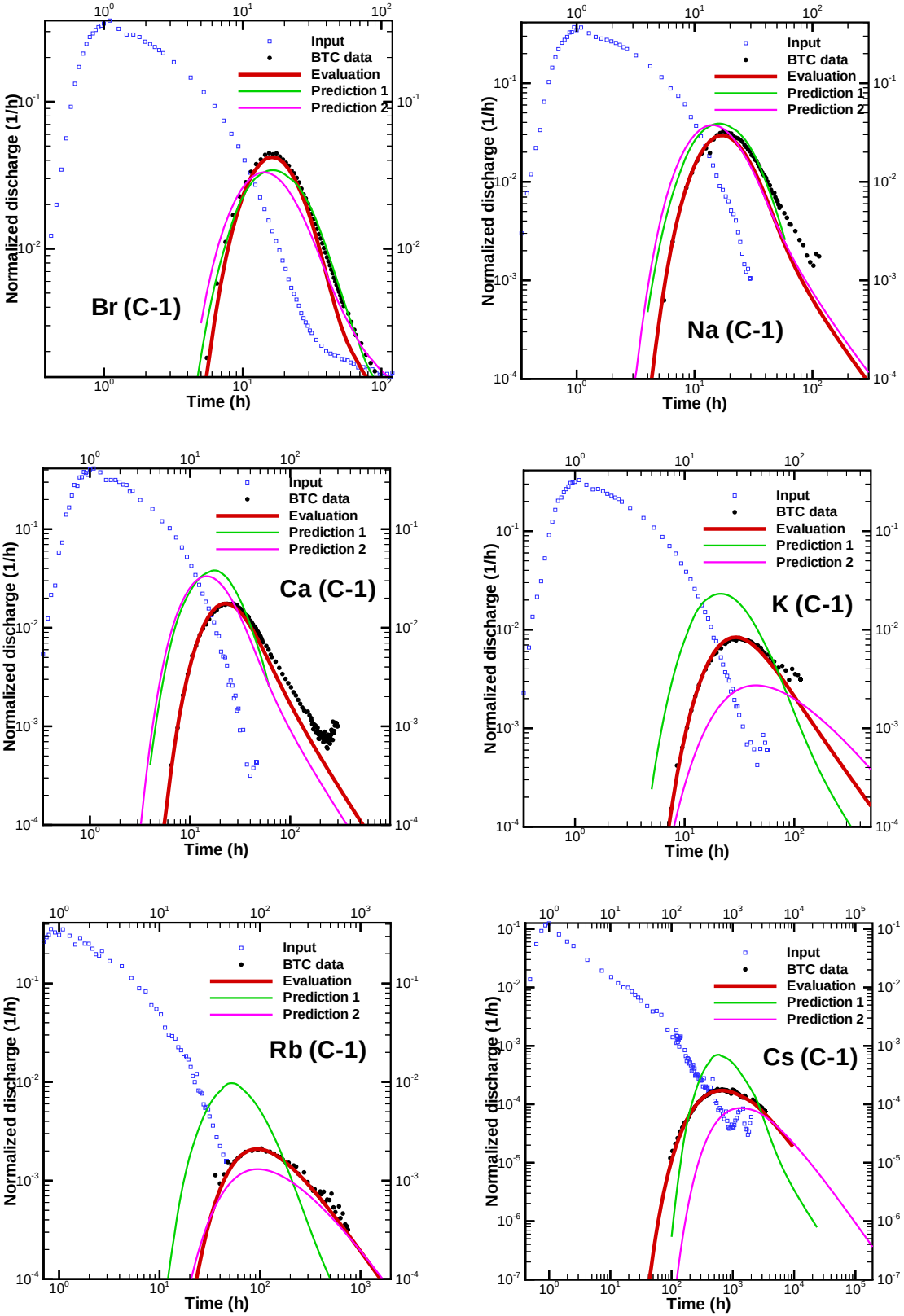

Figure 6.1: *Evaluation and prediction curves for test C-1, "Input" is the injection function, "BTC data" is the experimental data, "Evaluation" is the best fitted (calibrated) curve, "Prediction 1" is the predicted BTC using MIDS data, and "Prediction 2" is the predicted BTC using TRUE-1 (Feature A) estimated in-situ retention parameters.*

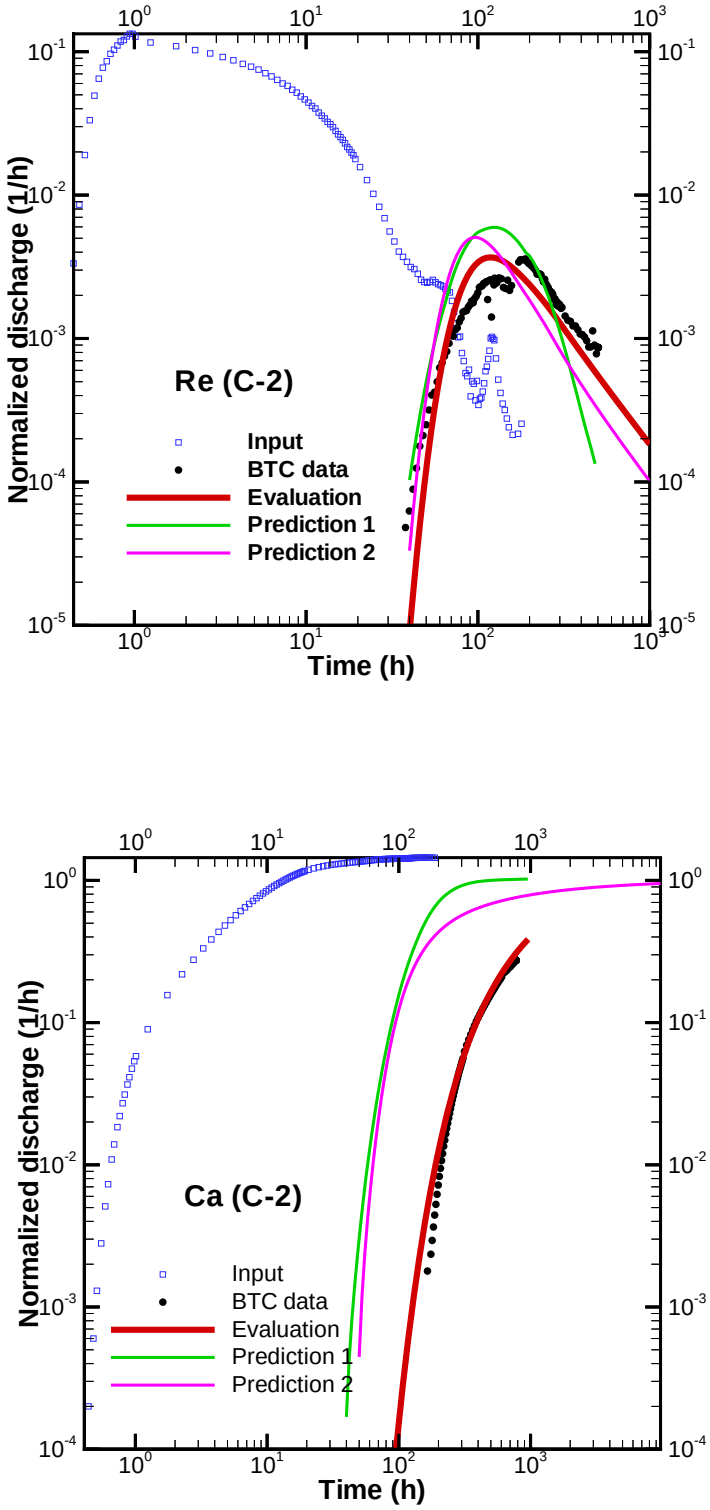

Figure 6.2: *Evaluation and prediction curves for test C-2, "Input" is the injection function, "BTC data" is the experimental data, "Evaluation" is the best fitted (calibrated) curve, "Prediction 1" is the predicted BTC using MIDS data, and "Prediction 2" is the predicted BTC using TRUE-1 (Feature A) estimated in-situ retention parameters.*

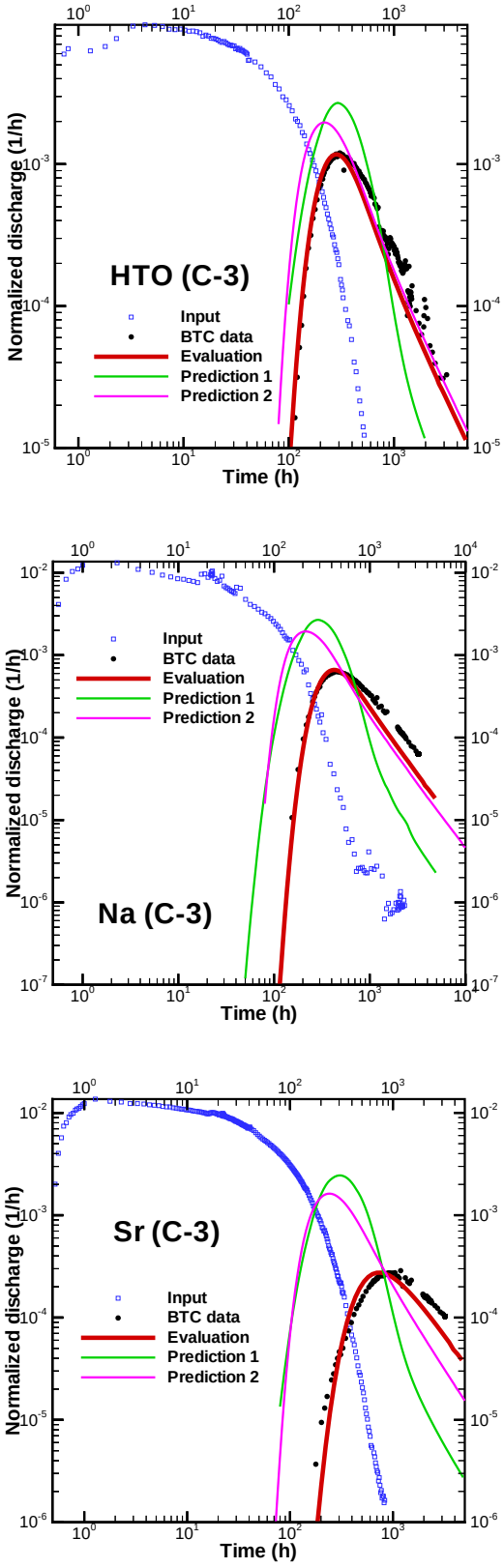

Figure 6.3: *Evaluation and prediction curves for test C-3, "Input" is the injection function, "BTC data" is the experimental data, "Evaluation" is the best fitted (calibrated) curve, "Prediction 1" is the predicted BTC using MIDS data, and "Prediction 2" is the predicted BTC using TRUE-1 (Feature A) estimated in-situ retention parameters.*

Table 6.3: Tracer diffusivity in water, D_w, at temperature relevant for TRUE Block Scale tests, D_w is the calculated water diffusivity at infinite dilution (Gray, 1972).

Tracer(s)	$D_w \times 10^6$ [m^2h^{-1}]
Br,Re,HTO	8.4
Na	4.8
Ca	2.8
Sr	2.8
K	7.2
Ba	3.0
Rb	7.3
Cs	7.3

where k, F, θ and K_d are the *in-situ* "effective" values of the respective parameters, and ψ is given in Table 6.1. The subscript "TR" emphasizes the dependence of a parameter on the tracer (For test C-1, TR = Br, Na, Ca, K, Rb and Cs). Note that $K_{d(\mathrm{TR})}$ is strongly dependent on the tracer and on the flow path, since effective sorption properties (which strongly depend, for instance, on mineralogy), may vary between flow paths. The parameters $k, F$and θ represent physical properties which are indepedent of the tracer but generally depend on the particular flow path of the test.

We now formulate the problem as follows: Given the calibrated *in-situ* parameter groups ψ and ζ (Table 6.1), can we estimate the *in-situ* values of k, F and θ for each test configuration, and $K_{d(\mathrm{TR})}$ for each tracer and test configuration?

We have three unknown physical parameters (k, F and θ) and 5 unknown sorption parameters ($K_{d(\mathrm{TR})}$) for C-1 test since $K_{d(\mathrm{Br})} = K_{d(\mathrm{Re})} = K_{d(\mathrm{HTO})} = 0$. Equation (6.3) can be written for 6 tracers in C-1 tests, hence we have 6 equations. To close the equation system (for test C-1) two additional constraints are required (see discussion in Chapter 2).

In want of a more comprehensive data set for the *in-situ* formation factor, and rather than arbitrarily assign a values, we shall introduce a new constraint as an empirical relation referred to as "Archie's law" which relates the *in-situ* porosity θ and the *in-situ* formation factor F as (Clennell, 1997):

$$F = \theta^m \tag{6.4}$$

With (6.4), we have only one independent (arbitrary) parameter in the six equations (6.3).

We choose *in-situ* porosity θ as the *arbitrary*, (effective) parameter. The exponential m in (6.4) is assumed to take two values: 1.3 and 1.6, which are considered as realistic bounds. We then compute all other parameters over a plausible range of θ values, for the three test configurations. The results are summarized in Tables 6.4-6.6. Different columns in Tables 6.4-6.6 quantify different processes/effects. The first and second columns are physical/retention properties (porosity, formation factor and parameter k). The last column are sorption coefficients that quantify mineralogical/geochemical (water/rock)/structural properties affecting sorption.

The steps in computing the values of Tables 6.4- 6.6 are as follows. First, for a given θ we compute F using (6.4). Then from (6.3) for the conservative tracer or Br (test C-1) we compute k as

$$k = \frac{\psi_{(\mathrm{TR})}}{(D_{w(\mathrm{TR})} F\,\theta)^{1/2}} \tag{6.5}$$

where the calibrated *in-situ* values of ψ for tests C-1, C-2 and C-3 and respective tracers, are given in Table 6.1. The diffusivity D_w is given in Table 6.3. The remaining 5 equations (6.3) are then used to compute K_d for Na, Ca, K, Rb and Cs as

$$K_{d(\mathrm{TR})} = \frac{1}{\rho}\left[\frac{\left(\psi_{(\mathrm{Br})}\right)^2}{k^2\, D_{w(\mathrm{TR})} F} - \theta\right] \tag{6.6}$$

where ρ is the density of the rock matrix.

All the parameter combinations given in Tables 6.4- 6.6 are in principle possible, and all would provide a close match between the measured and modelled BTCs, as discussed in the next section. However only a few of these may be considered as realistic combinations.

6.4 Alternative parameter estimation

The key difficulty with the "effective" parameter estimates in Tables 6.4- 6.6 is that the first step (e.g., estimating the slope k for test C-1 from Br BTC using Eq.(6.5)) is uncertain, since the retention effect on Br is relatively small. Thus, the estimate of k and the following estimates of K_d for sorbing tracers are also uncertain.

In particular, the calibrated parameter group values of Table 6.1 are most critical for retention parameter estimates. However, we see a two-order of magnitude difference between the value for Br and Cs, for instance in the C-1 tests. This implies that the reliability of the calibrated values of Table 6.1 increases with the sorptivity of the tracer: It is least reliable for Br and most reliable (or "robust") for Cs. In this sense, our estimates of Table 6.4-6.6 depend on the (uncertain) value of k for Br.

Of all retention parameters, k is most uncertain since no independent experimental information is available, apart from numerical simulations. By comparison, for K_d there are batch test data, with different fractions and durations (Byegård et al., 1998); thus *in-situ* K_d may be considered as a less uncertain parameter than *in-situ* k. In the following, we shall take advantage of two facts: First that the calibrated values of Table 6.1 are more robust for the sorbing tracers, and second that we may have some idea about the *in-situ* K_d based on the laboratory data base.

Consider the equation for sorbing tracers Eq.(2.4). From this equation we write

$$k = \left\{\frac{\psi^2_{(\mathrm{Br})}}{K_d}\right\}^{1/2}\left(\frac{1}{\rho D_w F}\right)^{1/2} = \left\{\frac{\psi^2_{(\mathrm{TR})}}{\eta\, K_d^{\mathrm{lab}}}\right\}^{1/2}\left(\frac{1}{\rho D_w \theta^m}\right)^{1/2} \tag{6.7}$$

Table 6.4: Estimation tables of effective parameters for C-1 tests. The asterix denotes most probable values.

C-1 ($m = 1.3$) $\theta(\%)$	$F \times 10^3$ [-]	k [1/m]	K_d [m^3/kg] Na-24	K_d [m^3/kg] Ca-47	K_d [m^3/kg] K-42	K_d [m^3/kg] Rb-86	K_d [m^3/kg] Cs-134
0.1	0.1259	37813	0.61E-05	0.60E-04	0.72E-04	0.58E-03	0.73E-02
0.4	0.7633	7678	0.24E-04	0.24E-03	0.29E-03	0.23E-02	0.29E-01
*0.8	*1.8794	*3460	*0.49E-04	*0.48E-03	*0.58E-03	*0.46E-02	*0.58E-01
1.2	3.1837	2171	0.73E-04	0.72E-03	0.87E-03	0.69E-02	0.87E-01
1.6	4.6276	1559	0.98E-04	0.96E-03	0.12E-02	0.92E-02	0.12E+00
2.0	6.1850	1206	0.12E-03	0.12E-02	0.14E-02	0.12E-01	0.15E+00
2.4	7.8393	978	0.15E-03	0.14E-02	0.17E-02	0.14E-01	0.17E+00
2.8	9.5787	819	0.17E-03	0.17E-02	0.20E-02	0.16E-01	0.20E+00

C-1 ($m = 1.6$) $\theta(\%)$	$F \times 10^3$ [-]	k [1/m]	K_d [m^3/kg] Na-24	K_d [m^3/kg] Ca-47	K_d [m^3/kg] K-42	K_d [m^3/kg] Rb-86	K_d [m^3/kg] Cs-134
0.1	0.0158	106570	0.61E-05	0.60E-04	0.72E-04	0.58E-03	0.73E-02
0.4	0.1456	17577	0.24E-04	0.24E-03	0.29E-03	0.23E-02	0.29E-01
0.8	0.4415	7139	0.49E-04	0.48E-03	0.58E-03	0.46E-02	0.58E-01
1.2	0.8447	4214	0.73E-04	0.72E-03	0.87E-03	0.69E-02	0.87E-01
1.6	1.3384	2899	0.98E-04	0.96E-03	0.12E-02	0.92E-02	0.12E+00
2.0	1.9127	2169	0.12E-03	0.12E-02	0.14E-02	0.12E-01	0.15E+00
2.4	2.5606	1711	0.15E-03	0.14E-02	0.17E-02	0.14E-01	0.17E+00
2.8	3.2768	1401	0.17E-03	0.17E-02	0.20E-02	0.16E-01	0.20E+00

Table 6.5: Estimation tables of effective parameters for C-2 tests. The asterix denotes most probable values.

C-2 ($m = 1.3$) $\theta(\%)$	$F \times 10^3$ [-]	k [1/m]	K_d [m^3/kg] Ca-47
0.1	0.1259	228000	1.15E-05
0.4	0.7633	46200	4.6E-05
0.8	1.8794	21000	9.21E-05
1.2	3.1837	13200	1.38E-04
1.6	4.6276	9600	1.84E-04
2.0	6.1850	7200	2.3E-04
2.4	7.8393	6000	2.76E-04
*2.8	*9.5787	*4920	*3.22E-04

C-2 ($m = 1.6$) $\theta(\%)$	$F \times 10^3$ [-]	k [1/m]	K_d [m^3/kg] Ca-47
0.1	0.0158	642000	1.15E-05
0.4	0.1456	108000	4.6E-05
0.8	0.4415	42600	9.21E-05
1.2	0.8447	25200	1.38E-04
1.6	1.3384	17400	1.84E-04
2.0	1.9127	13200	2.3E-04
2.4	2.5606	10200	2.76E-04
2.8	3.2768	8400	3.22E-04

Table 6.6: Estimation tables of effective parameters for C-3 tests. The asterix denotes most probable values.

C-3 ($m = 1.3$) $\theta(\%)$	$F \times 10^3$ [-]	k [1/m]	K_d [m^3/kg] Na-22	K_d [m^3/kg] Sr-85
0.1	0.1259	114000	1.32E-06	9.55E-05
0.4	0.7633	22800	5.29E-06	3.82E-05
0.8	1.8794	10200	1.06E-05	7.64E-05
1.2	3.1837	6600	1.59E-05	1.15E-04
1.6	4.6276	4680	2.12E-05	1.53E-04
*2.0	*6.1850	*3600	*2.65E-05	*1.91E-04
2.4	7.8393	2940	3.18E-05	2.29E-04
2.8	9.5787	2460	3.71E-05	2.67E-04

C-3 ($m = 1.6$) $\theta(\%)$	$F \times 10^3$ [-]	k [1/m]	K_d [m^3/kg] Na-22	K_d [m^3/kg] Sr-85
0.1	0.0158	318000	1.32E-06	9.55E-05
0.4	0.146	52800	5.29E-06	3.82E-05
0.8	0.442	21600	1.06E-05	7.64E-05
1.2	0.845	12600	1.59E-05	1.15E-04
1.6	1.34	8700	2.12E-05	1.53E-04
2.0	1.91	6600	2.65E-05	1.91E-04
2.4	2.56	5160	3.18E-05	2.29E-04
2.8	3.28	4200	3.71E-05	2.67E-04

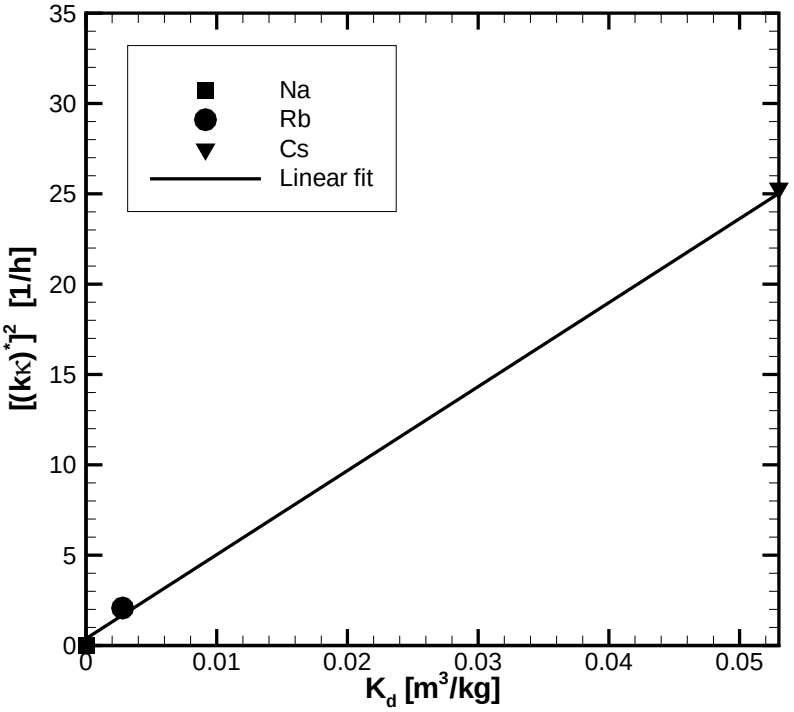

Figure 6.4: *Determination of the slope $[\psi_{(\mathrm{TR})}]^2/K_d^{\mathrm{lab}}$ using laboratory and tracer tests data for Na, Rb and Cs from test C-1; the slope is 465 m^3/(kg h). K_d laboratory values were obtained from batch tests on 1-2 mm fractions.*

In Eq.(6.7) we assumed that the *in-situ* sorption coefficient for all sorbing tracers scales linearly with a factor η, i.e., $K_d = \eta K_d^{\mathrm{lab}}$, where K_d^{lab} is the laboratory sorption coefficient chosen from the available data base (for a given type of test, size, fraction, duration, etc). We have also assumed Archie's law applicable in the above equation. If we can establish the slope $\psi_{\mathrm{TR}}^2/K_d^{\mathrm{lab}}$ by combining field and laboratory data, then for given θ and m we can compute k, if η is given.

In Figure 6.4 we determine the slope $\psi_{\mathrm{TR}}^2/K_d^{\mathrm{lab}}$ using three tracers of C-1 tests: Na, Rb and Cs; we get $\psi_{\mathrm{TR}}^2/K_d^{\mathrm{lab}} = 465$ m^3/(kg h). The K_d^{lab} values are taken from the 1-2 mm batch tests on generic Äspö material (Byegård et al., 1998), and ψ_{TR} from Table 6.1.

The expression for k is then

$$k = \frac{456}{\sqrt{\eta}}\,\theta^{-m/2}\,\frac{1}{(\rho D_w)^{1/2}} = \frac{153}{\sqrt{\eta}}\,\theta^{-m/2} \tag{6.8}$$

If we consider K_d obtained from batch tests on 1-2 mm fractions to be representative of effective *in-situ* K_d, then $\eta = 1$. In such a case, we can use Eq.(6.8) to estimate k. The results are given in Table 6.5 for two values of m, and compared for the same values of m with k as summarized in Table 6.7. We see that although the two estimates of k differ, the difference is within a factor 2.

Table 6.7: Comparison of k as obtained from Eq. (6.8) and Table 6.4, for different porosity θ and Archie's exponent m.

θ	k [1/m] $m = 1.3$ Eq. (6.8)	k [1/m] $m = 1.6$ Eq. (6.8)	k [1/m] $m = 1.3$ (Table 6.4a)	k [1/m] $m = 1.6$ (Table 6.4b)
0.4	5538	12678	7678	17577
0.8	3529	7281	3460	7139
1.2	2712	5264	2171	4214
1.6	2249	4182	1559	2899
2.0	1945	3498	1206	2169
2.4	1728	3024	978	1711
2.8	1563	2673	819	1401

Chapter 7

Retention heterogeneity

There is experimental evidence that the matrix porosity varies longitudinally (i.e., in the x, y-plane, as tracer particles move along the flow path), as well as depth-wise (i.e., in the z-direction, as the particles diffuse into the rock matrix). There are different physical and chemical reasons for spatial variability of retention properties. Within a given site on 10-100 m scale, we will generally encounter different rock types with different mineralogies and histories. Different history includes the formation of fractures, which implies that conducting fractures will be of different type. Moreover, different history may imply exposure to different chemical conditions by different fractures which can also results in the variability of retention properties (e.g., due to variations in mineralogy). For our current analysis, the significant fact is that we encounter spatial variations in the retention properties, irrespective of the origin.

In this Chapter, we shall illustrate potential effects of heterogeneity, and derive expressions for "effective" porosity.

7.1 Depth-dependent variability

There is evidence that porosity (when averaged over a core cross-sectional area) varies with depth, from the fracture surface toward the intact rock (Byegård et al., 2001; Kelokaski et al., 2001). Different cores exhibit different porosity profiles, however a consistent depth-wise decreasing trend is observed in most of the sampled cores.

To study potential effects of depth-dependent variability in porosity, we approximate this variability by an exponential function (Figure 7.1):

$$\theta = \theta_{\rm un} + (\theta_{\rm al} - \theta_{\rm un})\, \exp(-a\, z) \tag{7.1}$$

where $\theta_{\rm al}$ is the porosity at the fracture-matrix interface (i.e., for $z = 0$), and $\theta_{\rm un}$ is the porosity of the unaltered matrix away from the altered rim zone. The parameter a quantifies the extent of the altered rim zone.

Given the above porosity profile, we wish to quantify the penetration of different tracers in the matrix. The penetration profile will depend on the retention properties (formation factor F and K_d, if the tracer is sorbing), and on the boundary conditions in the fracture,

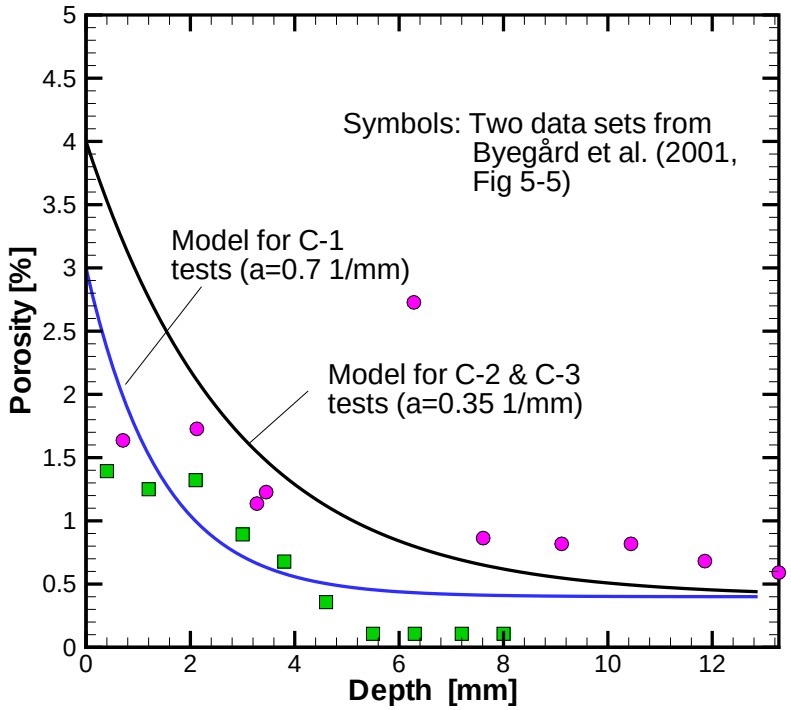

Figure 7.1: *Depth-wise trend in porosity variability; two data sets are shown from Byegård et al. (2001), together with exponential models for flow path I (C-1 tests), flow path II (C-2 tests) and flow path III (C-3 tests).*

i.e., concentration vs time. The governing equation for the concentration profile in the matrix is

$$\frac{\partial C}{\partial t} = \frac{\partial}{\partial z}\,\frac{D}{R}\left(\frac{\partial C}{\partial z}\right) \tag{7.2}$$

The boundary condition is specified as $C(0,t)$ which is the tracer concentration in the fracture. The pore diffusivity D is related to porosity based on Archie's law as

$$D = \frac{D_e}{\theta} = D_w\,\frac{F}{\theta} = D_w\,\frac{\theta^m}{\theta} = D_w\,\theta^{m-1} \tag{7.3}$$

The retardation factor in the matrix is related to porosity as

$$R = 1 + \frac{\rho K_d}{\theta} \tag{7.4}$$

Thus both D and R are depth-dependent. Whereas D is dependent only on porosity (through Archie's law), R is dependent both on porosity and K_d. Information on how K_d may vary with depth z is lacking. Evaluation of TRUE-1 tracer test data indicates that K_d is larger in the rim zone compared to the intact rock, which would imply conceptually a decreasing trend from the fracture surface into the rock. Since porosity also decreases with depth, this may result in their ratio (and hence R) as varying comparatively little with z. We shall therefore simplify the calculations of the concentration profile and assume R constant.

Furthermore, microfissures are presumably better connected close to the fracture surface in the altered rock compared to the intact rock deeper in the matrix. This would imply that the exponent m in the Archie's law (6.4) is depth-dependent, i.e., $m(z)$. Since data on m as a function of depth are not available, we propose a model for m in analogy to the model for porosity, namely

$$m(z) = m_{\rm un} + (m_{\rm al} - m_{\rm un})\,\exp(-a\,z) \tag{7.5}$$

where $m_{\rm un}$ is the value for the intact (unaltered) rock, and $m_{\rm al}$ is the value applicable at the transition from the fracture to the rim zone (matrix).

Ideally, $m = 1$ in the case where the rim zone consists of parallel microfissures with zero tortuosity and perfect connectivity (Clennell, 1997). We anticipate that in the first few tenths of a millimeter, from the fracture into the altered rim zone, the connectivity will be relatively high and tortuosity low, hence m will be at its minimum $m_{\rm al} < 1$. As we proceed deeper into the rim zone, the connectivity should decrease and tortuosity increase, whereby m increases; in the unaltered rock, m is anticipated to have a maximum value, in Eq.(7.5) denoted as $m_{\rm un}$. For illustration purposes, we shall assume $m_{\rm un} = 1.8$, which is consistent with MIDS data, and the lower bound (applicable for the rim zone in the very vicinity of the fractures, say over a few tenths of a millimeter), as $m_{\rm al} = 1.3$. We shall assume the transition parameter a to be identical for the porosity, and for m. Note that it would be difficult in practice to directly measure parameters $m_{\rm al}$ and a, although it is in principle possible.

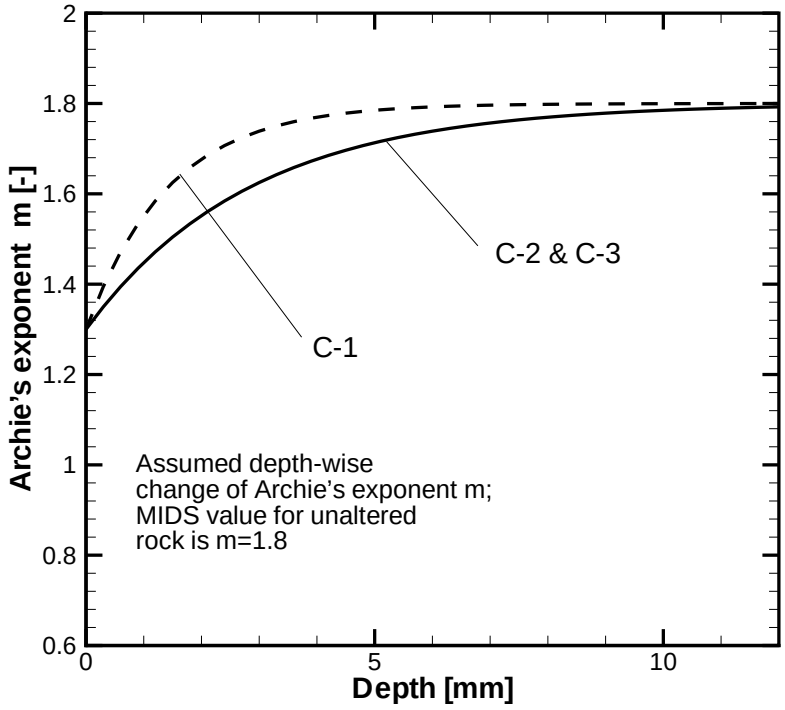

Figure 7.2: *Depth-wise trend in Archie's exponent m for C-1, and C-2 and C-3 tests.*

The governing equation then becomes

$$\frac{\partial C}{\partial t} = \frac{1}{R}\frac{\partial D(z)}{\partial z}\frac{\partial C}{\partial z} + \frac{1}{R}D(z)\frac{\partial^2 C}{\partial z^2} \tag{7.6}$$

where $D(z) = D_w[\theta(z)]^{m(z)-1}$, and $\theta(z)$ and $m(z)$ are given in Eq.(7.1) and Eq.(7.5), respectively.

The boundary condition $C(t,0)$ is proportional to the tracer discharge in the fracture at any given cross-section along the flow path. In the vicinity of the injection borehole, the $C(t,0)$ is applied over a relatively short time, giving least time for tracer penetration into the matrix. In the vicinity of the detection (pumping) borehole, the $C(t,0)$ is applied over longest time interval, giving most time for tracer penetration. In the following chapter, we consider both limits (boreholes).

The penetration profiles can be computed at times when the boundary condition is effectively terminated, implying that at a later time the tracer would slow down its penetration considerably. At the pumping borehole, for instance, the penetration profile for Cs would be computed for ca 3000 h, when the BTC data is terminated. Hence, although Cs will continue to penetrate further into the matrix after 3000 h, this is seen as irrelevant for the interpretation of the BTC which terminates at 3000 h. Penetration profiles computed at the injection and the pumping boreholes are viewed as relevant for interpreting the retention as reflected by the measured BTCs of the TRUE Block Scale tests.

In view of the different sorption properties for different tracers, each tracer will penetrate to a different depth during the TRUE Block Scale experimental time. This implies that each tracer "experiences" different porosity: for instance, Br the lowest porosity and Cs the highest porosity. To account for this difference in parameter estimation, we define a profile-averaged (referred to as "apparent") porosity, $\theta_{\rm app}$ for a given tracer:

$$\theta_{\rm app} \equiv \frac{1}{\int_0^\infty C(z,t)dz} \int_0^\infty \theta(z)\, C(z,t)\, dz \tag{7.7}$$

Note that $\theta_{\rm app}$ depends on time.

In the next chapter, we shall illustrate the penetration profiles, and their impact on $\theta_{\rm app}$, as part of an iterative estimation procedure.

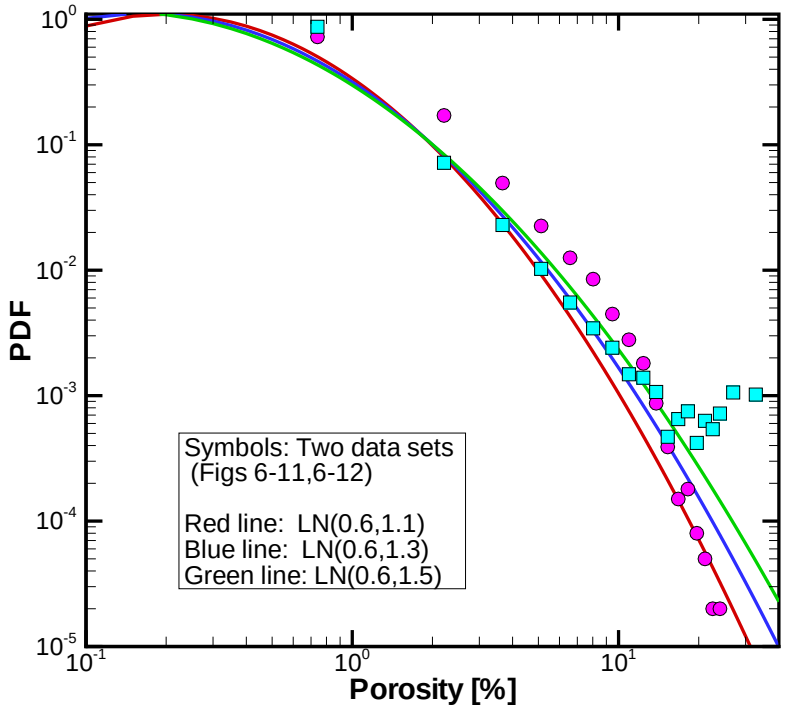

Figure 7.3: *Longitudinal variability in porosity: Two data sets over a ca 20 cm^2 area from Byegård et al. (2001), and a log-normal model for three sets of parameters.*

7.2 Longitudinal variability

In Byegård et al. (2001) it was clearly shown for TRUE-1 Feature A that the retention in altered rock core samples (diffusion and sorption) can be better reproduced by modelling if porosity is assumed to vary along the surface of the core cross-section (here referred to as longitudinal variability); porosity variability over the cross-sections was inferred independently using PMMA porosity data. On the surfaces of the investigated cores, the porosity variability was found to be approximately log-normally distributed (Figure 7.3). Comparative data from TRUE Block Scale intercepts are also available (Kelokaski et al., 2001), which demonstrate both depth-wise and longitudinal variations of porosity.

In the following, we outline a methodology to account for the longitudinal variability, and derive expressions for "effective" porosity.

The key parameter group in our evaluation is $\beta\kappa$ defined for the heterogeneous case as

$$\beta\kappa = \int_0^\tau \frac{(\theta F R D_w)^{1/2}}{b}\, d\vartheta \tag{7.8}$$

where in the general case, all parameters can vary (longitudinally) over the fracture surface, i.e., along any trajectory between injection and detection borehole. We first write the above

integral in a discrete form:

$$\beta\kappa = \Delta\tau \sum_{i=1}^{N} \frac{1}{b_i} \left(\theta_i \, D_w \, F_i R_{(i)}\right)^{1/2} \tag{7.9}$$

Thus if the water residence time τ is discretized along the flow path into N equal segments, the retention parameters could be assigned values for each segment. Invoking the linear assumption $\beta = k\,\tau$ where k corresponds to $1/b$ in an average (effective) sense, we write the above expression as

$$\beta\kappa = N\,\Delta\tau \left[\frac{1}{N} \sum_{i=1}^{N} \frac{1}{b_i} \left(\theta_i \, D_w \, F_i R_{(i)}\right)^{1/2}\right] \tag{7.10}$$

$$\approx k\,\tau \left[\frac{1}{N} \sum_{i=1}^{N} \left(\theta_i \, D_w \, F_i R_{(i)}\right)^{1/2}\right] = k\,\tau \left\langle (\theta \, D_w \, FR)^{1/2} \right\rangle \tag{7.11}$$

where angular brackets imply ensemble average. In other words, we have invoked in the last step the "ergodicity assumption", implying that the flow path is sufficiently long such that approximately all statistical variability is captured, whereby ensemble and space average operations are equivalent. If we assume Archie's law applicable in the form $F = \theta^m$, then for any given tracer, the expression for κ writes

$$\kappa = \left\langle \left(\theta^{m+1} + \theta^m \, \rho K_d\right)^{1/2} \right\rangle \sqrt{D_w} \tag{7.12}$$

Consider first a non-sorbing tracer with $K_d = 0$:

$$\kappa = \left\langle \theta^{(m+1)/2} \right\rangle \sqrt{D_w} \tag{7.13}$$

Let θ be log-normally distributed (Byegård et al., 2001; see also Figure 7.3) with θ_G as the geometric mean and $\sigma_{\ln\theta}$ the log-standard deviation. Then, for any given pair $\theta_G, \sigma_{\ln\theta}$, we estimate the slope k from the calibrated parameter group ψ (see Table 6.1) as

$$k = \frac{\psi}{\left\langle \theta^{(m+1)/2} \right\rangle \sqrt{D_w}} = \frac{\psi}{\theta_G^{(m+1)/2} \sqrt{D_w}} \exp\left[-\sigma^2_{\ln\theta} \, \frac{(m+1)^2}{8}\right] \tag{7.14}$$

Thus we see that smaller θ_G implies a smaller slope k, and similarly greater variability (i.e., larger $\sigma^2_{\ln\theta}$) implies a larger slope k.

Expression (7.14) suggests an "effective" porosity[1] θ_{eff} for retention of non-sorbing tracers. Eq.(7.14) writes by definition

$$k = \frac{\psi}{\theta_{\text{eff}}^{(m+1)/2} \sqrt{D_w}} \tag{7.15}$$

[1] By "effective" we imply here parameters that are used in the transport model in exactly the same manner as their uniform counterparts.

In other words, θ_{eff} replaces a uniform porosity value for *non-sorbing tracers*, which yields the same k. From Eq.(7.15) we have

$$\theta_{\text{eff}} = \theta_G \, \exp\left(\frac{(m+1)^2 \, \sigma^2_{\ln\theta}}{4}\right) \tag{7.16}$$

which defines θ_{eff} in terms of the log-normal statistical parameters for θ (θ_G and $\sigma^2_{\ln\theta}$) and m. Since $m > 1$, we see from Eq.(7.16) that θ_{eff} is always greater than the arithmetic mean of θ, which is always greater than θ_G. In other words, the effective θ for inferring k is larger than the common averages, such as arithmetic or geometric means, if Archie's law is applicable.

For a sorbing tracer, we have from (7.11)

$$\psi = k\langle(\theta^{m/2} D_w K_d \rho)^{1/2}\rangle = k\langle\theta^{m/2}\rangle (D_w K_d \rho)^{1/2} \tag{7.17}$$

whereby

$$K_d = \left(\frac{\psi}{k}\right)^2 \frac{1}{\rho \, D_w} \frac{1}{\langle\theta^{m/2}\rangle^2} = \left(\frac{\psi}{k}\right)^2 \frac{1}{\rho \, D_w} \frac{1}{\theta_G^m} \exp\left(-\sigma^2_{\ln\theta} \frac{m^2}{4}\right) \tag{7.18}$$

assuming K_d to be a uniform (effective) value, and k is estimated from (7.14). In (7.18), we have assumed that K_d is sufficiently large (e.g., for Rb or Cs) such that θ^{m+1} is negligible relative to $\theta^m \, \rho K_d$. Also, we have assumed that density ρ is uniform. In the following chapters, we shall illustrate the effect of longitudinal heterogeneity on the estimation of *in-situ* retention parameters.

Finally, we derive effective porosity for relatively strongly sorbing tracers for which $1 + \rho K_d/\theta \approx \rho K_d/\theta$. Based on similar reasoning as above, we get for *sorbing tracers*

$$\theta_{\text{eff}} = \theta_G \, \exp\left(\frac{m^2 \, \sigma^2_{\ln\theta}}{4}\right) \tag{7.19}$$

We see that whereas θ_{eff} for non-sorbing tracers is always greater than the arithmetic mean, for the sorbing tracers θ_{eff} is greater than the arithmetic mean only is $m > \sqrt{2}$, which is likely to be the case in most applications.

Chapter 8

Accounting for retention heterogeneity: Evaluation results

In this chapter, we summarize iteration steps for estimating plausible ranges of *in-situ* retention parameters for each tracer of the C-1, C-2 and C-3 tests accounting for retention heterogeneity.

In the suggested procedure, we build on the analysis of the previous chapters, and account for the depth-wise deterministic trend in the porosity, as well as for the longitudinal porosity variability; models for the heterogeneity are qualitatively consistent with available data and conceptual models.

Step 1: Postulate θ and m heterogeneity models

We postulate a depth-wise porosity trend following an exponential model as presented in Figure 7.1. Available data indicate that along the TRUE Block Scale flow paths a coating is present with relatively large porosity (Andersson et al., 2002b); thus in the first millimeter of the "matrix" we anticipate relatively large porosity which is difficult to infer experimentally. Limiting values are postulated as 3% and 0.4% for flow path I (C-1 tests), and 4% and 0.4% for flow paths II and III (C-2 and C-3 tests, respectively); the latter two flow paths indicate somewhat stronger retention properties, hence higher values. Note that the assumed variability in porosity includes all the immobile zones, fault breccia as well as fault gouge, which are in contact with the flow path. The transition parameter a (see Eqs.(7.1) and (7.5)) is assumed as 0.35 1/mm for C-1, and 0.7 1/mm for C-2 and C-3 tests (Figure 7.3).

The longitudinal porosity variation is assumed to follow a log-normal distribution model, consistent with findings of Byegård et al. (2001). The geometric mean of the porosity (which is independent of the log-standard deviation), is assumed to depend on the penetration of a tracer in the "matrix", as will be explained below. The log-standard deviation is considered a sensitivity parameter, with the lower limit of 1.1 being consistent with the data of Byegård et al. (2001). The upper limit is set arbitrarily to 1.5. If Byegård et al. (2001) found a log-standard deviation of 1.1 on a sample of 5 cm scale, then a larger log-standard deviation can be expected for the entire flow path, if the integral scale of the

longitudinal variations is larger than the sample (≈ 5 cm) size.

The heterogeneity in porosity implies heterogeneity of the diffusivity through Archie's law. Since we have evidence of relatively large tortuosity and small connectivity for the unaltered rock, and anticipate relatively small tortuosity and large connectivity in the altered rim zone, we postulate a depth-wise increasing trend of the Archie's exponent m; the limiting values are 1.3 in the vicinity of the flow path, and 1.8 in the unaltered rock. Note that 1.8 is the value valid for MIDS data since $\theta = 0.004$ and $F = 0.00005$ (Cvetkovic et al., 2000). We assume an increasing exponential model as for m, with an identical transition parameter a as for the porosity (i.e., 0.35 1/mm for C-1, and 0.7 1/mm for C-2 and C-3); the assumed profiles for m are given in Figure 7.2

Step 2: Assume R_0

Once the depth-wise profiles (trends) for the porosity and the exponent m are postulated (Figures 7.1-7.2), and a longitudinal statistical model is assumed, we select an initial value for the retardation coefficient of the rock "matrix" (referred to as R_0), for example, consistent with MIDS data.

Step 3: Compute tracer penetration

With R_0 postulated, and the depth-wise porosity and m trends assumed, we can compute a one-dimensional penetration of different tracers at the injection and pumping boreholes, using Eq.(7.6). The boundary condition is set at the injection borehole as the tracer injection function, and the pumping borehole as the measured BTC. The penetration profiles are computed at times, corresponding roughly to the "end" of the injection curve, i.e. BTC, for a given tracer (Figure 8.1-Figure 8.2), after which the penetration is anticipated to slow down significantly.[1]

Step 4: Compute "apparent" (depth-averaged) θ_{app} and m_{app}

Since we assume a depth-wise trend in the porosity and m, different penetration by different tracers implies that each tracer "experiences" a somewhat different porosity and exponent m. We define an "apparent" (depth-averaged) porosity and exponent m, and compute them as weighted by the penetration profile Eq.(7.7). For instance, for HTO the penetration is relatively large, since sorption is zero, hence HTO "experiences" the highest and the lowest porosity. By contrast, Cs penetrates the least since sorption is relatively strong, hence Cs "experiences" only the largest porosity, which has a decisive effect of

[1] These curves can be compared to the analytical solution if the porosity profile is assumed uniform with constant concentration in the fracture:

$$C(z,t)/C_0 = \operatorname{erfc}\left(\frac{1}{2}\frac{z}{\sqrt{tD/R}}\right) \tag{8.1}$$

where $D = FD_w/\theta$ is the pore diffusivity. We have made this comparison and found consistent results.

estimates of *in-situ* K_d. Hence the actual profile assumed is decisive for estimates of K_d, whereas the limiting lower bound for the unaltered rock is decisive for estimates of k.

Step 5: Infer k from non-sorbing tracer BTC

Once "apparent" (depth-averaged) porosity and exponent m are determined, the flow-dependent parameter k can be inferred. In particular, the depth-averaged $\theta_{\rm app}$ is considered as the geometric (independent of variability) mean of the statistical model, where from an effective porosity $\theta_{\rm eff}$ is computed using $\theta_{\rm app}$, $m_{\rm app}$ and $\sigma_{\ln\theta}$ from derived expression (7.16). With $\theta_{\rm eff}$ and $m_{\rm app}$, k is determined as

$$k = \frac{\psi[\text{calibrated}]}{\theta_{\rm eff}^{(m_{\rm app}+1)/2}\sqrt{D_w}} \tag{8.2}$$

We emphasize that $1/k$ [L] may be interpreted as a measure of the half-aperture. However, in view of the fact that we have lumped all immobile zones into our "matrix", $1/k$ cannot be considered directly related to the physical/geometrical half-aperture, but rather a "half-aperture" in a generalized sense, as a characteristic length scale for diffusive mass transfer into the "matrix".

Step 6: Infer K_d for each tracer

Once k is estimated, we can infer K_d for each of the sorbing tracers. Using depth-averaged $\theta_{\rm app}$ and the "matrix" density ρ (here assumed 2700 kg/m^3), we can compute the "apparent" retardation coefficient as $R_{\rm app} = 1 + \rho K_d/\theta_{\rm app}$ where

$$K_d = \left(\frac{\psi[\text{calibrated}]}{k}\right)^2 \frac{1}{\rho\, D_w}\, \frac{1}{\theta_{\rm app}^{m_{\rm app}}}\, \exp\left(-\sigma_{\ln\theta}^2\, \frac{m_{\rm app}^2}{4}\right) \tag{8.3}$$

will generally be different than the assumed initial value of R_0 (Step 2). We then "manually" iterate the procedure by assuming a new R_0 value that is closer to $R_{\rm app}$, until we get $R_{\rm app} \approx R_0$. Once $R_{\rm app} \approx R_0$ is achieved, the iterative procedure is terminated and we consider the determined parameters k, K_d and $\theta_{\rm app}$ as *in-situ* estimates.

Step 7: Infer K_a for each tracer

We estimate the *in-situ* surface sorption coefficient K_a as

$$K_a = \frac{\zeta[\text{calibrated}]}{k} \tag{8.4}$$

where ζ is given in Table 6.1.

The entire iterative procedure is outlined in Figure 8.3. The estimated *in-situ* parameters are summarized in Tables 8.1-8.3, exemplified for flow path I (C-1 tests), for the different tracers. The procedure was applied for C-1 tests only since too few sorbing tracer breakthroughs are available for the C-2 and C-3 tests.

Table 8.1: Estimation tables of *in-situ* K_d for the C-1 test, where we account for longitudinal and depth-wise variability in the porosity and diffusion coefficient.

C-1	k [1/m]	K_d [m^3/kg]				
		Na-24	Ca-47	K-42	Rb-86	Cs-134
$\sigma_{\ln\theta} = 0$	20 900	7.32E-06	4.93E-05	4.82E-05	2.8E-04	3.5E-03
$\sigma_{\ln\theta} = 1.1$	6 500	1.84E-05	1.07E-04	1.11E-04	6.62E-04	7.9E-03
$\sigma_{\ln\theta} = 1.3$	4 090	3.36E-05	1.2E-04	2.08E-04	1.25E-03	1.5E-02
$\sigma_{\ln\theta} = 1.5$	2 380	5.52E-05	3.24E-04	3.49E-04	2.17E-03	2.58E-02

Table 8.2: Estimation tables of *in-situ* K_a for C-1 test, where we account for longitudinal and depth-wise variability in the porosity and diffusion coefficient.

C-1	K_a [m]				
	Na-24	Ca-47	K-42	Rb-86	Cs-134
$\sigma_{\ln\theta} = 0$	2.01E-07	1.15E-05	2.07E-05	1.44E-04	4.32E-04
$\sigma_{\ln\theta} = 1.1$	6.46E-07	3.70E-05	6.65E-05	4.62E-04	1.39E-03
$\sigma_{\ln\theta} = 1.3$	1.03E-06	5.87E-05	1.06E-04	7.33E-04	2.2E-03
$\sigma_{\ln\theta} = 1.5$	1.76E-06	1.01E-04	1.82E-04	1.26E-03	3.78E-03

Table 8.3: Estimates of the "apparent" porosity, θ_{app} Eq.(7.7) which account for the fact that porosity and diffusivity vary depth-wise, and that different tracers penetrate to different depths.

C-1	θ_{app} [%] Eq.(7.7)		
	$\sigma_{\ln\theta}$ =1.1	$\sigma_{\ln\theta}$ =1.3	$\sigma_{\ln\theta}$ =1.5
Br	0.51	0.51	0.51
Na	1.16	1.16	1.27
Ca	1.44	1.44	1.60
K	1.51	1.51	1.66
Rb	1.70	1.70	1.85
Cs	1.72	1.72	1.87

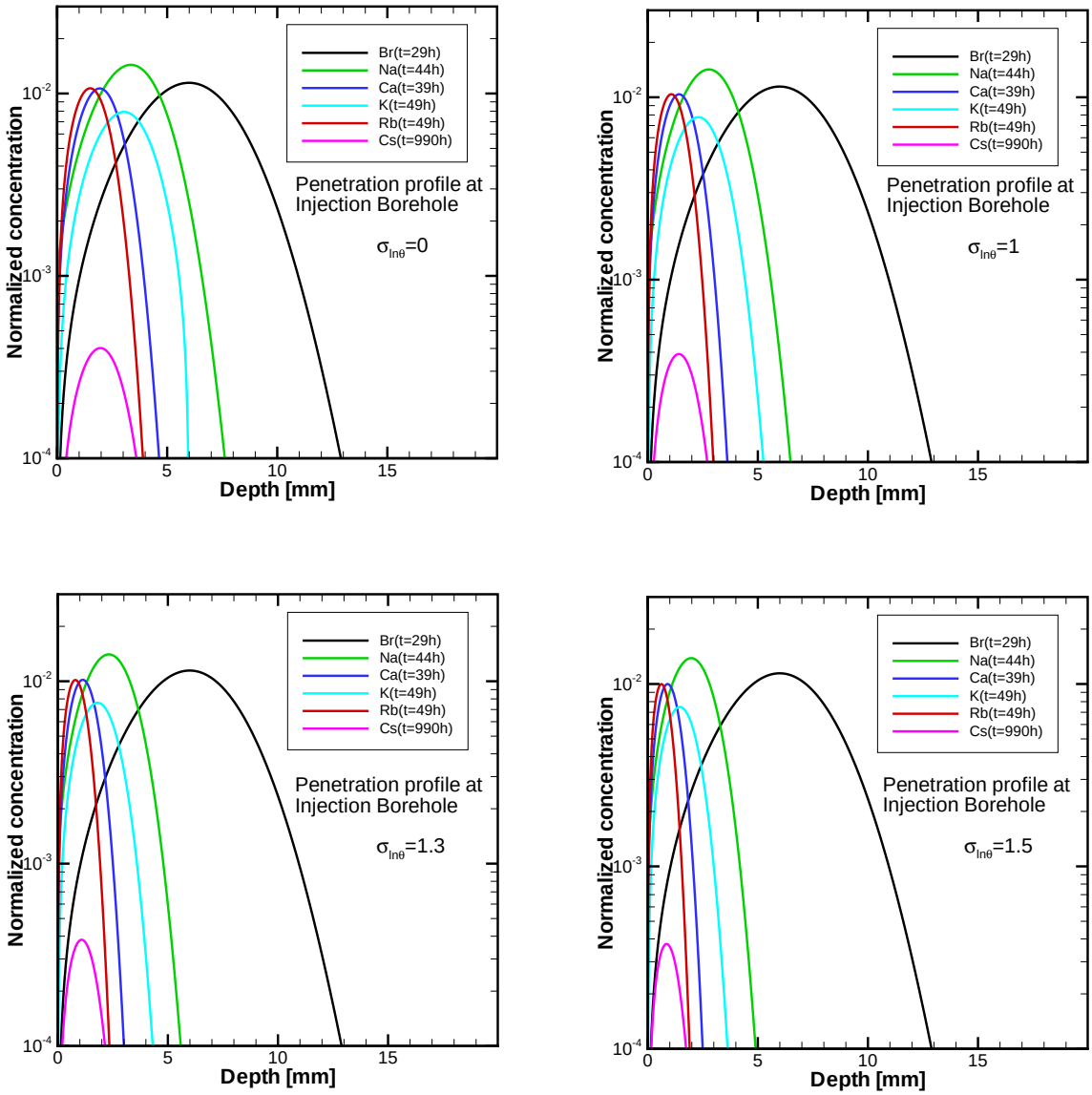

Figure 8.1: *Penetration profiles at the injection borehole for different tracer of the C-1 tests at times indicated in parenthesis for each tracer. These times correspond approximately to times when injection curves for respective tracers have decreased to a fraction of their peak value.*

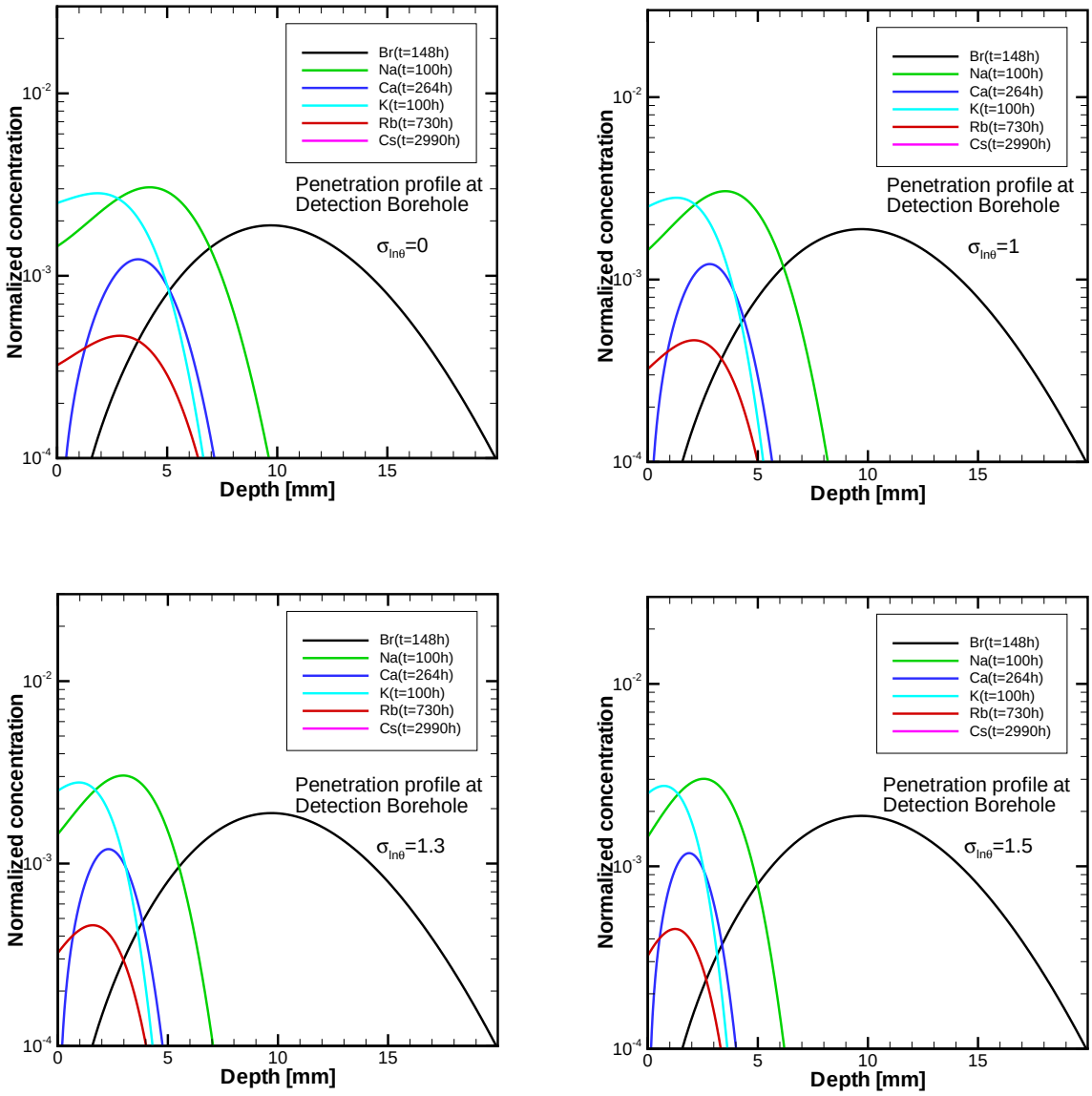

Figure 8.2: *Penetration profiles at the pumping borehole for different tracer of the C-1 tests at times indicated in parenthesis for each tracer. These times correspond approximately to times when BTCs for respective tracers have decreased to a fraction of their peak value.*

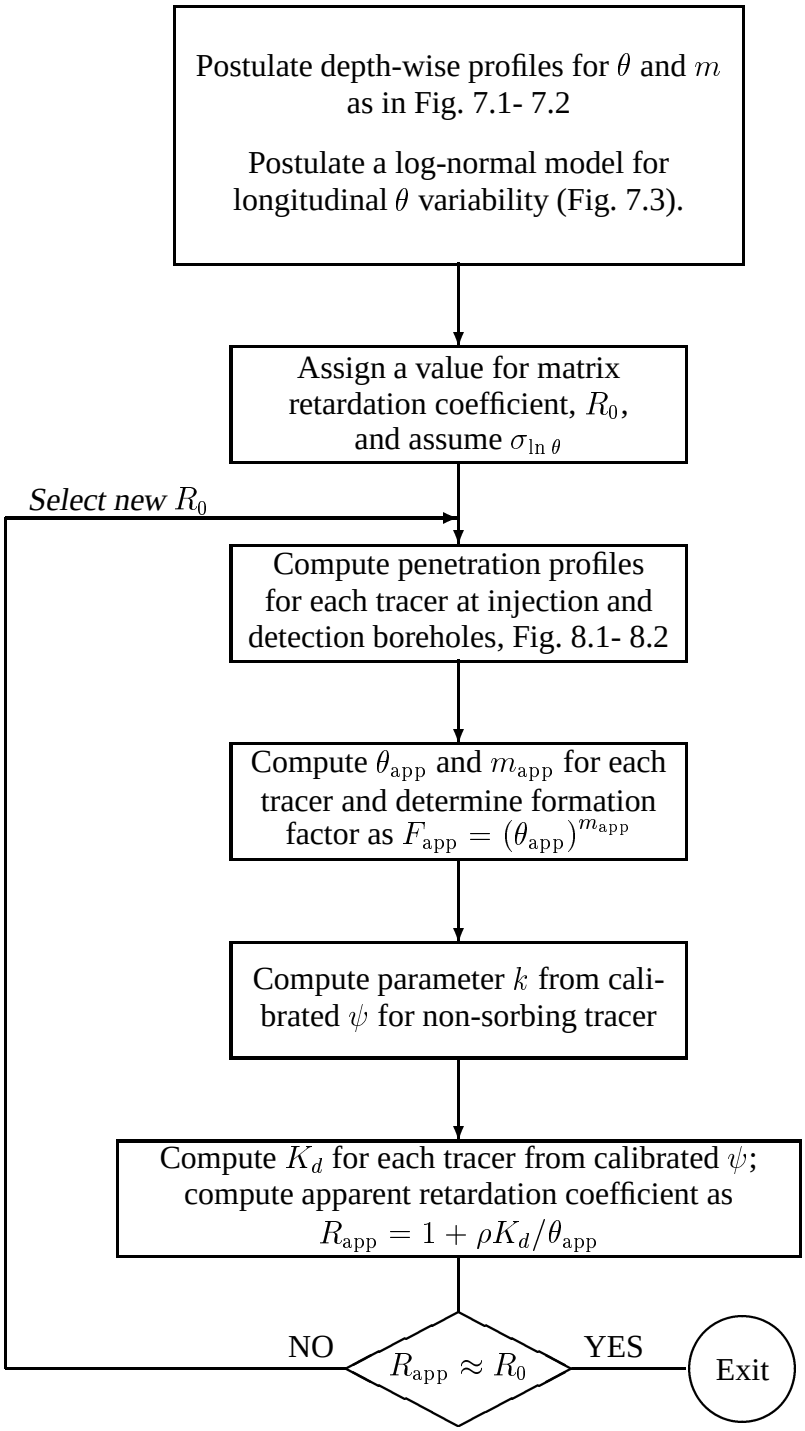

Figure 8.3: *Iterative procedure for estimating in-situ retention parameters, which accounts for vertical (depth-wise) and longitudinal variability in porosity and diffusivity; the porosity and diffusivity are assumed linked through Archie's law.*

Table 8.4: Estimates of the "apparent" Archie's exponent m, $m_{\rm app}$ computed in analogy with $\theta_{\rm app}$ Eq. (7.7) which account for the fact that porosity and diffusivity vary depth-wise, and that different tracers penetrate to different depths.

C-1	$m_{\rm app}$ [–]		
	$\sigma_{\ln\theta}$ =1.1	$\sigma_{\ln\theta}$ =1.3	$\sigma_{\ln\theta}$ =1.5
Br	1.78	1.78	1.78
Na	1.65	1.65	1.63
Ca	1.60	1.60	1.57
K	1.59	1.58	1.56
Rb	1.55	1.55	1.52
Cs	1.55	1.55	1.52

Table 8.5: Estimates of the "apparent" formation factor obtained using Archie's law with "apparent" porosity ($\theta_{\rm app}$) and exponent ($m_{\rm app}$).

C-1	$F_{\rm app} \equiv (\theta_{\rm app})^{m_{\rm app}} \times 10^4$ [–]		
	$\sigma_{\ln\theta}$ =1.1	$\sigma_{\ln\theta}$ =1.3	$\sigma_{\ln\theta}$ =1.5
Br	0.83	0.83	0.83
Na	6.4	6.4	8
Ca	11	11	15
K	13	13	17
Rb	18	18	23
Cs	18	18	23

Table 8.6: "Equivalent" porosity, $\theta_{\rm eff}$ as defined in Eq.(7.16). We emphasize that effective porosity for retention depends on the tracer and degree of variability, implying enhancement of retention for increasing variability.

C-1	$\theta_{\rm eff}$ [%] Eq.(7.16)		
	$\sigma_{\ln\theta} = 1.1$	$\sigma_{\ln\theta} = 1.3$	$\sigma_{\ln\theta} = 1.5$
Br	1.18	1.64	2.43
Na	2.59	3.56	5.58
Ca	3.16	4.32	6.77
K	3.30	4.51	7.00
Rb	3.68	5.00	7.65
Cs	3.71	5.04	7.72

Chapter 9

Discussion

The conditions which any tracer particle (ion) encounters on its "journey" from the injection (A) to the pumping (B) borehole are complex, regarding geometry, flow conditions, retention properties (porosity, diffusivity, etc). A three-dimensional model for flow and retention processes, could, in principle, describe all these complexities. However, the limited information available (few borehole intercepts and limited laboratory data) does not warrant a detailed (microscopic) flow-retention model.

The basic assumption of our evaluation model is the existence of *dual porosity*, here applied in a Lagrangian framework. In other words, there is a void space (of unit porosity) which is the opening of the fracture (referred to as "aperture") where advection takes place, and a (less than unity) porosity of the rock "matrix". As a tracer particle migrates from A to B, carried by water through the high porosity (void) regions of the fracture, it is temporarily "trapped" in the low porosity zones ("matrix") where the flow is essentially immobile; thus the low porosity regions are the "retention zones", or zones where retention takes place.

9.1 Conceptualization of retention heterogeneity

The simplest conceptualization of the above simulation is one of a parallel plate, with a uniform fracture aperture and uniform matrix (e.g., Neretnieks, 1980). Although this conceptual model presumably captures the main effects, it is clear from the available information that the matrix is nothing like a uniform block, but rather a conglomerate of complex superimposed structures, consisting of microfissures and smaller and larger "pieces" of altered rock (breccia) down to finer and finer particles (fault gouge). Moreover, the complexities of microscopic rock structure are most apparent in the rim zone, say up to 10 cm from the fracture surface, and in particular in the immediate vicinity of the fracture surface (say a few millimeters). Since the sorbing tracers are retained in this narrow zone, understanding the effect of (microscopic) heterogeneity in the altered rim zone is important for understanding (macroscopic) retention seen in the TRUE Block Scale *in-situ* tests.

There is evidence that even over a relatively small surface area of a fracture (core size), porosity varies from point to point on say a millimeter scale (e.g., Figures 6-11 and 6-12 in Byegård et al., 2001); this variability is apparently random (statistical). Such variability

has also been reported using samples of varying size (including fragments) from TRUE Block Scale structures (Kelokaski et al., 2001; Figures Figures 3-10, 3-13, 3-17, 3-27, 3-34, 3-43 and 3-50). Moreover, measurements of tracer penetration in core intercepts show the variability in penetration depth over a relatively small (millimeter) scale (Figures 6-5, 6-7, 6-9, Byegård et al., 2001; e.g., Figures 3-24, 3-31, 3-42 and 3-48 in Kelokaski et al., 2001). Furthermore, there is evidence that porosity when averaged over a relatively small volume (about 1 mm depth), varies in a deterministic manner, monotonically decreasing from the fracture surface (Figure 5-5, Byegård et al., 2001). The important issue then is how to "assemble" these different data into a consistent integrated conceptual picture of the retention heterogeneity.

The conceptual model for heterogeneity can be described from an "observer" which would be "attached" to a tracer ion, migrating from A to B. As the ion (particle) moves, it is occasionally retained in the immobile zones of the "matrix"; the physical/chemical basis for these "excursions" (or retention)[1] are diffusion and sorption (in this discussion we leave out, for simplicity, surface sorption). The retention process for a single particle is quantified in probabilistic terms. The probability of particle "excursions" depends on the combination of flow and retention properties, which vary from point to point on a millimeter scale. At locations of small aperture, low flow rate, large porosity, large K_d, the probability of a particle to make an "excursion" into the immobile part of the system, would be larger; in our model, this is quantified by a larger parameter B (2.2), which integrates these effects along trajectories.

The "matrix" here can mean any saturated immobile part of the system, where a combination of diffusion and sorption takes place; thus breccia and fracture coating (with its comparatively large porosity) is part of the heterogeneous "matrix". In other words, a tracer particle may be temporarily trapped on either side of the trajectory, i.e., in the matrix proper or "matrix" of rock fragments (breccia) and/or fracture coating.

Once the particle is temporarily trapped by the "matrix", it diffuses (penetrates) into the rock. At the actual fracture-matrix interface, the porosity encountered by the particle, at a given longitudinal location, is maximum; it is say a few percent, but could be significantly larger. The porosity then decreases quite rapidly, as the particle diffuses deeper into the matrix. If the particle manages to penetrate to tens of centimeters of the matrix proper, it encounters an unaltered (intact) rock with a relatively low porosity, say in the range 0.1-0.4%. The nature of diffusion is such that once a particle enters the matrix proper (which is assumed to be of large extent), it may take infinite time for it to leave the matrix; the probability for this however is small. As a rule, the particle will leave the matrix after a finite time, will re-enter the fracture, and continue its migration toward the pumping borehole (B). It can then get trapped and released at another location, and another, which macroscopically yields the accumulated retention effect at B. For the non-sorbing ions (e.g., Br), the "excursions" (or "trapping") into the immobile zones are relatively short, since only diffusion is active in the matrix; hence the comparatively small retention observed.

[1] Note that retention is assumed here reversible; hence "excursions" are only temporary since the particle sooner or later is released and continues the "journey".

In summary, we can provide a conceptual model for heterogeneous porosity as follows. Due to geometrical/structural variations (existence of microfissures of different sizes and lengths), the porosity varies longitudinally (along the trajectories (transport paths)) at the fracture-rock interface; this variation is statistical and observable on the millimeter scale. Moreover, the "connectivity" of the pores (microfissures), also varies. Although we do not have quantitative information on the correlation, larger porosity locations presumably imply existence of microfissures which extend deeper into the matrix, and hence larger connectivity. This is consistent with the data on say a millimeter scale variability of porosity observed over core intercepts (Figure 6-11, 6-12, Byegård et al., 2001), as well as the observations of varying tracer penetration (Figures 6-5,6-7,6-9, Byegård et al., 2001). Furthermore, if we average the porosity over 1 mm slices depth-wise, we expect a depth dependent variability, reflecting the attenuation of micro-fissure connectivity; this would then explain the PMMA measurements of depth variation profiles (Byegård et al., 2001; Kelokaski et al., 2001).

Finally, we comment on the formation factor F which in our analysis has been related to the porosity using Archie's law. The miscrofissure structure is presumably such that the exponent m is expected to be relatively low at the fracture-rock interface, monotonically increasing with the depth, reaching an asymptotic (maximum) value in the unaltered rock. This implies relatively large diffusion (due to good connectivity) at the fracture-rock interface, and relatively low diffusion deeper in the rock matrix. In Tables 6.4- 6.6 we have treated m as a sensitivity parameter, and have assigned it two limiting values, whereas in Chapters 7 and 8 we have assumed m to vary with depth, following an exponential model, similar as for θ.

9.2 Effect of retention heterogeneity: A simplistic example

The impact of retention heterogeneity is one of the important issues addressed in this report. In this section, we shall consider the simple (and classical) example of a flow "channel", attempting to demonstrate in a generic way how longitudinal porosity variations affect retention.

Let the flow rate q advect a tracer along a flow path of width w, length L and uniform half-aperture b. If the porosity of the rock matrix is uniform, say θ, the solution of the transport for pulse injection is

$$\gamma(t) = \frac{H(t-\tau)B}{2\sqrt{\pi}(t-\tau)^{3/2}} \exp\left[-\frac{B^2}{4(t-\tau)}\right] \tag{9.1}$$

where

$$B \equiv \frac{2Lw\sqrt{\theta F D_w R}}{q} \tag{9.2}$$

with F being the formation factor, and R the retardation coefficient of the matrix for sorbing tracers. Let us now assume that Archie's law is applicable in the form $F = \theta^m$; B then

writes

$$B = \frac{2Lw\sqrt{\theta^{m+1} D_w R}}{q} \tag{9.3}$$

Consider the case where the porosity is spatially variable in the longitudinal direction; we shall first consider the non-sorbing case.

9.2.1 Non-sorbing tracer

Non-sorbing tracers are significant for TRUE Block Scale tracer test evaluation since the flow-dependent retention parameter β, or its linearization counterpart k, are inferred from the BTCs of the non-sorbing tracers.

The exact expression for B in this case writes

$$B = \frac{2w\sqrt{D_w}}{q} \int_0^L \theta^{\frac{m+1}{2}}(x)\, dx \tag{9.4}$$

The above expression can be approximated by

$$B \approx \frac{2Lw\sqrt{D_w}}{q} \langle \theta^{\frac{m+1}{2}} \rangle \tag{9.5}$$

where

$$\langle \theta^{\frac{m+1}{2}} \rangle \approx \frac{1}{L} \int_0^L \theta^{\frac{m+1}{2}}(x)\, dx \tag{9.6}$$

is the statement of ergodicity (Dagan, 1989), i.e., we assume that L is sufficiently large relative to the integral scale of θ such that the ensemble and spatial averages can be exchanged.

Let us now assume that θ follows a log-normal distribution consistent with the data of Byegård et al. (2001) (see Section 9.1). Moreover, we shall assume that the parameter values of Figure 7.3 are applicable, i.e., the geometric mean is $\theta_G = 0.006$, and the log-standard deviation is $\sigma_{\ln\theta} = 1.1$. If $\sigma_{\ln\theta} = 0$, then the entire "channel" area in contact with the tracer has a uniform porosity of 0.006. With $\theta_G = 0.006$ and $\sigma_{\ln\theta} = 1.1$, 18% of the channel area is with porosity below 0.2%, 10% area with porosity > 0.02 and 2% of the area with porosity > 0.05. Thus we see that for a factor 3, the low porosity $< 0.006/3 = 0.002$ covers almost two times larger area (18%) than the larger porosity $> 3 \times 0.006 \approx 0.02$ which covers only 10% of the channel area. In other words, the statistical variations of the matrix porosity following a log-normal distribution have in effect increased the fraction of low porosity area to a greater extent than the larger porosity area. Nevertheless, the fact that porosity is variabile *enhances* retention, as will be demonstrated below.

Following the above definition of B, we have

$$B = \frac{2Lw\sqrt{D_w}}{q} \theta_G^{\frac{m+1}{2}} \exp\left[\frac{(m+1)^2 \sigma_{\ln\theta}^2}{8}\right] \tag{9.7}$$

which is an exact expression (provided conditions are "ergodic"). Hence we see from the above expression that stronger variability (i.e., larger $\sigma_{\ln\theta}$) directly enhances retention. For instance, let $m = 1.6$. Then for $\sigma_{\ln\theta} = 1.1$, we have

$$B = \frac{2.86\, Lw\sqrt{D_w}}{q} \tag{9.8}$$

This can be compared to

$$B = \frac{0.51\, Lw\sqrt{D_w}}{q} \tag{9.9}$$

which is applicable if there is no variability, i.e., $\sigma_{\ln\theta} = 0$ and the uniform porosity is $\theta_G = 0.6\%$. In other words, porosity variability has enhanced retention by a factor 6. If $\sigma_{\ln\theta} = 1.7$ (which for a flow path length of tens of meters is realistic given that 1.1 was found on a 5 cm scale sample by Byegård et al. (2001)), we have

$$B = \frac{5.9\, Lw\sqrt{D_w}}{q} \tag{9.10}$$

which is a retention enhancement by over one order of magnitude.

Here we wish to emphasize that the enhancement is stronger due to the assumed relationship between F and θ through Archie's law. Namely, Archie's law implies that the impact of porosity is greater than if the relationship between F and θ did not exist. To demonstrate this point, consider the case where F =const. i.e., independent of porosity. Then we have

$$B = \frac{2Lw\sqrt{FD_w\theta_G}}{q}\, \exp\left[\frac{\sigma^2_{\ln\theta}}{8}\right] \tag{9.11}$$

For $\sigma_{\ln\theta} = 1.7$, we get

$$B = \frac{0.74\, Lw\sqrt{D_w}}{q} \tag{9.12}$$

which is only 40% larger than the case without variability; this can be compared to over 1000% increase in the case F is related to θ through Archie's law (and specific value of $m = 1.6$).

Finally, we recall our derived expressions for effective porosity Eq.(7.16). It implies that if Archie's law is applicable, then the effective porosity for retention of non-sorbing tracers is

$$\exp\left[(m+1)^2\, \sigma^2_{\ln\theta}/4\right] \tag{9.13}$$

larger than θ_G. In our above example, with $\sigma_{\ln\theta} = 1.1$, we have that $\theta_{\text{eff}} = 7.7\theta_G$; in other words, effective porosity for retention is almost 8 times larger than the uniform porosity with $\sigma_{\ln\theta} = 0$, where the uniform porosity is the variability-independent geometric mean porosity, θ_G. In other words, effective porosity porosity, θ_{eff} is dependent on the variability.

With $\sigma_{\ln\theta} = 1.7$, for instance, we would have a factor 132, i.e., effective porosity for retention would be 132 times larger then the variability-independent, uniform porosity, θ_G. Note that the impact on retention is not proportional to the porosity, but rather to its square root.

In summary, we have demonstrated above that longitudinal (statistical) variability of porosity *enhances retention*, since effective porosity increases with variability. This is in spite of the fact that increase in the variability (i.e., in $\sigma_{\ln\theta}$) effectively increases low porosity area to a greater extent than the high porosity area. The relatively strong effect of porosity variability follows from the fact that diffusivity and porosity are assumed related, hence heterogeneity in porosity implies heterogeneity in the diffusivity, following Archie's law. Without this relationship, porosity variability still enhances retention, but to a lesser extent. The fact that longitudinal variability in porosity increases θ_{eff} affects our estimates of *in-situ* β (or k).

9.2.2 Sorbing tracer

The exact expression for B in this case writes

$$B = \frac{2w\sqrt{D_w}}{q} \int_0^L \theta^{\frac{m+1}{2}}(x)\,\sqrt{R(x)}\,dx \tag{9.14}$$

We shall consider here relatively strongly sorbing tracers such that $1 + \rho K_d/\theta \approx \rho\, K_d\, \theta$ is applicable. The above expression can then be approximated as

$$B \approx \frac{2Lw\sqrt{D_w \rho\, K_d}}{q}\,\langle\theta^{\frac{m}{2}}\rangle \tag{9.15}$$

where

$$\langle\theta^{\frac{m}{2}}\rangle \approx \frac{1}{L}\int_0^L \theta^{\frac{m}{2}}(x)\,dx \tag{9.16}$$

Following the above definition of B, we have

$$B = \frac{2Lw\sqrt{D_w\,\rho K_d}}{q}\,\theta_G^{\frac{m}{2}}\,\exp\left[\frac{m^2\,\sigma^2_{\ln\theta}}{8}\right] \tag{9.17}$$

Recalling the expression Eq.(7.19), we see that effective porosity for retention of sorbing tracers is

$$\exp\left[m^2\,\sigma^2_{\ln\theta}/4\right] \tag{9.18}$$

larger than θ_G. We see that although larger variability even here implies a larger effective porosity, the effect is smaller than for non-sorbing tracers.

Table 9.1: Comparative effect of heterogeneity in porosity on *in-situ* parameter estimates for Cs in the C-1 tests. The geometric mean porosity (which corresponds to the "uniform" porosity) and the Archie's exponent are indicated in the parenthesis.

Cs (C-1 tests)	Depth var. $(\theta; m)$	K_d [m^3/kg]	k [1/m]
$\sigma_{\ln\theta} = 0$	YES	0.0035	20 900
	NO (0.03;1.3)	0.21	760
	NO (0.03;1.8)	0.21	1800
	NO (0.004;1.8)	0.028	30 600
$\sigma_{\ln\theta} = 1.5$	**YES**	**0.026**	**2380**
	NO (0.03;1.3)	1.61	170
	NO (0.03;1.8)	2.82	200
	NO (0.004;1.8)	0.38	3400

9.3 Signifi cance of retention heterogeneity for *in-situ* estimates

Tables 6.4- 6.6 provide estimation matrices, i.e., retention parameter ranges where we do not explicitly account for retention heterogeneity, and treat all parameters as uniform "effective" values. For instance, if we estimate the "matrix" porosity for a flow path to be say in the range 0.8-1.2%, then Tables 6.4- 6.6 give the corresponding estimates of the slope k, and the sorption coefficients for the tracers, for the three flow paths. Our analysis of Chapter 7 had the objective to derive expressions for effective porosity, and improve our understanding of the notion of effective porosity for retention.

We computed the penetration profile and showed that the penetration depth varies between different tracers. The implications are significant for porosity estimates, since the depth-wise variability of porosity implies that different tracers "experience" different porosity. For instance, the "apparent" (penetration-averaged, Eq.(7.7)) porosity for Cs could be up to 3 times larger than the corresponding porosity for Br.

Using equations of Chapter 7, we can show that the estimated *in-situ* slope k decreases with increasing porosity variability, whereas the estimated *in-situ* K_d for Rb and Cs increase. If we neglect the depth-wise variability in porosity, then the estimated K_d for Rb and Cs may be considered too large, for increasing longitudinal variability in porosity. This point is exemplified in Table 9.1 for Cs in the C-1 tests.

We see in Table 9.1 considerable differences in our *in-situ* estimates if we account for longitudinal and/or depth-wise variability in porosity, and if we do not.

Consider first the case where $\sigma_{\ln\theta} = 0$ (no longitudinal variability). The estimate where we assume depth-wise variability yields a too large k and relatively small K_d. When depth-wise variability is ignored, we can assume different (uniform) porosity values. Here we

compare 3 cases: Two cases where porosity is assigned limiting values of our depth-wise trend (3% and 0.4%, Figure 7.1) with $m = 1.8$, and one case where the porosity is 3% with $m = 1.3$, i.e., we test the limiting values of m with porosity 3%.[2] We see that two of the three cases yield plausible values of k (760 and 1800 1/m), however, the corresponding K_d values are too large. In the case $\theta = 0.4\%$, K_d is realistic, however, k is unrealistically large.

When longitudinal variability is accounted for ($\sigma_{\ln\theta} = 1.5$), if depth-wise variability is neglected we get too large estimates of *in-situ* K_d, whereas realistic estimates are obtained for k. Only in the case (noted as bold) where we account for both longitudinal and depth-wise variability, do we have estimates of k and K_d which both appear realistic; we consider this case as the most plausible. It is worth noting that Archie's exponent is a relatively robust parameter, as its range 1.3-1.8 has a limited impact on k and K_d, at most a factor 2 difference.

9.4 Generalized transport-retention model

In this section we discuss the generalization of the transport-retention model presented in Chapter 2, consistent with the transport-retention models which have been used by different modelling teams within the TRUE Block Scale Project (Poteri et al., 2002).

The problem of tracer transport and retention is formulated by "partitioning" the tracer into a *mobile* component (with concentration C) and one or more *immobile* components with concentrations C_i^*, where $i = 1, 2, .., N$ and N is the total number of immobile zones. Mass balance equations in their most general form are given by

$$\frac{\partial C}{\partial t} + \mathbf{V}\cdot\nabla C - \nabla\cdot\mathbf{D}\cdot\nabla C = F(C, C_1^*, C_2^*, ..., C_N^*; \mathbf{x}, t) \tag{9.19a}$$

$$\frac{\partial C_i^*}{\partial t} = F_i^*(C, C_1^*, C_2^*, ..., C_N^*; \mathbf{x}, t) \tag{9.19b}$$

where F and F_i^* define the interaction/exchanges between the mobile and immobile zones. In the general case, these interactions are non-linear, dependent on space and time. The velocity vector $\mathbf{V}$ quantifies advection due to groundwater flow, and the tensor $\mathbf{D}$ quantifies hydrodynamic dispersion. The concentrations C, C^* are defined for a given support volume (REV), consistent with the support volume of the advection velocity, $\mathbf{V}$. The dispersion tensor $\mathbf{D}$ reflects velocity fluctuations on the sub-REV scale.

For linear retention processes, F and F_i^* are linear functions of C and C_i^* and/or their spatial derivatives.

We assume the source/sink terms consistent with diffusion and sorption into immobile zones, and write the transport equations as

[2] Note that we do not consider it realistic to assign $m = 1.3$ to the case of porosity 0.4%, since for low porosity we anticipate relatively low connectivity and large tortuosity, hence large m.

$$R(\mathbf{x})\,\frac{\partial C}{\partial t} + \mathbf{V}\cdot\nabla C - \nabla\cdot\mathbf{D}\nabla C + \sum_{i=1}^{N}\frac{\alpha_i\,\theta_i(\mathbf{x})\,D_i(\mathbf{x})}{b_i(\mathbf{x})}\,\frac{\partial C_i^*}{\partial z}\;|_{z=0} = 0 \qquad (9.20a)$$

$$R_{m(i)}(\mathbf{x})\,\frac{\partial C_i^*}{\partial t} - \frac{\partial}{\partial z}\,D_i(\mathbf{x})\,\frac{\partial C_i^*}{\partial z} = 0 \qquad (9.20b)$$

where we have neglected radioactive decay and omitted internal or external sink/sources of tracer; the external sink/source are given as boundary conditions.

The quantities given in Eqs.(9.20a)-(9.20b) are:

N –	total number of retention zones
i –	index of retention zone ($i = 1, 2, ..., N$)
$\mathbf{D}(\mathbf{x})$ –	hydrodynamic dispersion tensor [L^2/T]
$b_i(\mathbf{x})$ –	generalized "half-aperture" for the different retention zones [L]
$D_i(\mathbf{x})$ –	pore diffusivity of rock matrix [L^2/T]
$\theta_i(\mathbf{x})$ –	porosity of rock matrix of retention zone "i" [-]
α_i –	fraction of fracture unit area in contact with retention zone "i" ($0 < \alpha_i \leq 1$) [-]
$K_a(\mathbf{x})$ –	surface sorption coefficient for fracture [L]
$C(\mathbf{x}, t)$ –	mobile tracer concentration [M/L^3]
$C_i^*(\mathbf{x}, t)$ –	immobile tracer concentration in retention zone "i" [M/L^3]
$R(\mathbf{x})$ –	retardation coefficient for the fractures [-] defined as $1 + K_a/b$ where K_a [L] is the surface sorption coefficient
$R_{m(i)}(\mathbf{x})$ –	retardation coefficient for retention zone "i" [-]
$\mathbf{V}$ –	advection velocity defined on an appropriate scale [L/T]
z –	distance perpendicular to plane of fracture [L]
$\mathbf{x}$ –	Cartesian position vector [L] (in 1D, 2D or 3D)
t –	time [T]

Equations (9.20a)-(9.20b) can in principle account for all type of heterogeneity for which data are available, both in terms of flow and retention. Different simplifications of Eqs.(9.20a)-(9.20b) can be considered, different techniques of solution, and different strategies to account for random/deterministic flow and retention heterogeneity. Equations (9.20a)-(9.20b) have been the basis for transport modelling within the TRUE Block Scale program.

In the general case, Eqs.(9.20a)-(9.20b) need to be solved numerically. However, analytical solutions can be obtained if diffusion is assumed unlimited in all retention zones for the duration of the tests. In such a case, we obtain the solution for a pulse of unit mass, as (neglecting for simplicity decay and surface sorption)

$$\gamma(t) = \frac{H(t-\tau)\,B}{2\sqrt{\pi}(t-\tau)^{3/2}}\,\exp\left[\frac{-B^2}{4(t-\tau)}\right] \qquad (9.21)$$

where

$$B \equiv \sum_{i}^{N} \int_{0}^{\tau} \frac{\alpha_i \, \theta_i \, \sqrt{D_i R_{m(i)}}}{b_i} \, d\vartheta \tag{9.22}$$

where γ [1/T] is tracer discharge, and τ is the water residence time for a trajectory. Note that all parameters in the integrand can be spatially variable, following a trajectory. The integral retention parameter B is a random variable, in general correlated to τ. The effect of dispersion is accounted for by averaging over all trajectories using a joint probability density function $f(\tau, B)$.

Assuming that the local retention parameters θ, D and K_d are uniform, effective values, we can write

$$B \equiv \sum_{i}^{N} \beta_i \, \alpha_i \, \theta_i \, \sqrt{D_i R_{m(i)}} \tag{9.23}$$

where

$$\beta_i \equiv \int_{0}^{\tau} \frac{d\vartheta}{b_i} \tag{9.24}$$

Extending the linear assumption $\beta = k\tau$ to all retention zones, we write

$$\beta_i = k_i \, \tau \tag{9.25}$$

where k_i [1/L]. We then have

$$B \equiv \tau \sum_{i}^{N} k_i \, \alpha_i \, \theta_i \, \sqrt{D_i R_{m(i)}} \tag{9.26}$$

We first define an effective "diffusion time" t_d as

$$t_d \equiv \left[\sum_{i}^{N} k_i \, \alpha_i \, \theta_i \, \sqrt{D_i R_{m(i)}} \right]^{-2} \tag{9.27}$$

For infinitely strong diffusion, $t_d = 0$ and diffusion is instantaneous, whereas $t_d \to \infty$ implies that diffusion takes infinite time and has no effect. Note that t_d accounts for mass transfer in all the retention zones.

Using t_d, a "retention time" T is defined as

$$T \equiv B^2 = \frac{\tau^2}{t_d} \tag{9.28}$$

The "retention time" T provides a compact measure of the retention effect for diffusion/sorption: It can be shown that the peak of γ is proportional to $1/T$, and that the peak arrives at the time $t = \tau + T/6$. In the absence of retention, $t_d \to \infty$, whereby $T \to 0$; then $\gamma \to \delta(t - \tau)$ and the peak arrives at $t = \tau$.

9.5 Comparative measures of retention

We seek suitable relative (dimensionless) measures for retention which can be used to compare retention of different flow paths (tests), as well as retention for given flow paths as evaluated/interpreted by different TRUE Block Scale modelling teams.

To this end, we shall use T and t_d as defined in the previous section.

Let RC denote a dimensionless measure referred to as "retention capacity", defined as

$$\frac{T}{\tau} = \frac{\tau}{t_d} \equiv RC \tag{9.29}$$

Since T may be interpreted as the "retarded" tracer residence time, due to diffusion/sorption, RC corresponds to a "sorption coefficient" for diffusion/sorption. For RC=0, there is no retention due to diffusion/sorption, whereas large RC implies strong retention due to diffusion/sorption (which in turn implies short t_d). It must be emphasized that RC is not independent of the water residence time, as is the equilibrium sorption coefficient; diffusion/sorption is a non-linear retention process, where $T \sim \tau^2$ is an approximation.

In the following we shall use t_d and RC to compare retention along TRUE-1 and TRUE Block Scale flow paths.

Calibration of the model Eqs.(9.20a)-(9.20b) (for unlimited diffusion), is effectively a calibration of three parameters: one retention parameter t_d, and two advection/dispersion parameters (for instance, the mean and variance of water residence time $\langle\tau\rangle$ and σ_τ^2, or mean velocity and dispersivity).[3]

In Table 9.2 we summarize the calibrated t_d for the TRUE-1 and TRUE Block Scale tests. The first observation is that the calibrated (*in-situ*) values are considerably smaller (i.e., *in-situ* retention is considerably larger) than predicted by MIDS data. The second observation is that relative to MIDS t_d, *in-situ* t_d for TRUE-1 and TRUE Block Scale C-1 tests are relatively close, within a factor 5 for the sorbing tracers. We emphasize that similar material retention properties for all three TRUE-1 tests (STT-1, STT-1b and STT-2) were estimated (Cvetkovic et al., 2000); we also note that TRUE-1 and TRUE Block Scale C-1 tests constitute 90% of all sorbing tracer tests with the TRUE program; in other words, there is comparatively little information for estimating retention properties of flow paths II and III from C-2 and C-3 tests, respectively. Third, from the few sorbing tracers considered in C-2 and C-3 tests, t_d in Table 9.2 indicates that flow path II (C-2) has strongest retention properties, and flow path I (C-1) the weakest, and that flow path III (C-3) has stronger retention properties than flow path I (C-1).

A further comparison between flow paths is given in Table 9.3 using the dimensionless measure RC ("retention capacity"). We see again that the values are comparable for the sorbing tracers for TRUE-1 and C-1; TRUE-1 (STT-1 tests) exhibits somewhat stronger "retention capacity". We also include the unaltered matrix sorption coefficient (dimensionless). If the rock was a compact (unaltered) matrix without fractures, then retention

[3]Note that $\langle\tau\rangle$ and σ_τ^2 can be related to the mean velocity and dispersion coeffi cient, if an advection-dispersion process is assumed.

Table 9.2: Calibrated *in-situ* diffusion time t_d for TRUE-1 and TRUE Block Scale flow paths. Smaller t_d indicates stronger retention. For comparison, we show t_d for MIDS retention parameters with an assumed "aperture" (characteristic length scale of the mobile water space) as 1 mm.

TRACER	t_d [h] TRUE-1	t_d [h] C-1	t_d [h] C-2	t_d [h] C-3	t_d [h] MIDS
HTO	32	625	18	72	1.5×10^5
Na	32	69	–	29	1.5×10^5
Sr	21	–	–	8	10^5
Ca	–	12	1.7	–	–
K	4	–	–	–	–
Ba	0.7	–	–	–	3200
Rb	0.1	0.48	–	–	640
Cs	0.006	0.04	–	–	43

would effectively be equilibrium retardation with $1 + \rho K_d/\theta$ as the retardation coefficient. From Table 9.3 we see that RC is about 25% of $\rho K_d/\theta$ for the TRUE-1 flow path, and around 10% for the TRUE Block Scale flow path I (C-1), whereas RC is larger than $\rho K_d/\theta$ for C-2 and C-3 tests. However, it must be emphasized that in contrast to $\rho K_d/\theta$ for equilibrium sorption, RC for diffusion/sorption is *not* independent of the water residence time; in the present case (due to linearization of β) it is proportional to the water residence time. Thus we see that RC is relatively large for flow paths II and III, due to the dependence on the water residence time.

Finally, we correlate RC with $\rho K_d/\theta$ in Figure 9.1 for TRUE-1 and C-1 tests. We see that the TRUE-1 line has a greater slope indicating that the physical retention parameters (θ, D and $1/b$) are somewhat higher for the TRUE-1 flow path than for the TRUE Block Scale flow path I (C-1).

Table 9.3: Dimensionless measure "retention capacity" RC for TRUE-1 and TRUE Block Scale flow paths. The water residence time for TRUE-1 is the mean 7 h, for C-1 15 h, C-2 140 h, and for C-3 250 h. Larger RC indicates stronger retention. All quantities are dimensionless. Note that RC is not independent of the water residence time, but in this case proportional to it.

TRACER	RC TRUE-1	RC C-1	RC C-2	RC C-3	$\rho K_d/\theta$ MIDS
HTO/Re/Br	0.2	0.02	7.8	2	0
Na	0.2	0.2	–	8.5	1
Sr	0.3	–	–	31	3.2
Ca	–	1.3	84	–	?
K	3.8	–	–	–	?
Ba	10	–	–	–	135
Rb	70	31	–	–	270
Cs	1 170	375	–	–	4050

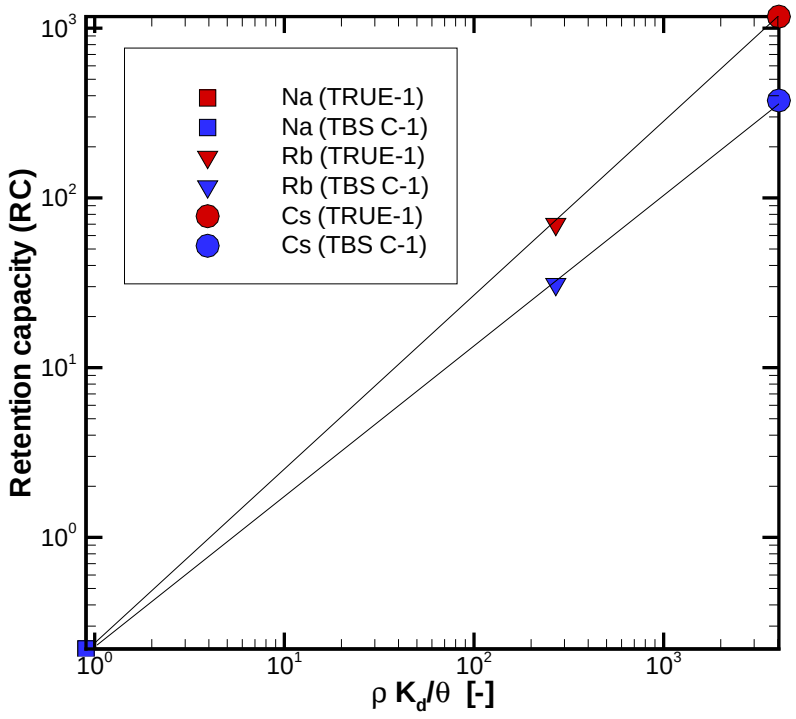

Figure 9.1: *Correlation between calibrated (in-situ) RC for TRUE-1 and flow path I (C-1) with $\rho K_d/\theta$, as given in Table 9.3. A greater slope for TRUE-1 indicates somewhat stronger retention due to larger values of the physical retention parameters θ, D and $1/b$.*

Chapter 10

Summary and conclusions

10.1 Summary points

Conceptualization and model

- We view the crystalline rock in a quasi-three-dimensional sense: as one, or several, interconnected two-dimensional fractures/structures with a heterogeneous void space. Tracers are advected with the water flow through the void space (fractures), and are subject to surface sorption and one-dimensional diffusion/sorption into the rock "matrix". The "matrix" is viewed as heterogeneous pore space with $\theta < 1$ and essentially immobile water. The immobile water adjacent to the flow path, including that of fault breccia, larger fault gouge fractions, fracture coating, are all viewed as part of the "matrix"; all the mobile water is viewed as part of a "fracture", characterized by a characteristic length scale referred to as "aperture".

- A linear retention model is assumed applicable for evaluating and interpreting BTCs of the TRUE Block Scale tests that is based on the dual porosity (parallel plate) concept (Neretnieks, 1980; Cvetkovic et al., 1999). Thus we assume that diffusion takes place into essentially unlimited retention (immobile) zones, for the time scales of the tests. Two important assumptions for the evaluation are: (a) the flow-dependent retention parameter β can be linearized as $\beta = k\,\tau$ where k [1/L] is applicable for a given flow path; (b) matrix porosity and diffusivity are related through the so-called Archie's law $F = \theta^m$ where F is the formation factor, θ is the porosity and m is a parameter which quantifies the connectivity/tortuosity of the matrix pore space ($m = 1$ indicates no tortuosity and perfect connectivity).

Calibration

- The parameter groups $\psi \equiv k\kappa$ (for retention in the matrix) and $\zeta \equiv k\,K_a$ (for surface sorption) have been calibrated for each tracer and flow path as summarized in Table 6.1; this calibration was done jointly with the calibration of water residence time moments $\langle\tau\rangle$, σ_τ^2 for each flow path. The groups ψ and ζ can be used as integral measures of retention. Comparing ψ for non-sorbing tracers, and ψ and ζ groups for

Na and Ca, we see that flow path II (C-2) exhibits the strongest retention and flow path I (C-1) the weakest.

- A key step in our estimation procedure uses the non-sorbing BTC for obtaining the parameter k as

$$k = \frac{\psi[\text{calibrated}]}{\theta^{(m+1)/2}\sqrt{D_w}}$$

The uncertainty in estimating k stems from three facts: (i) We do not have the *in-situ* water residence time distribution $g(\tau)$, hence the calibration of ψ, $\langle\tau\rangle$ and σ_τ^2 is not unique; (ii) we do not currently have sufficiently representative statistical *in-situ* information for determining the effective porosity, θ, for different flow paths; (iii) we do not have direct data on the Archie's exponent, and hence do not have representative values of m. Once k is determined (given all the uncertainty), the next key step is estimation of K_d and K_a from calibrated ψ and ζ for sorbing tracers.

Retention heterogeneity

- Important *in-situ* information, independent of the BTCs, is available on retention heterogeneity as summarized by Byegård et al. (2001, Figures 6-11,6-12 and 5-5). We find the data of Byegård et al. (2001) of particular interest since they have shown that porosity variability yields closer model representation of tracer penetration through core samples. Although the data are for the TRUE-1 Feature A, we regard it as qualitatively representative for TRUE Block Scale flow paths. We emphasize that the data of Byegård et al. (2001) are consistent with data of Kelokaski et al. (2001) obtained from TRUE Block Scale intercepts. The data from Byegård et al. (2001) indicates a relatively large longitudinal variability (Figure 7.3) on a small sample area; hence the longitudinal variability for the entire flow path is anticipated considerably larger. This implies that a comprehensive data set is required for quantitative statistical estimation. Moreover, the data of Kelokaski et al. (2001) are relatively limited and capture only a small part of the microscopic structural complexity. We therefore consider the data available from intercepts (Kelokaski et al., 2001; Byegård et al., 2001) as qualitative, rather than quantitative information.

- We postulate that both the "matrix" porosity and the connectivity/tortuosity exponent m, exhibit a depth-wise trend (Figure 7.3). Specifically, for flow path I (C-1), porosity decreases from 3% to 0.4% over approximately 2 mm scale, consistent with Figure 5-5 of Byegård et al. (2001), and m increases from 1.3 to 1.8, where 1.8 is consistent with the unaltered MIDS data. The increasing trend in m (Figure 7.2) reflects a decline in connectivity (increase in tortuosity) from the fracture surface toward the unaltered rock. Since flow paths II and III (C-2 and C-3 tests) show stronger retention, we assume the porosity and m profiles for C-1 tests and C-2, C-3 tests as slightly different (Figure 7.1 and Figure 7.2).

- Consistent with Figures 6-11,6-12 of Byegård et al. (2001), the porosity and diffusivity are assumed to vary randomly in the longitudinal direction; the basic ran-

dom field is that of porosity, assumed log-normally distributed. The diffusivity is a random field derived from porosity using Archie's law, where the exponent m is assumed uniform in the longitudinal direction.

- The longitudinal variability in retention parameters can be directly accounted for in our model, whereas the depth-wise variability cannot. Our approach is to account for depth-wise variability in an approximate manner, by computing one-dimensional penetration profiles in the vicinity of the injection and pumping boreholes, using the measured input tracer discharge curves and BTCs as boundary conditions. A penetration profile is computed at the time the boundary condition decreases to zero (see Figure 8.1 and 8.2, for specific times), after which the tracer penetration will increase much slower and eventually decrease.

Accounting for retention heterogeneity

- We developed an iterative procedure (Figure 8.3) for estimating *in-situ* values of K_d and K_a for all sorbing tracers and flow paths. Tracer penetration depends on the "matrix" retardation coefficient which depends on the unknown value of K_d. Hence we assign an initial value of the retardation coefficient, and change it for each iteration until the assigned and estimated values of the "matrix" retardation coefficient are approximately equal. All penetration profiles of Figure 8.1- 8.2 have been determined in this manner.

- Based on the computed penetration profiles (which differ at the injection and pumping boreholes), we defined an "apparent" porosity $\theta_{\rm app}$ for the entire flow path; this value is representative of the porosity (based on the assumed porosity profile of Figure 7.1), which a given tracer "experiences" during its penetration. The deeper the penetration (e.g., for non-sorbing tracers), the smaller the apparent porosity. The computed values of $\theta_{\rm app}$ depend on the tracer and the flow paths, and are summarized in Table 8.3.

- Similarly as for porosity, we define an "apparent" exponent in Archie's law, $m_{\rm app}$; this value is also tracer-dependent, as the penetration depth differs between tracers, depending on their sorption/diffusion properties. With $\theta_{\rm app}$ and $m_{\rm app}$, we define an "apparent" formation factor $F_{\rm app}$. Thus $\theta_{\rm app}\, F_{\rm app}\, D_w$ is a "lumped" measure for the whole flow path of the effective diffusivity applicable for a given tracer; the values of $F_{\rm app}$ are given in the Table 8.3.

- We derived an expression for effective porosity $\theta_{\rm eff}$ (7.16) for non-sorbing tracers, defined as the equivalent uniform porosity that accounts for the spatial variability in the retention parameter group κ. The effective porosity depends on $\theta_{\rm app}$ and on the log-standard deviation of the porosity, $\sigma_{\ln\theta}$; hence $\theta_{\rm eff}$ is also tracer-dependent. We summarize the values in the Table 8.3. We find $\theta_{\rm eff} \geq \langle\theta\rangle$, i.e., the effective porosity is always larger than the arithmetic mean porosity for non-sorbing tracers.

For sorbing tracers, effective porosity is greater than the arithmetic mean porosity for $m > \sqrt{2}$ which would be applicable in most cases.

Hydrodynamic control of retention

- Using the developed iterative procedure, we have estimated k in the range 2380-6500 1/m for C-1. For C-2 and C-3, the values are considerably larger: 8100-22400 1/m for C-2, and 3800 - 10500 1/m for C-3. Thus, we have an uncertainty range of approximately factor 3. The k value for C-2 and C-3 may be considered as overestimates. One possible explanation is that for flow paths II and III (C-2 and C-3 tests), the porosity profile shown in Figure 7.1 underestimates the real values, in view of the fact that the heterogeneity model "lumps" all immobile (retention) zones into a single, heterogeneous one. In fact, we can show that a modest change of the profiles in Figure 7.1, yields lower values of k for C-2 and C-3 tests. Another explanation is that *in-situ* k is large since it accounts for all voids with mobile water of a flow path, hence eluding a simple geometrical interpretation, as would be applicable for a uniform fracture ("channel"). Interestingly, the estimates of k from the non-calibrated FracMan (JNC/Golder) simulations obtained from correlating τ, β yielded k(C-1)=4700 1/m, k(C-2)=11500 1/m and k(C-3)=6370 1/m (Figure 4.3); in other words, the largest value is also for flow path II (C-2).

- Estimates of k for the three flow paths based on a homogeneous "channel" model can be made for comparison as follows. Using the calibrated mean water residence time $\langle\tau\rangle$ in Table 6.2, we compute the width of a flow path $w = \langle\tau\rangle Q/2bL$, where Q is the injection flow rate in Table 3.2 and L is the estimated flow path length. Assuming that for all flow paths the aperture is $2b$=1 mm, and that L(C-1)=20 m, L(C-2)=70 m and L(C-3)=90 m, we get w(C-1)=2 m, w(C-2)=1.2 m and w(C-3)=0.2 m. We can compute $\beta = 2wL/Q$, from which we estimate $k = \beta/\langle\tau\rangle$. The result is k(C-1)=2000 1/m, k(C-2)=2000 1/m and k(C-3)=2400 1/m. Thus we see that the homogeneous "channel" k values are consistent between flow paths, and are consistent with the lower bound of our estimates from BTC data. Consistent with a generalized interpretation of the characteristic length b, BTC data integrates retention effects along a structurally complex mobile water space, which yields a larger "apparent" or "effective" contact area, than would be obtained for a homogeneous "channel". Note that assuming a 2 times smaller aperture would yield two times larger k.

10.2 Concluding remarks

- The main difficulty in modelling TRUE Block Scale tracer tests for evaluation and interpretation is that the *in-situ* data base on retention material properties is limited, implying relatively large degree of freedom in parameter estimation; the challenge

has been to set appropriate *constraints* which are process-based and realistic using all available relevant information.

- In our evaluation, the key constraint is based on the fact that tracers of *strongly* varying sorbing properties were injected *simultaneously*, and hence are subject to identical physical processes (advection, dispersion, diffusion); another important constraint is based on the assumption that the immobile water ("matrix") porosity and diffusivity can be deterministically related by an empirical relationship referred to as Archie's law.

- Evaluation results indicate that the basic dual porosity transport model (linear mass transfer controlled by a concentration gradient as Fickian diffusion from the mobile to the immobile water with simultaneous sorption) captures the main features of the observed breakthrough curves; in other words, this model seems to account for the most dominant effects on the experimental time scales of the TRUE Block Scale tests.

- Retention parameters are grouped as: (i) material properties pertinent to the immobile zone (porosity θ, formation factor F, sorption coefficients K_d and K_a) and flow-related (hydrodynamic control) parameter $\beta = k\tau$ pertinent to the mobile zone; although individual effective retention parameters are strictly non-unique, we provide what we consider are *most probable* estimates based on Tables 6.4-6.6 for $m = 1.3$ as:

  - MATERIAL PROPERTIES: θ(C-1)=0.8%, θ(C-2)=2.8%, θ(C-3)=2%; F(C-1)=0.0019, F(C-2)=0.009, F(C-3)=0.006. K_d values are summarized in Table 10.2 and K_a values in Table 10.2.
  - HYDRODYNAMIC CONTROL: k(C-1)=3460 1/m, k(C-2)=4900 1/m, k(C-3)=3600 1/m; note that advective (water) travel times are roughly in the range 5-100 h (C-1), 40-400 h (C-2) and 100-1000 h (C-3), hence β is variable according to $\beta = k\,\tau$ and is found in the range: $2 \leq \beta$(C-1)≤ 39 yr/m, $22 \leq \beta$(C-2)≤ 224 yr/m, $41 \leq \beta$(C-3)≤ 411 yr/m.

  The approximate analysis in Chapter 8 indicates that effective parameters of Tables 6.4-6.6 would be somewhat different if depth-wise variability was directly accounted for (see Table 9.1 for Cs in C-1 tests); further analysis is required however for providing more accurate values.

- Comparison of retention parameter estimates from TRUE-1 Feature A scale of 5 m with TRUE Block Scale estimates indicate that material effective properties are comparable; thus it appears that no particular upscaling considerations are required for effective material properties from 5 m to say 15-30 m.

Table 10.1: Estimation tables for most probable effective K_d for TRUE Block Scale C-tests extracted from Tables 6.4- 6.6. The additional estimated $K_d = 0.32$ m^3/kg is for Ca-47 in C-2 tests. Included in the Table are MIDS values and the estimated *in-situ* range for TRUE-1 Feature A (Cvetkovic et al., 2000), as well as the K_d for fault breccia and gouge from Andersson et al. (2002b).

TRACER	C-1 $K_d \times 10^3$ [m^3/kg]	C-3 $K_d \times 10^3$ [m^3/kg]	TRUE-1[1] $K_d \times 10^3$ [m^3/kg]	MIDS[2] $K_d \times 10^3$ [m^3/kg]	TBS[3] $K_d \times 10^3$ [m^3/kg]	TBS[4] $K_d \times 10^3$ [m^3/kg]
Na	0.049	0.027	0.007-0.06	0.0014	0.003	0.047
Sr	-	0.19	0.024-0.32	0.0047	0.04	0.3
Ca	0.48	-	-	-	0.03	0.3
K	0.58	-	-	-	0.1	1.2
Rb	4.6	-	1.7 - 4.5	0.4	0.9	6.7
Cs	58	-	30-56	6	10	67

[1)] From Table 9.4 in Cvetkovic et al. (2000).
[2)] From Table 1.2 in Cvetkovic et al. (2000).
[3)] Estimated K_d for fault gouge material, size fraction $\geq 125\mu$m (Tullborg et al., 2000).
[4)] Estimated K_d for crushed material size fraction $\leq 63\mu$m (Andersson et al., 2002b).

Table 10.2: Estimation tables for most probable K_a for TRUE Block Scale C-tests obtained as ζ/k where k is extracted from Tables 6.4- 6.6, and ζ is given in Table 6.1. Included are the MIDS values (Cvetkovic et al., 2000).

TRACER	C-1 $K_a \times 10^3$ [m]	C-2 $K_a \times 10^3$ [m]	C-3 $K_a \times 10^3$ [m]	MIDS $K_a \times 10^3$ [m]
Na	0.0012	-	0.116	0.0007
Sr	-	-	0.133	0.008
Ca	0.069	0.049	-	-
K	0.125	-	-	-
Rb	0.867	-	-	0.5
Cs	2.6	-	-	8

10.3 A few open issues

Modelling of TRUE Block Scale tracer tests for parameter estimation and interpretation with the LaSAR approach could be improved by addressing a number of issues; we list below a few such issues and related tasks.

- A more comprehensive analysis of the upscaling of material retention properties from the microscopic scale to a meter scale is needed. The key issue is the relationship between *effective material properties* for retention on the field scale and results from small scale measurements, such as those obtained for porosity with the PMMA technique. One particular task is to statistically analyse the small scale porosity measurements from TRUE Block Scale *in-situ* samples reported in Kelokaski et al. (2001).

- The development of a en efficient methodology for estimating β from field measurements is required on the scale of TRUE Block Scale tests and larger. The particular issue is under what conditions does the linear relationship $\beta = k\tau$ (consistent with the classical model) apply, and how an "effective retention aperture" $2b_{\text{eff}} \equiv 2/k$ can best be estimated in the field. The specific task is to analyse existing TRUE Block Scale discrete fracture network simulation results and also carry out updated simulations and statistically analyse the hydrodynamic control of retention as quantified by β.

- Retention over longer transport times would be influenced by the limited capacity of the rim zones with its relatively strong retention properties; the time-dependence of the retention process and impact of the finite capacity of the rim zone on transport need to be further addressed. One possibility to account for finite retention zones is to use the framework of Cvetkovic et al. (1998).

- Sorption coefficient for the immobile zone (matrix) as determined from batch experiments is found to be time-dependent at least for some nuclides, such as Cs, indicating possible presence of kinetic effects for sorption in the immobile zone. Potential effects of such kinetics need to be studied, in particular to what extent they may affect the interpretation and evaluation of TRUE Block Scale tracer test results. A special case of such kinetics would be irreversible sorption. The framework of Cvetkovic et al. (1998) allows for incorporating sorption effects in the immobile zone.

- Current retention model assumes a single diffusion rate. The complexity of the rim zone may require a more general mass transfer model with multiple diffusion (mass transfer) rates at any given point along the flow path. The task would be to apply the modelling framework developed by Cvetkovic and Haggerty (2002) and re-evaluate breakthrough curves to assess whether a more general mass transfer (retention) model would yield a more consistent interpretation and evaluation of the TRUE Block Scale tracer tests.

- Direct impact of fracture intersection zones (FIZ) on *retention* appears impossible to discriminate from TRUE Block Scale BTCs (Cvetkovic and Uchida, in prep.). The possible impact of FIZ as sinks may be deduced indirectly, in view of the fact that tracer recovery for the different flow paths varies, being selectively relatively high: ca 100% (C-1), ca 80% (C-2) and ca 70% (C-3). However, further analysis is required for a better understanding of the potential impact of fracture intersection zones on tracer transport through a fracture network.

- The estimated retention parameters of Tables 6.4-6.6 represent effective values and were obtained *without* explicitly accounting for longitudinal or depth-wise variability in material retention properties. The analysis of Chapter 8 shows the potential effect of variability in porosity; if accounted for, this variability may imply that *in-situ* values of K_d and k for a given porosity given in Tables 6.4-6.6 may actually be lower (see Table 9.1). A more comprehensive analysis is required however to further expand results of Chapter 8 and more fully account for small scale variability in the estimation of retention material properties for TRUE Block Scale flow paths.

Bibliography

Andersson, J., Elert, M., Hermansson, J., Moreno, L., Gylling, B., and Selroos, J.-O. (1998). Derivation and treatment of the flow wetted surface and other geosphere parameters in the transport models FARF31 and COMP23 for use in safety assessment. Technical Report R-98-60, Swedish Nuclear Fuel and Waste Management Co.(SKB).

Andersson, P., Byegård, J., Holmqvist, M., Skålberg, M., Wass, E., and Widestrand, H. (2001). TRUE Block Scale Project tracer tests stage. Tracer tests, Phase C. International Progress Report IPR-01-33, Swedish Nuclear Fuel and Waste Management Co.(SKB).

Andersson, P., Byegård, J., and Winberg, A. (2002a). TRUE Block Scale Project. Final report #2(4). Tracer tests in the block scale. Technical Report TR-02-14, Swedish Nuclear Fuel and Waste Management Co.(SKB).

Andersson, P., J., B., Dershowitz, W., Doe, T., Hermanson, J., Meier, P., Tullborg, E., and Winberg, A. (2002b). TRUE Block Scale Project. Final report #1(4). Characterisation and model development. Technical Report TR-02-13, Swedish Nuclear Fuel and Waste Management Co.(SKB).

Andersson, P., Ludvigson, J., Wass, E., and Holmqvist, M. (2000a). TRUE Block Scale Project tracer tests stage. Interference tests, dilution tests and tracer tests, Phase A. International Progress Report IPR-00-28, Swedish Nuclear Fuel and Waste Management Co.(SKB).

Andersson, P., Wass, E., Holmqvist, M., and Fierz, T. (2000b). TRUE Block Scale Project tracer tests stage. Tracer tests, Phase B. International Progress Report IPR-00-29, Swedish Nuclear Fuel and Waste Management Co.(SKB).

Byegård, J., Johansson, H., Skålberg, M., and Tullborg, E.-L. (1998). The interaction of sorbing and non-sorbing tracers with different Äspö rock types: Sorption and diffusion experiments in the laboratory scale. Technical Report TR-98-18, Swedish Nuclear Fuel and Waste Management Co.(SKB).

Byegård, J., Widestrand, H., Skålberg, M., Tullborg, E., and Siitari-Kauppi, M. (2001). First TRUE Stage: Complementary investigation of diffusivity, porosity and sorptivity of Feature A-site specific geologic material. International Cooperation Report ICR-01-04, Swedish Nuclear Fuel and Waste Management Co.(SKB).

Clennell, M. (1997). *Tortuosity: A guide through the maze*, pages 299–344. Geological Society Special Publication No. 122.

Cvetkovic, V., Cheng, H., and Selroos, J. (2000). Evaluation of tracer retentionn understanding experiments (first stage) at Äspö. International Cooperation Report ICR-00-01, Swedish Nuclear Fuel and Waste Management Co.(SKB).

Cvetkovic, V., Dagan, G., and Cheng, H. (1998). Contaminant transport in aquifers with spatially variable hydraulic and sorption properties. *Proceedings of the Royal Society of London*, 454:2173–2207.

Cvetkovic, V. and Haggerty, R. (2002). Transport with multiple-rate exchange in disordered media. *Physical Review E*, 65:051308.

Cvetkovic, V., Painter, S., and Selroos, J. (2002). Comparative measures for radionuclide containment in the crystalline geosphere. *Nuclear Science and Engineering*, 142:292–304.

Cvetkovic, V., Selroos, J. O., and Cheng, H. (1999). Transport of reactive tracers in rock fractures. *Journal of Fluid Mechanics*, 378:335–356.

Dagan, G. (1989). *Flow and Transport in Porous Formations*. Springer-Verlag, New York.

Dershowitz, W., Cladouhos, T., and Uchida, M. (2001). Äspö Task Force, Task 4E and 4F - Tracer tests with sorbing tracers. International Cooperation Report ICR-01-02, Swedish Nuclear Fuel and Waste Management Co.(SKB).

Gray, D. (1972). *American Institute of Physics Handbook*. McGraw-Hill, New York.

Kelokaski, M., Oila, E., and Siitari-Kauppi, M. (2001). Investigation of porosity and microfracturing in granitic rock using the 14C-PMMA technique on samples from the TRUE Block Scale site at the äspö Hard Rock Laboratory. Technical Report IPR-01-27, Swedish Nuclear Fuel and Waste Management Co.(SKB).

Neretnieks, I. (1980). Diffusion in the rock matrix: An important factor in radionuclide retention. *Journal of Geophysical Research*, 85:4379–4397.

Poteri, A., Billaux, D., Dershowitz, B., Gomez-Hernandez, J.-J., Cvetkovic, V., Hautojärvi, A., Holton, D., Medina, A., and Winberg, A. (2002). TRUE Block Scale Project. Final report #3(4). Modelling of flow and transport. Technical Report TR-02-15, Swedish Nuclear Fuel and Waste Management Co.(SKB).

Winberg, A. (1997). Test plan for the TRUE Block Scale experiment. International Cooperation Report ICR-97-02, Swedish Nuclear Fuel and Waste Management Co.(SKB).

Winberg, A., Andersson, P., Hermanson, J., Byegård, J., Cvetkovic, V., and Birgersson, L. (2000). Final report on the first stage of the tracer retention understanding experiments. Technical Report TR-00-07, Swedish Nuclear Fuel and Waste Management Co.(SKB).